

Dear Professor Sierra,

We have now completed the edits to our manuscript titled: "*Robust Ecosystem Demography (RED): a parsimonious approach to modelling vegetation dynamics in Earth System Models*".

Attached is a file containing the point by point responses to each reviewer's comments, and a latexdiff file showing the extensive changes that we have made to our paper. We believe that these changes have made our study much more coherent and robust.

We have added Dr Anna Harper from the University of Exeter as a co-author, as she provided driving data for our study and also invaluable insights during the revision process.

Thank you in advance for taking the time to look over our revisions. We look forward to your decision.

Yours sincerely,

Arthur Argles and Peter Cox (on behalf of co-authors)

Response to Reviewer 1:

Robust Ecosystem Demography (RED): a parsimonious approach to modelling vegetation dynamics in Earth System Models

Arthur P. K. Argles, Jonathan R. Moore, and Peter M. Cox on behalf of co-authors. (*on behalf of the co-authors*)
22nd April 2020

We thank the reviewer for their extremely detailed review. Most of the suggestions were on technicalities within the literature and definitions used within the paper. We address each of the queries raised below. The relevant reviewer comments are written in italics below followed by our responses in plain font with the changes given in blue.

Reviewer:

In this paper, Argles and co-authors introduce the ‘Robust Ecosystem Demographic’ (RED) model. RED is introduced as an alternative to cohort-based vegetation demographics models, and its justifications are largely presented as being in opposition to more complex approaches that discretize tree size and age since disturbance. Instead of discretizing age since disturbance and tracking individual cohorts performance, RED makes several simplifying assumptions including:

- 1. Productivity for each plant size class is not calculated as a function of it’s resource availability within a PFT x age class matrix (as for a typical ecosystem-demography based VDM) and instead is assumed to scale with plant size, as per the idealized ‘Metabolic Scaling Theory’.*
- 2. Thus, there is no possibility of relative plant size determining competition for light, and hence productivity and growth, and thus all plants of a given PFT are supposed to occupy the same area.*

Response (1):

While it is true that we do not explicitly model light competition (except with respect to the net growth-rate of the recruitment flux), it is not true that plant size has no impact on growth-rate or that all plants of a given PFT occupy the same area. In RED we assume allometric relationships relating tree mass to growth-rate (Equation 2) and crown area (Equation 3). We have clarified these assumptions.

Reviewer:

- 3 The horizontal area is divided into said PFT tiles, and another tile wherein disturbance and seed establishment occur.*

Response (2):

This is an interesting way of viewing RED, but it’s not quite how we see it. In fact, PFT-dependent disturbance occurs across the whole of the grid-box, as does seed establishment. The confusion may arise from the fact that the latter is affected by light-competition

and therefore depends on the unvegetated fraction of the grid-box. We have clarified these points in a revised model description.

Edit:

“Spreading is homogeneous across the entirety of the grid-box, but only seedlings established within ‘unoccupied space’ will survive to join the plant cohort.”

Edit:

“Disturbance mortality rates from γ_d can in principle be both PFT-dependent and mass-dependent (e.g. to capture forestry practices).”

Reviewer:

On account of these various simplifications the model can be solved analytically for a given productivity and mortality rate and RED is generally proposed as an alternative method for the simulation of some aspects of vegetation demographics in Earth system models (ESMs). I appreciate the novelty of this approach, and think it is important that a diversity of avenues are taken towards improving the representation of the terrestrial carbon cycle within ESMs.

While this is an interesting set of concepts, and potentially an interesting ‘middle ground’ in complexity of representation of vegetation demographics, there are numerous issues with the presentation, description and validation of the model that I find problematic in this paper.

First, in the introduction, there is insufficient explanation of the existing diversity of approaches to the simplification of forest models. A class of models already exists which is much closer conceptually to RED, e.g. the POP (Haverd et al., 2014) and ORCHIDEE-MICT (Yue et al., 2018) models, that also track different size or age cohorts within a single tile devoted to each PFT. While RED additionally provides a DGVM capacity in the form of the competition for seed recruitment, it seems that this class of models certainly requires description at the very least.

Response (3):

As suggested, we now compare and contrast RED with these other published models, within our revised discussion and introduction.

Edit:

“In a similar vein other models have limited the number of cohort dimensions. The POP model (Haverd et al., 2014), uses stand-age cohorts as the dimension for population dynamics, every time-step applying crowding and resource limited mortality rates. Another example is the ORCHIDEE-MICT (Yue et al., 2018), which disaggregates the populations of a PFT into patch cohort functional types, with transitions between cohorts diagnosed when the average basal diameter passes a threshold.”

Edit:

“This is a distinct approach relative to other intermediate complexity DGVMs which are based on

patches defined by time since disturbance, such as the POP or ORCHIDEE-MICT models (Haverd et al., 2014; Yue et al., 2018)."

Reviewer:

Further, despite the numerous mentions of the PPA approach, the paper does not actually describe this alternative approach to defining 'tractable' solutions to demographic modeling. A comparison of the RED and PPA approaches would be interesting, in particular given the fact that the PPA requires slightly more parameters than RED. This is particularly relevant given that the PPA is also implemented in the GFDL ESM. A comparison of the RED and PPA approaches would be interesting, in particular given the fact that the PPA requires slightly more parameters than RED. This is particularly relevant given that the PPA is also implemented in the GFDL ESM.

Response (4):

We have included a description on PPA in the discussion and how this relates to the minimum overlap assumption within RED.

Edit:

"Finally, we assume that competition is only significant for the lowest 'seedling' mass class. This enables us to represent gap dynamics among plants and resultant stages in succession. This represents a significant simplification compared to other approaches involving the Perfect Plasticity Assumption (PPA), as used within DGVMs such as LM3-PPA or CLM(ED) (Fisher et al., 2015; Weng et al., 2015), where canopies are assumed to perfectly fill gaps through photomorphism (Strigul et al., 2008). In LM3-PPA the radiative flux is limited by the available gap fraction in a given crown layer. PPA parallels our gap boundary condition at the lowest mass class (equation (6)), but in RED the growth of a cohort is purely dictated by the the disaggregation of total growth assimilate assuming metabolic scaling (equation (11))."

Reviewer:

Instead of a description of the relevant literature, the current justification statements in the introduction focus on somewhat vague assertions that full ED-type size-and age structured approximations are too cumbersome. A comparison with more similar models would be helpful, as would a more general depiction of the pro's and cons of the approach used here. The model clearly has some benefits in terms of simplicity and tractability, but also has some drawbacks in terms of reduced ecological fidelity compared to real ecosystems. Given this, it would be good if the paper at some point addresses the questions for which RED would and would not be appropriate.

Response (5):

As suggested, we have now included a discussion of the pros and cons of RED, and the implications for its applications, within the revised Discussion section. We have also explained where more complex approaches (such as ED) are required.

Edit:

“Our previous work in evaluating demographic equilibrium theory for regional forest inventory datasets in North America (Moore et al., 2018) and using RAINFOR sites for South America (Moore et al., 2020), has provided the theoretical basis for the development of RED. In those studies we found that tree-size distributions within observed forests can be satisfactorily understood in terms of demographic equilibrium in the size dimension alone. This is a reduction in complexity compared to other cohort models which are based on patch age, and yet an improvement in ecological fidelity compared to older phenomenological DGVMs such as TRIFFID (Cox, 2001). The modular design of RED allows for easy coupling to land-surface schemes, merely requiring the per unit grid-box total carbon assimilate rate and any additional mortality disturbance rates as inputs for each grid-box (Figure 2). In principle, RED allows scope for more complex tree size-dependent processes, although in this first study we chose to assume size-independent (but spatially varying) mortality rates for each PFT. Our previous work suggests that this is a good first-order assumption (Moore et al., 2018, 2020).”

Edit:

“There are inevitably weaknesses with any particular modelling approach. For RED, a current limitation is for competition to lead to a single PFT at each location within each co-competing vegetation class (i.e. tree, shrub, grass). The PFT with the highest equilibrium fraction will end up excluding sub-dominant PFTs within the same vegetation class. It was necessary for us to account for this eventual competitive exclusion to derive zero-drift steady-states for the global runs presented in Section 3.2.1. Such competitive exclusion is a common problem in DGVMs (Fisher et al., 2018). Currently, RED would not be the most appropriate DGVM to answer important questions regarding the role of biodiversity in ecosystem function (Pavlick et al., 2013; Levine et al., 2016). More sophisticated DGVMs are required to simulate plant diversity, such as individual-based models (Fischer et al., 2016), and DGVMs specifically-designed to capture sub-gridscale patch dynamics (Longo et al., 2019a,b). Adapting our ‘gap’ boundary condition (equation 7) appears to be a promising way to allow greater PFT diversity in RED, without unduly increasing model complexity. We see this as a key priority for future research.”

Reviewer:

Many demographic model development activities, for example, as specifically motivated by a desire to include greater diversity of functional types in ESMs, and to predict their distribution as a function of their plant traits, which in most models primarily impact upon growth. Removing the ability of the model to simulate growth-based competition for light, and indeed, to simulate a diversity of trees within the same class, means that this RED would not be suitable for that problem.

Response (6):

Agreed. The introduction has been rewritten to explain how in RED we choose to trade model complexity for reduced parameter uncertainty. This trade-off seems to be appropriate for the purposes of modelling large-scale forest demography and carbon storage (Moore et al., 2018, 2020), but it is indeed less appropriate for applications related to forest ecology and diversity.

Reviewer:

Further, the introduction suggests that part of the motivation for resolving tree size is to introduce size-dependant physiological processes, but by introducing the metabolic scaling of productivity from an arbitrary reference size to all of the other classes, RED is also unable to simulate how tree size actually affects physiology - e.g. plant hydraulics, light availability, fire damage, allometry (and thus allocation and demand for nutrients in pools of different stoichiometry), size dependant rooting depth (and thus uptake of water and nutrients), burial by snow, etc. Many developments of demographics models are specifically motivated by the representation of size, so again, RED could not be used for those types of question.

Response (7):

RED is a demography model which requires net PFT growth rates and disturbance rates as inputs. In the study presented in this paper, net PFT growth-rates were provided by the JULES land-surface scheme. In principle, details on the tree size distribution can be fed back into JULES (or any other land-surface scheme) to enable size-dependent processes to be included (for example to represent size-dependent drought mortality). We include these possible future developments in our new Discussion section.

Edit:

“RED is currently being coupled to the JULES Land Surface Model, replacing TRIFFID as the default DGVM within that framework. In parallel, significant improvements are being made to the representation of physiological processes in JULES, most notably through the representation of non-structural carbohydrate (‘SUGAR’, Jones et al. (2019)), and through the inclusion of a coupled model of stomatal conductance and hydraulic failure under drought stress (‘SOX’, Eller et al. (2018, 2020)). Plans are also being made to derive the mortality rates for RED from the INFERNO forest-fire model (Burton et al., 2019). These developments will allow us to simulate the effects of size-dependent tree mortality rates within the near future.”

Reviewer:

As a parallel, RED also does not provide discretization of the time-since-disturbance continuum, and instead really divides the grid cell into various PFT tiles, with resolved height, and one ‘gap’ tile, where new seedlings compete for space. Many demographic model developments are motivated by the ability to represent how the development along the successional trajectory impacts physiological boundary conditions. Examples of this include simulating the dominance of N fixers in early succession, of the matrix of post-fire disturbance conditions (including the vertical co-existence of grass and trees), representation of variation in light conditions to capture successional composition shift and the horizontal variation of vegetation height in systems which are buried by snow.

Response (8):

As pointed out above (response 2), this picture of RED is not correct. We have clarified this in the revised model description. The other points concerning the age-dependent (rather than size-dependent) processes are covered in our revised introduction and discus-

sion (see our response 3).

Reviewer:

I am also highly skeptical of the authors claim that mortality rates can be backed out from spatial coverage of a particular PFT. Given that only a single not very convincing validation is presented, I remain far from convinced that this is a reasonable model inversion method. While it might be mathematically plausible, given the myriad simplifying assumptions of the model, I'd like to see how robust the mortality estimates are to variations in the seed production rates and minimum size, as well as assumptions on the spatial arrangement of crowns, and indeed, the uncertainties in the estimates of PFT areal coverage.

Response (9):

As requested, we have carried-out a sensitivity analysis to show how our estimates of mortality-rates depend on the model parameters (α , m_0) along with the ‘observed’ PFT areal coverage and UKESM carbon assimilate input. This is included as a new Appendix C.

Edit:

The diagnosed mortality rates in figure 6 are sensitive to variation in model inputs and parameters. The mortality rate, γ , can be found for the continuous solutions by rearranging the boundary condition equation (6), substituting in Eq.(B2) and Eq.(B13):

$$\gamma = \frac{\alpha P_{eq} a_0}{m_0} \left(\frac{1 - \nu_{eq}}{\nu_{eq}} \right) \left[1 + \frac{1}{2\mu_0} + \frac{1}{8\mu_0^2} \right] \quad (1)$$

The key external inputs to this equation are the observed PFT fraction ν_{eq} and the net assimilate P_{eq} . In addition, our estimates of γ are dependent on the internal model parameters, α and m_0 . The red lines in Figure C1 demonstrate how the estimate of γ depends on these four inputs. The black dashed lines in Figure C1 indicate how uncertainties in each input relate to uncertainties in γ , for ‘true’ values typical of a tree PFT. We estimate uncertainties in the observed PFT fraction (e.g. from remote-sensing) to be $\pm 5\%$, and uncertainties in P (e.g. from JULES) to be $\pm 20\%$, leading to errors of $\pm 17\%$ and $\pm 20\%$ respectively. Likewise, $\pm 20\%$ uncertainties in the internal parameters α and m_0 lead to $\pm 12\%$ and $\pm 20\%$ uncertainties in γ . Combining these sources of uncertainty leads to an overall uncertainty in our inferred estimate of γ of about $\pm 35\%$. "

Reviewer:

Lastly, the paper has some issues with clarity that I have tried to cover in some detail in the following comments. Some of the excessive mathematical details could be moved to the appendix as they rather detract from the flow of the paper. A more informed and nuanced description of how the model fits into existing demographic model literature and of it's strengths and weaknesses would, I think, be more useful for the general readership.

Response (10):

As suggested, we have moved mathematical details concerning carbon conservation to appendix A and the equilibrium state to Appendix B. The pros and cons of RED are

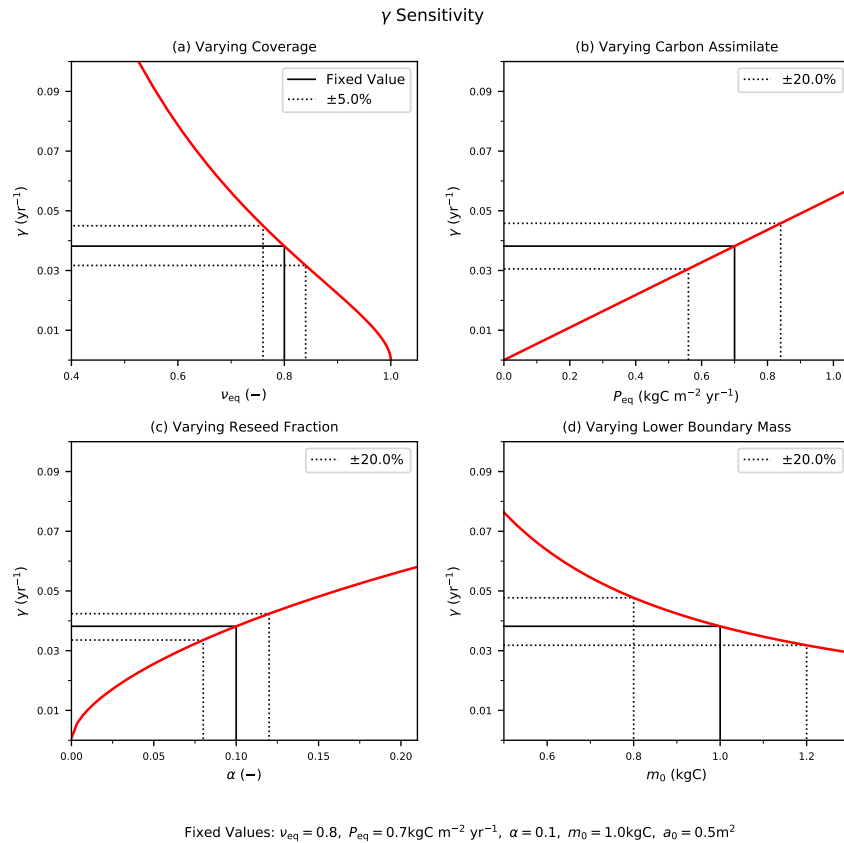


Figure 1: The sensitivity of the mortality rate to assumed input variables: coverage, ν_{eq} (a), and carbon assimilate rate, P_{eq} (b), and model parameters: reseed fraction, α (c) and boundary mass, m_0 (d). The solid black line indicates the fixed values with corresponding $\pm 20\%$ (b,c,d) or $\pm 5\%$ (a) variation (dotted black lines).

discussed in more detail in our revised Discussion section (as outlined above in response 5).

Specific Comments

Reviewer:

P1, L21: The statements in these first three sentences all need references.

Response (11):

Done.

Edit:

“A key requirement of Earth System Science is to estimate how much carbon the land surface will take-up in the decades ahead (Ciais et al., 2014). This is an important component of the total carbon budget consistent with avoiding global warming thresholds, such as 2 C (Schleussner et al., 2016). Unfortunately, projections of future land carbon storage still span a wide-range (Brovkin et al., 2013; Friedlingstein et al., 2014; Arora et al., 2019).

Reviewer:

P2, L7: I'm not sure what to take from this assertion that uncertainty 'can be attributed' to CO2 responses and regrowth. It can also be attributed to a lot of other features of LSMs. Is it really necessary to state this so definitively?

Response (12):

Agreed - we have now removed this phrase.

Reviewer:

P2, L9: You didn't really describe or define what a DGVM is yet.

Response (13):

DGVM now defined at the point of use.

Edit:

"The representation of plant communities within Earth System Models (ESMs) is achieved through the use of Dynamic Global Vegetation Models (DGVMs). DGVMs employ a variety of biophysical, biogeographical and biochemical processes to simulate growth, competition and recruitment of vegetation. The variety in the number and resolution of the processes contributes to the differences found at the Earth System level."

Reviewer:

P2, L15: Here it is indicated that 'processes that are dependant on size' is a core motivation for the implementation of this concept, but RED actually ignores that size of all except the reference tree, using an assumption to scale to the other size classes. There are lots of processes that do actually depend on size (hydraulics, allocation, fire mortality, competition for light, wind damage, snow burial, etc.) and so this is a genuine justification for using a size-structured model, but it does not apply to RED. Therefore, a different justification is required.

Further, in ED-type models, the faster regrowth after disturbance is typically predicted on the use of multiple tree types that exist in early, mid and late successional systems (as opposed to an average, slower growing tree).

Response (14):

Please see our responses to points in (1), (2) and (7) above.

Reviewer:

P2, L21: This is true, but you are also going to get lots of different outcomes of climate change from alternative parameterizations of RED - parameters that are absent from the simpler model are really just assumed to be fixed in RED (e.g. the decay coefficient of productivity with size, seed production, competition parameters). Making the parameters either assumed constants or round numbers doesn't make their uncertainties go away. It would be more interesting to investigate these uncertainties and illustrate a succession experiment under a range of model assumptions.

Response (15):

Previous studies testing RED equilibrium profiles against observed forest demography for north and south America (Moore et al., 2018, 2020), suggest that our simplifying assumptions are sufficient to capture tree size distributions in many locations. However, we agree that it is important to assess the sensitivity of our simulations to the assumed fixed parameters. This is why we have included a new sensitivity analysis in Appendix C, as per (9) above.

Reviewer:

P2, L24: Cohort models are numerically unwieldy and no-doubt more expensive, but as you attest later in the paper, it is disingenuous to state that they make a new patch every timestep when in fact ED-derived models immediately fuse the newest patch to the next largest one.

Response (16):

The algorithm used to ‘fuse’ patches is arguably an arbitrary feature of such models. However, we have toned-down our implied criticism of these alternative approaches in the introduction.

Reviewer:

P2, L26: Cohort models can either track tree age or tree size, so adding this here to distinguish RED from a cohort model doesn't really make sense.

Response (17):

The norm for cohort model is to track both tree age and tree size. As stated within the sentence RED is a “simplified” cohort model, the simplification being not tracking tree size.

Reviewer:

P3, L5: The way in which this equation is presented seems overly contrived. Surely it can be presented such that the dn/dt is the sole term on the left hand side?

Response (18):

We choose to write the equation in this way, because the lhs is essentially the continuity equation for a conserved variable (in this case tree number), while the rhs contains the source and sink terms. This is a standard way to write Fokker-Planck type equations.

Reviewer:

Neither $g(m)$ nor $\lambda(m)$ appear in the actual equation, so this is again a little hard to get ones head around.

Response (19):

The terms g and γ (Rather than λ ?) appear in equation 1. We choose not to write these explicitly as functions of mass (e.g. “ $g(m)$ ”) for clarity. Again, this is standard practice.

Reviewer:

P3, L11: What did Niklas and Spatz find or do, briefly?

Response (20):

We have edited this sentence to include "...consistent with the meta-analysis of field-based measurements by of Niklas and Spatz (2004).."

Reviewer:

P3, L16: I do not understand how the last term translates into fractional area, when it looks like it should just return 'area'. Further, is there no constraint on the area the trees can occupy? That seems strange and needs further discussion.

Response (21):

This term returns fractional area because of the dimensions of " a " (m^2) and " n " (number/kgC/ m^2). Integrating over mass-classes therefore yields a unit of (m^2/m^2).

Reviewer:

P4, L1: I'm not sure why you need to state that the model conserves carbon three times. All vegetation models must conserve carbon. This isn't very surprising.

Response (22):

This subsection describes the discrete equations for RED. The discrete form is now derived in appendix A, using the conservation of mass as a constraint on the net fluxes of plants moving between the mass classes. We now make this clear at the beginning of the subsection.

Edit:

"We wish to produce a model of vegetation demography that can be updated numerically and which explicitly conserves vegetation carbon, providing a constraint on the number of plants moving between mass classes in the discrete form."

Reviewer:

P4, L3-15: I'm not sure what purpose is served by this sequence of equations.

Response (23):

Please see response (22) above.

Reviewer:

P4, L20: This equation would be easier to read if it were split into terms for seed recruitment and growth.

Response (24):

The equation as written shows that seedling recruitment depends on the fraction of net-assimilate which goes into seedling production (α), the net-assimilate (P), and the frac-

tional gap area (s). We have added a sentence below the equation to make this clearer.

Edit:

“Therefore, the rate of recruitment F_0 is the ratio of a fraction of the carbon assimilate allocated to reproduction, αP , and m_0 , multiplied by the gap area s .”

Reviewer:

P4, L23: The PPA assumes minimum overlap of crowns within each layer of the canopy. It distinctly does not assume no overlap of PFTs. It assumes that canopies are arranged into layers and within each layer there is no overlap. Competition for light occurs at the boundary of the layers and is a strong control on ecosystem assembly. In fact, much of RED is highly contradictory to the PPA concept, given the MST rejects the need to different growth parameters as a function of light availability (as demonstrated convincingly for tropical forests by Farrior et al. (2016)). I think it's thus a little disingenuous to cite the PPA here as a justification for this assumption.

Response (25):

Based-on the reviewers' own comments here, it sounds to us like the minimum overlap assumption in RED and PPA are indeed related. However, the potential relationship to PPA is just an aside, so we have removed the reference to PPA here to avoid further concern from the reviewer on this point.

Reviewer:

P4, L25: “injected”? How do trees get injected?

Response (26):

Changed to “recruited”.

Reviewer:

Figure 1: I don't find figure 1 particularly informative. It would be better to have a depiction of the actual area available for seeds and to illustrate how the different PFTs might affect the allocation to each PFT. This figure just tells me that shrubs are smaller than trees.

Response (27):

Others who have seen this diagram have found it useful, so we have retained it despite the reviewer's opinion on this point.

Reviewer:

P5, L4: The calculation of the area occupied by each PFT, as it is introduced here, needs a lot more explanation. In the description on L16 of P3, it simply states that the area of all the mass classes is added together, such that there is no overlap between the canopies of the trees in each plant type. This implicitly assumes that all the trees are in the ‘canopy’ layer, (using PPA terminology) and thus by implication that they should all get the same amount of light. Of course, via use of equation 2, the actual light environment of the plants

is divorced from assumptions about their spatial arrangement, but it seems like a strong assumption to me to include no possibility of additional canopy layers. What happens when the total amount of space occupied by the plants exceeds the ground area available?

Response (28):

Our gap boundary condition given by equation 12 ensures that there are no steady-state solutions where the total vegetated fraction exceeds one. We have added a sentence to clarify this point.

Edit:

“This ‘gap’ boundary condition results in there being no equilibrium solution where the amount of coverage exceeds 1. Doing so would halt the recruitment flux such that mortality processes would bring the fractional coverage back below unity.”

Reviewer:

P5, L5: It should be noted here that the Cox 2001 paper is at-least inspired by the Lotka-Volterra approach, to better allow connection of this concept to community ecology literature.

Response (29):

Agreed. Rewritten as “..this is a similar competition regime to the Lotka-inspired TRIF-FID model..”

Reviewer:

P5, L7: Later on you state that the coexistence between PFTs of the same type doesn't actually work, so this statement that Eqn 12 allows for coexistence is a little misleading.

Response (30):

Here we mean by “inter-functional group” we mean tree-shrub-grasses. We make that clearer in a revised sentence.

Edit:

“...allows for the co-existence between inter-functional groups (trees, shrubs and grasses) of PFTs. For instance, a PFT such as Broadleaf Deciduous Tree can co-exist with a Deciduous Shrub and C3 Grass.”

Reviewer:

P5, L8: This allows succession as you note, but only between the PFT of different classes, not within a given class, unless I'm mistaken? . Figure 3: I'm not really sure what this Figure is supposed to illustrate. What are the red dotted lines in the middle of the triangle? There are three heavy double headed black arrows and not one (as implied by the legend).

Response (31):

Figure 3 shows that the RED equilibrium state can be determined using observed areal cover plus either growth or mortality rate. [We have removed this figure.](#)

Reviewer:

Eq 28 and 29: These equations need a bit more explanation and description. This section feels like you are making a concerted effort to lose readers. Is it really necessary that everyone understands how the equilibrium solution of the model is derived? Could this go in an appendix?

Response (32):

Equation 28 is important in the derivation of the analytical equilibrium. We have now moved the derivation into the description (Appendix B2) and have included more explanation on the mathematical expressions:

Edit:

To solve for the discrete model equilibrium, we start from the flow equation from Eq.(4) with the term $\partial N/\partial t \rightarrow 0$:

$$\gamma N_i + F_i = F_{i-1} \quad (2)$$

considering the population flux - equation (5), we find N_i in relation to the lower mass class, N_{i-1} :

$$N_i = N_{i-1} \left[\frac{g_{i-1}/(m_i - m_{i-1})}{g_i/(m_{i+1} - m_i) + \gamma} \right] = N_{i-1} \lambda_i \quad (3)$$

(Further down in appendix B2)

An expression for the total stand density at equilibrium, N_{eq} , can be derived. Using equation (B.18), we can represent any population of mass class i in terms of the lowest mass class N_0 :

$$N_i = N_0 \prod_{j=1}^i \lambda_j \quad (4)$$

Therefore, when finding the total number of stands relative to N_0 we get:

$$N_{eq} = N_0 \left[1 + \sum_{i=1}^I \prod_{j=1}^i \lambda_j \right] = N_0 X_N \quad (5)$$

where X_N describes the sum of the all mass classes as a proportion of N_0 .

(Further down in appendix B2)

We can repeat the same process for coverage:

$$\nu_i = N_0 a_i \prod_{j=1}^i \lambda_j \quad (6)$$

and using allometric relationship (equation 3):

$$\nu_i = N_0 a_0 \left(\frac{m_i}{m_0} \right)^{\phi_a} \prod_{j=1}^i \lambda_j \quad (7)$$

This gives the total coverage, ν_{eq} as:

$$\nu_{eq} = N_0 a_0 \left[1 + \sum_{i=1}^I \left(\frac{m_i}{m_0} \right)^{\phi_a} \prod_{j=1}^i \lambda_j \right] = N_0 a_0 X_\nu \quad (8)$$

Reviewer:

P10, L1: As I said above, I am highly skeptical that this is a robust way of estimating turnover, given the uncertainties to do with seed production and spatial extent.

Response (33):

As response (9) and (15) states, we have conducted a sensitivity analysis for the RED equilibrium mortality within the new appendix C.

Reviewer:

P10, L8: So, productivity was derived from JULES using TRIFFID? Were the outputs saved for each month? Is there interannual variability? This needs a bit more detail.

Response (34):

We have appended more detail around the UKESM input:

Edit:

“The UKESM simulation provides NPP and local litterfall per unit area of each PFT. We multiply by PFT fraction to get the grid-box mean values required to drive RED (using ESA landcover data, as explained below).”

Reviewer:

P11, L3: Is this really how succession works in Amazonian forests? I think it's really mostly trees that are present in the formation of small to medium sized gaps.

Response (35):

In typical succession you see the establishment of faster-growing PFTs (C3, Esh), but ultimately slower-growing trees often dominate. We see this sort of successional dynamics in RED transient simulations, as shown in Figure 4 (now Figure 10).

Reviewer:

P11, L5: Can you illustrate the dependence on alpha and m_0 ?

Response (36):

See responses (9), (15) and (33). This is now done in appendix C.

Reviewer:

P12, L11: What are we to take from this illustration of ‘succession’ in the model? There isn’t any comparison with data, nor an illustration that the model fixes the issue of slow recovery from disturbance that was raised in the introduction. What controls the area fractions of the smaller PFTs? Is there always some gap fraction dedicated to them? How is this equilibrium maintained?

Response (37):

Data on forest regrowth is unfortunately difficult to find. However, this successional sequence is broadly consistent with ecological understanding and other DGVMs. We show it here to demonstrate the dynamical nature of the model. Sub-dominant PFTs occupy space left by dominant PFTs (as determined by our gap lower boundary condition - equation 12). For all PFTs the equilibrium is maintained as a balance between mortality and seedling recruitment (which is dependent on net growth-rate and competition through equation 11). We have added text below Figure 4 (now Figure 10) to clarify.

Appended onto the bottom of the caption on Figure 10:

“The ultimate steady-state is determined by the balance between recruitment and mortality (equation (6)). Intra- and inter-PFT occurs here through the shading of seedlings, which implies that just a fraction of the gridbox (s, ‘space’ or ‘gap’ fraction) is available to grow seedlings (equation (7)).”

Reviewer:

Figure 6: The inputs of productivity taken from JULES do not, for example, allow BETs to grow outside of the tropics, and so many of the critical questions related to the prediction of biome boundaries that are asked of DGVMs cannot be addressed in this circular analysis.

Response (38):

In fact JULES does allow BET to grow outside of the tropics. We have revised the colour scale of Figure 6 (now 5) to make this clearer. However, we also sense that the reviewer is under a false impression about the nature of RED. RED is a model of forest demography that is driven by net growth-rates and mortality rates that can come from land-surface models or observations. In this study we have driven RED with fluxes from the JULES land-surface scheme, but the current paper is not about JULES or even JULES-RED. We clarify this point in the model introduction (as per response 34).

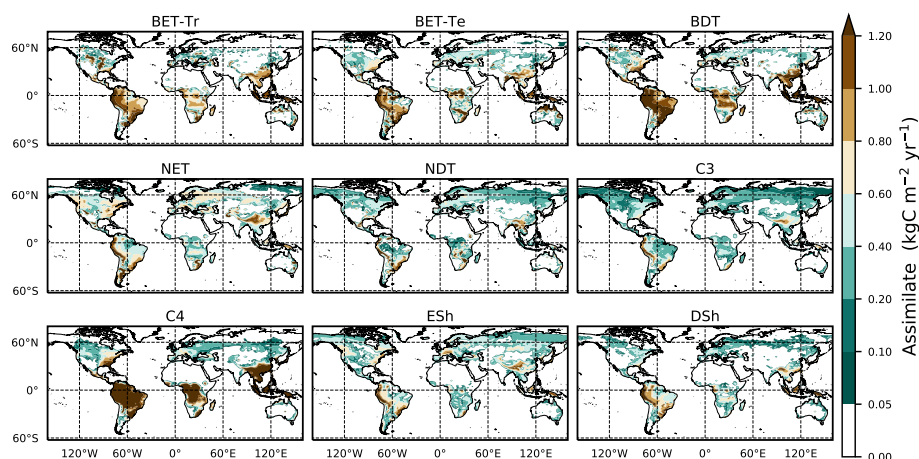


Figure 2: Mean net assimilate P assimilate (equation (8)) from UKESM between 2000-2010. The mean is constructed by setting any negative growth rates to zero.

Reviewer:

P14, L1: It seems that reproducing the PFT map should be a trivial matter

given the productivity inputs illustrated in Figure 6.

Response (39):

We are simply performing a model inversion to analytically solve for the RED dynamical steady-state. We have not seen this approach from another stand-alone DGVM.

Reviewer:

P 16 L8 This is confusing because the reference to Figure 10 comes before it is described. The use of the mortality rates in these simulations is not described in this section until now.

Response (40):

We have moved the mortality section so that it is now before the global dynamical plot.

Reviewer:

P17, L1: To what does this ‘diagnosed mortality rates’ refer? Isn’t this sentence about diagnosing mortality rates? This adds another layer of confusion onto my previous comment.

Response (41):

We can see how this might be confusing. Therefore, we have rearranged the sections to be more clearer ([Modelling setup](#) → [Equilibrium mortality rates](#) → [Local simulation](#) → [Global simulations](#)).

Reviewer:

Figure 9: This color map does not allow one to distinguish between most of the lower turnover areas. You need some sort of logarithmic variation in color with mortality rate.

Response (42):

As suggested, we have now used a logarithmic color map in Figure 9.

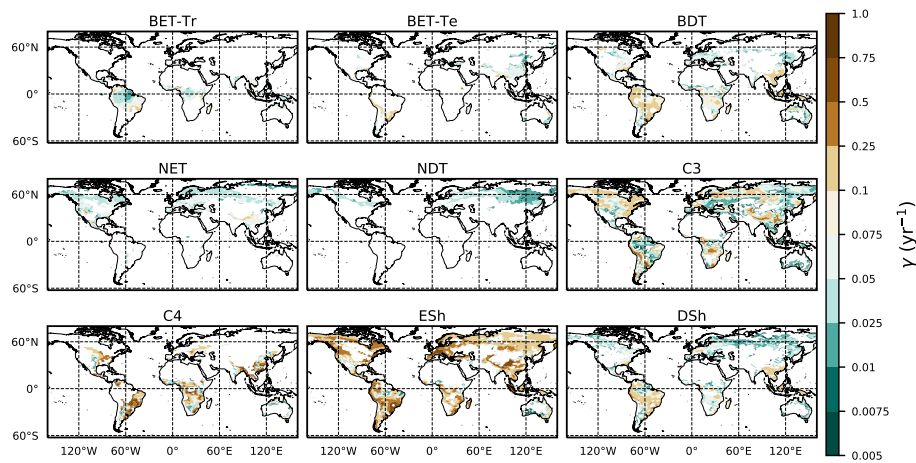


Figure 3: Diagnosed maps of mortality rates γ for each PFT, as required for consistency with the ESA observations and the UKESM growth rates. White areas correspond with zero coverage and/or zero growth.

Reviewer:

Referee: P17, L8: How influential is the minimum recruit size? This needs to be illustrated.

Response (43):

As stated in (9), (15), (33) and (36) we have carried out a sensitivity analysis in appendix C which includes the sensitivity to m_0 .

Reviewer:

P17, L10: The sentence that begins “Under the assumption” isn’t a whole sentence. Moreover, what is the aim of defining a ‘healthy’ environment? You need to state what you are trying to achieve first. . .

Response (44):

We have rewritten this statement for clarity. The use of ‘healthy’ is indeed rather vague – so we have clarified this to ‘dominant’.

Reviewer:

P17, L12: This is a very quick and potentially confusing switch to discussing the growth is as this mortality ratio and not mortality (you should maybe also re-state what is (μ_0 ??) a non-standard quantity.

Response (45):

We think reviewer means μ_0 (there appears to be an error in the reviewer document)? We have defined μ_0 before this sentence (within the steady state section). μ_0 is the ratio of mortality to growth-rate ($m_0\gamma/g_0$).

Reviewer:

P17, L13: This number seems extraordinarily high for the stem turnover rate of tropical forests? Comparison with data is, of course, where this aggrega-

tion idea is problematic, as mortality rates have clearly been shown to vary with tree size (Lines et al., 2010; Johnson et al., 2018), and thus the range of tree size with which one can compare these rates is unclear, particularly the lower size boundary.

Response (46):

The reviewer appears to be confusing μ_0 with γ , we therefore have clarified μ_0 as per response(45). The sensitivity of the lowest boundary and the derived γ see the sensitivity analysis with m_0 , (as with previous responses (9), (15), (33) and (36)) see appendix C. Assumptions of size independence of mortality has provided credible fits of size structure of the entire US forest inventory database (Moore et al., 2018) and plots across the tropics (Muller-Landau et al., 2006b; Lima et al., 2016; Moore et al., 2020). Interestingly, within Johnson et al. (2018) (Supplementary Figure 10), the plots have a similar mortality distribution within our papers analysis .

Reviewer:

P17, L13: Table 3 contains goodness of fit metrics, and not estimates of mortality.

Response (47):

A simple typo – we should have referenced Table 4 here. Now corrected.

Reviewer:

P17, L15: The ‘value within the paper’ doesn’t state which paper, nor why it needs converting. Thus is very confusing.

Response (48):

We have made this clearer.

Reviewer:

Referee: P18, L1: This text on the differences between the Moore paper value and this value (which are indeed extraordinarily close and probably don’t need excusing) would be better spent describing first how the Moore method differs from RED. This section assumes the reader is familiar with, for example, the non-discretized nature of the Moore method.

Response (49):

We have outlined the non-discretized form within Appendix B, which we now refer to and have added text to explain the relationship to the Moore et al. (2020) paper.

Reviewer:

P18, L5: “Potentially providing a future constraint on ESM growth rates for PFTs.” is not a whole sentence.

Response (50):

We have removed this sentence.

Reviewer:

Figure 10: The mortality numbers in figure 10 for tropical forests seem too high. (0.07- 0.08). Again, it's hard to know what mortality rates they can be compared to. In Table 4, the numbers are different from the figure, perhaps because they are area weighted, but this isn't really clear from the text.

Response (51):

This is because of a difference of sampling - “non-zero” grid-box fractions (figure 10) versus top quartile grid-boxes . We now use the same subset for all grid-boxes to calculate the mortality rates in figure 10 (now figure 7) (the top quartile of non-zero grid-box fractions) and make it more obvious what we are doing.

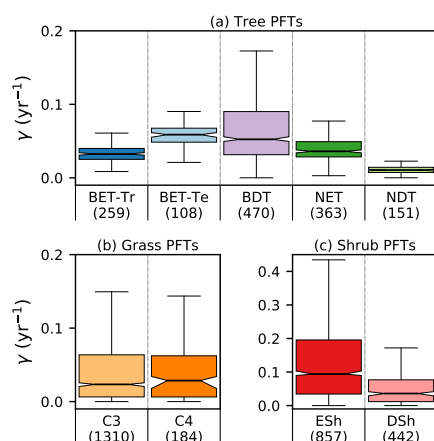


Figure 4: Diagnosed mortality rates for (a) trees, (b) grasses and (c) shrubs in the top quartile of coverage. Notches within the box represent the confidence bounds of the median. The confidence bounds are estimated using a bootstrap method. Bracketed numbers represent the number of grid-points.

Reviewer:

P18, L11: I'm not sure what “within the top 25% of coverages” means, nor what this is trying to achieve. Further, there is no data in figure 10, so I am not sure why one is supposed to conclude that the model captures the data well. Maybe you actually mean figure 11, which reduces the RED estimate, but only down to about double the observations. Given the a doubled mortality rate is approximately equal to a halved biomass, I'm not sure that this provides a very convincing validation. Further, many estimates of mortality are lower than this. Lewis et al. (2004) find mortality rates of tropical forest from 1.5-1.7%, for example.

Response (52):

There are a few things the reviewer raises here – the seemingly arbitrary “top 25%” of coverage and the fitted mortality rates being too high. Firstly, we picked this threshold to identify areas where PFTs have greater coverage – and therefore mortality rates hypothetically closer to an undisturbed baseline. We have included a sensitivity analysis in Appendix C of how the diagnosed mortality rates depend on other model parameters (as stated in our previous responses (9), (15), (32), (34) and (40).

Reviewer:

P20, L4: I could not find a definition of DET prior to this usage here.

Response (53):

We now refer to appendix B and have stated the definition of DET in the introduction.

Edit:

“ This paper presents a simplified cohort model (*Robust Ecosystem Demography (RED)*) which updates the number of trees in each mass class, but does not separately track tree-age or patch-age. RED assumes that the tree size-distribution of a forest is determined by how the rates of tree growth and mortality vary with tree size (Kohyama et al., 2003; Coomes et al., 2003; Muller-Landau et al., 2006b; Lima et al., 2016). We follow many other studies in assuming that tree-growth rates vary with the three-quarter power of tree mass ($m^{3/4}$), as suggested by metabolic scaling theory (West et al., 1997). Where tree mortality rate can also be assumed to be approximately independent of tree mass, the demographic equation yields equilibrium tree-size distributions which follow a Weibull distribution. This is sometimes termed *Demographic Equilibrium Theory (DET)* (see Appendix B). These simplifications significantly reduce the number of free parameters in RED, but still enable it to fit forest inventory data in North America (Moore et al., 2018) and South America (Moore et al., 2020). ”

Reviewer:

P22, L1-10: I'm not sure what to take from this section about fire. The last line seems to suggest that RED overestimates fire mortality, when figures 12 and 13 seem to show the opposite. The logic of this section needs tightening.

Response (54):

The purpose this section is to investigate if we see a raised mortality rate in regard to areas with fire disturbance and land-use. We have now changed figure 12 (now figure 9) and removed figure 13 to indicate this more clearly and rewritten the paragraph:

Edit:

There is a need to better understand the influence of mortality arising from disturbance events such as droughts and fire in order to constrain model projections (Pugh et al., 2020). Here we investigate if the equilibrium mortality rates implicitly capture areas of disturbances, by comparing the mean tree mortality rate to fire and land-use surveys (the mean mortality is defined here by weighting grid-box γ values by grid-box fractional coverages). There are a number of surveys relating stand mortality in regions prone to wildfires (Swaine, 1992; Kinnaird and O'Brien, 1998; Peterson and Reich, 2001; Van Nieuwstadt and Sheil, 2005; Prior et al., 2009; Staver et al., 2009; Brando et al., 2014). In a broad sense, post-fire mortality rates can range from 0.06 yr^{-1} to catastrophic rates around 0.8 yr^{-1} and can vary quite considerably depending on tree species, fire frequency and drought severity. The drought-fire interaction is responsible for significantly increasing mortality post-fire and can be a driving cause of regional die-back (Allen et al., 2010; Brando et al., 2014). Using the ESA FIRE_CCI dataset (Chuvieco et al., 2019) we can estimate the burnt vegetation fraction per year. Taking the average burnt vegetation fraction for the months between 2000 and

2010, and converting into annual burn rate we gain an estimate of fire severity.

Another key issue is anthropogenic land-use and land-use change (Nepstad et al., 2008; Haddad et al., 2015). Fragmentation of natural forests is understood to raise the mortality of the remaining forest and to decrease the overall resilience of the ecosystem (Esseen, 1994; Laurance et al., 1998; Jönsson et al., 2007). In order to maintain a near-constant agricultural fraction, regular disruption such as grazing is needed to prevent re-colonisation and secondary succession (Dorrough and Moxham, 2005; Van Uytvanck et al., 2008; Chaturvedi et al., 2012). We carry out a comparison with land-use using the 2000 ESA LC_CCI inferred crop coverages (Li et al., 2019).

In Figure 9, we see the derived observations for burn area (a) and crop fraction (b), along with the derived mean γ for the tree PFTs (c). From Figure 9 (d), we see that there are areas of large mortality ($\gamma > 0.075 \text{ yr}^{-1}$) that do correspond to areas where we see large fire activity (burn rate $> 0.1 \text{ yr}^{-1}$) and increased crop fraction (> 0.25). However, large burn rates are seen to overlap in parts of central Brazil around the Cerrado region, Southern Africa and North Western Australia where fires are understood to play a significant part within the ecosystem (Coutinho, 1990; Medeiros and Miranda, 2008; Prior et al., 2009; Staver et al., 2009). There are also some areas of agriculture which correspond to deforestation, such as in the Atlantic forests of Brazil and in Indonesia (Higuchi et al., 2008; Curran et al., 2004). Areas of increased disturbances result in grasses and shrubs dominating (Figure 3).

Analysis of the RED equilibrium is an indirect approach to estimating tree mortality based on simple yet mechanistic principles of demography, and relying on few inputs (vegetation cover and assimilate). It is however conditional on the assumed estimates of vegetation coverage and net rates of assimilation.

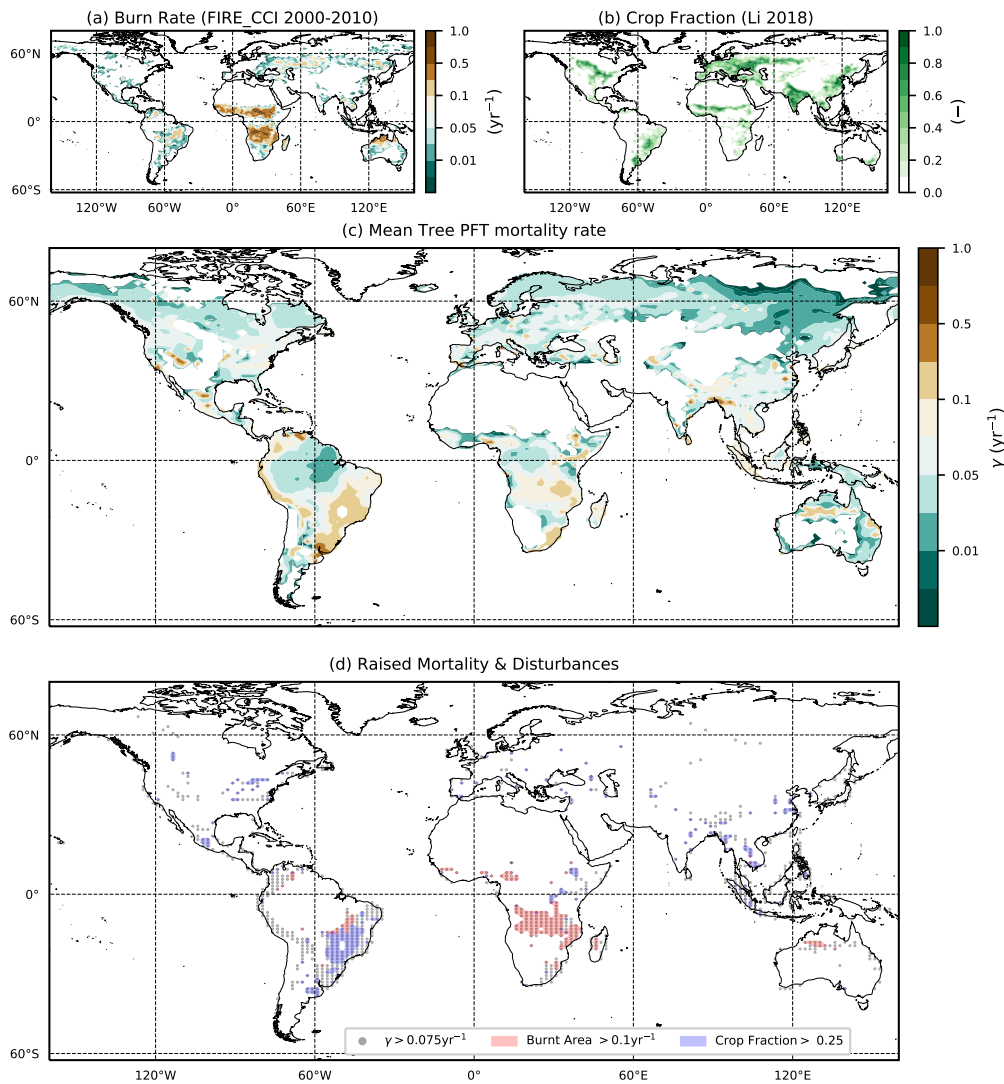


Figure 5: Comparison of diagnosed mortality rates, with observation-based maps of fire and land-use. (a) annual burnt area fraction from the ESA FIRE_CCI dataset; (b) crop fraction from the ESA LC_CCI 2000 dataset; (c) diagnosed mortality rate γ for the tree PFTs (BET-Tr, BET-Te, BDT, NET, NDT); (d) overlap of areas of higher tree mortality rates ($\gamma > 0.075 \text{ yr}^{-1}$) with areas of fire (Burnt Area $> 0.1 \text{ yr}^{-1}$) and agriculture (Crop Fraction $\geq 30\%$).

Reviewer:

P23, L1-6: This, and the paragraph above, are in need of more references.

Response (55):

As per the response above (54), we have now included more references.

Reviewer:

P23, L6: This statement about patch merging is incorrect in its assertion that patches can only be merged after a certain age in ED-type models. Further, it does not illustrate that this is actually problematic, and simply asserts as

such. Fusion criteria are indeed to some extent arbitrary, but that this is a genuine problem has not actually been demonstrated.

Response (56):

We have now removed the statement. As stated previously (response (5)), we have now sought to discuss both the pros and cons of RED relative to other DGVMs.

Reviewer:

P23, L7: Which important features is it designed to capture exactly? This hasn't really been stated.

Response (57):

We have now more clearly stated the important features of second-generation DGVMs within our updated introduction and discussion sections (as stated in response (5)).

Reviewer:

P23, L16: Metabolic scaling theory has been widely debunked by numerous studies comparing its predictions with observations (Muller-Landau et al., 2006a; Russo et al., 2007; Coomes et al., 2011; Rüger and Condit, 2012) in particular where asymmetric competition for light (e.g. in forests) is important.

Response (58):

The reviewer is perhaps confusing metabolic scaling theory for tree growth-rate as a function of tree mass ($g \propto m^{3/4}$), with an extension of metabolic scaling-theory to simulate forest demography (Brown et al., 2004). Observed tree-size distributions do not seem to be consistent with the latter, but do seem consistent with the former, as discussed in Moore et al. (2020). We have revised the introduction to clarify (response 53).

Reviewer:

P23, L18: I am not sure how the seed model allows you to capture the effects of light competition. It allows you to represent the impacts of recruitment competition, but seems to me that it explicit does not include light competition.

Response (59):

Agreed that we do not explicitly represent light competition. We have now removed this statement for the sake of clarity.

Reviewer:

P24, L1: It is stated here that equation 12 is a promising method to deal with the problems of coexistence in RED, but equation 12 is already part of RED, thus how can it be the solution? Further, I do not know what 'gap boundary conditions' refers to here.

Response (60):

Co-existence can be achieved by having competition coefficients less than 1. This model paper is RED version 1, there is always scope for future improvements to the model in

this topic.

Reviewer:

P24, L4: I am skeptical, without further much more robust testing and illustration, that these relationships would be meaningful.

Response (61):

Noted. We hope that future work involving closed-form DET and RED will help provide some illustration. See our responses concerning the sensitivity of this method for determining γ .

Reviewer:

P24, L13: I do not think that this model is 'based on' the ideas of the PPA in any meaningful way. The idea of the PPA is primarily concerned with how trees fill space, which is specifically ignored by RED, and also on the division of the canopy into discrete layers, which is definitively at-odds with the metabolic scaling method of disaggregating production solely based on tree size.

Response (62):

As per response (4) and (25) we have now edited and removed the specific mentions of PPA from the manuscript.

Reviewer:

P24, L16: It apparently can be fitted, but I'd argue that there has been no validation presented to show that this is 'effective'.

Response (63):

We have also tested for robustness in our new appendix C. (see also response to points (9), (15), (33), (36), (43) and (52)).

Response to Reviewer 2:

Robust Ecosystem Demography (RED): a parsimonious approach to modelling vegetation dynamics in Earth System Models

Arthur P. K. Argles, Jonathan R. Moore, and Peter M. Cox on behalf of co-authors. (*on behalf of the co-authors*)

22nd April 2020

The referee was mainly concerned with specific detail, they did raise other points but mainly found that the paper was a bit confusing. We address each of the queries raised below. The relevant reviewer comments are written in italics below followed by our responses in plain font, changes are detailed in blue font.

Reviewer:

The authors present a model development work on vegetation demography, and seek to incorporate it into an earth system model. The framework provides a simplified solution to model the global vegetation distribution based on the “Metabolic Scaling theory”. Both the topic and the model concept are very interesting. However, there are numerous errors and ambiguous expressions throughout the current manuscript. The model descriptions are not clear enough, especially for the equations and units. At some points, I have to stop to calculate the units of each term. I’m also not fully convinced by the model outputs and validations. Extra information are necessary to be provided for a proper judgement, e.g., how the NPP data was created, which climate forcing and vegetation map were used. I suggest an overall revision and reorganization of the manuscript. My major question about this approach is how it can be used in transit-time simulations, especially for the future projections. From a modelling aspect, the model simply ignored many factors that can be modified due to climate change. Nevertheless, it would be very exciting if enough evidences support that some important emergent properties from land ecosystems would remain constant in a fast changing world.

Response (1):

We thank the reviewer for their comments and have sought to make edits that make the model paper clearer and help clarify definitions. On the point of the NPP data, we ran RED offline using outputs from the UKESM climate model. UKESM calculates phenology and litter fluxes using climatic data per area of each PFT (rather than per gridbox). We have elaborate further within the discussion on how RED can be used in transient simulations of future climate simulations. RED was built to be parameter sparse to reduce uncertainty at the global level. As seen from the results within the paper it is possible to capture regional vegetation accurately even within such a parasimonious model.

Edit:

“RED is currently being coupled to the JULES Land Surface Model, replacing TRIFFID as the default DGVM within that framework. In parallel, significant improvements are being made to the representation of physiological processes in JULES, most notably through the representation

of non-structural carbohydrate ('SUGAR', Jones et al. (2019)), and through the inclusion of a coupled model of stomatal conductance and hydraulic failure under drought stress ('SOX', Eller et al. (2018, 2020)). Plans are also being made to derive the mortality rates for RED from the INFERNO forest-fire model (Burton et al., 2019). These developments will allow us to simulate the effects of size-dependent tree mortality rates within the near future."

Specific Comments

Reviewer:

P1 Abstract

L7: cohort-based models?

Response (2):

We further elaborate on this term within the abstract.

Edit:

"More advanced cohort-based patch models are now becoming established in the latest DGVMs. These models typically attempt to simulate the size-distribution of trees as a function of both tree-size (mass or trunk diameter) and age (time since disturbance)."

Reviewer:

..L8:These models

Response (3):

Corrected "These typically..." to "These models typically...".

Reviewer:

..L14:I feel it should not be the major reason to argue that RED would be a great contribution. Only mentioning the computing cost is not convincing enough.

Response (4):

We agree that this is not the definitive reason for the development of RED. Indeed the development of RED is driven by the need to have a robust and parameter sparse model of forest demography for global applicationslaw of parsimony. We therefore state that the additional problem arising from the balance of representation of ecological processes versus the number of uncertain parameters.

Edit:

"This approach can capture the overall impact of stochastic disturbance events on the forest structure and biomass, but at the cost of increasing the number of parameters and ambiguity when updating the probability density function (pdf) in two-dimensions."

Reviewer:
..L15:pdf?

Response (5):

We have appended “(pdf)” to the initial mention of “probability density function...” in the sentence beforehand.

Reviewer:
..L19:solvable?

Response (6):

Corrected typo.

Reviewer:
..L26:Why only compared to this dataset

Response (7):

We compare to this dataset partly because this dataset is classified using the same PFTs used within the UKESM.

Reviewer:
..L41:2K? not clear enough, references needed

Response (8):

We have added in a reference to the Paris Agreement and changed the units to degree centigrade.

Edit:

“This is an important component of the total carbon budget consistent with avoiding global warming thresholds, such as 2°C (Schleussner et al., 2016).”

Reviewer:
..L47:keep update with the new results?

Response (9):

We have now removed the reference to the GCB (Global Carbon Budget) results to streamline the introduction.

Reviewer:
..L44-51: The logic here is unclear. I assume that the authors want to stress the large uncertainties in modeling land C budget. But the topic of the study is model development, rather than uncertainty analysis. So I suggest to use 1-2 sentences to describe the uncertainty topic and go to the model development faster.

Response (10):

We agree that the motivation for including land C budget could be more concise. Uncertainty arising from the representation and parameterisation of processes is part of the motivation for RED. We have also included more discussion of other published models (see response 36).

Reviewer:

..L53: According to my knowledge, LUC prediction is from another sector, which is not from DGVM. Provide the LUC examples here seems irrelevant to the modeling of this study. Also, why the authors only picked examples from RCP8.5.

Response (11):

Agreed. Therefore, we only mention it in passing;

Edit:

“Beyond the fertilisation effect and land-use change, significant uncertainty arises from the representation of vegetation demographics such as recruitment, competition and mortality (Brovkin et al., 2013; Ahlström et al., 2015).”

Reviewer:

P2

..Line 2: Rewrite the sentence and focus on the topic of this study. Generally, DGVM includes biochemical, biogeographical, biophysical processes and other factors influencing vegetation.

Response (12):

We have changed the sentence to be more encompassing of what a DGVM includes.

Edit:

“The representation of plant communities within Earth System Models (ESMs) is achieved through the use of Dynamic Global Vegetation Models (DGVMs). DGVMs employ a variety of biophysical, biogeographical and biochemical processes to simulate growth, competition and recruitment of vegetation. The variety in the number and resolution of the processes contributes to the differences found at the Earth System level.”

Reviewer:

..Line 5: How to define complex. What about the other “complex” models.

Response (13):

We have clarified this as “individual based models”.

Reviewer:

..Line 10: Why non-individual based models cannot do that?

Response (14):

Valid point, we now have redefined this as:

Edit:

“In the second-instance, individual based models can explicitly represent a multitude of biological and ecosystem processes at a individual plant level (Smith, 2001; Sato et al., 2007).”

Reviewer:

..Line 13: What is top-down models? Area based?

Response (15):

Yes, we think of top-down models as phenomenological models such as Lotka-Volterra. We clarify this point in the introduction.

Edit:

“DGVMs range from the simplistic, older, top-down approaches to that of complex individual-based DGVMs. For example, in the first instance the TRIFFID model (Cox, 2001) simulates the fractional area of each Plant Functional Type (PFT) using phenomenological Lotka-Volterra equations.”

Reviewer:

..Line 15: are significantly simpler and more computationally efficient(reference?).

Response (16):

We have edited the paragraph in the model description removing this statement.

Reviewer:

Line 17: over-estimated(reference?)

Response (17):

We have now provided a reference: (Burton et al., 2019).

Reviewer:

..Line 34: The previous paragraph only explain one benefit of RED: reduce computational cost. To me, it is at least not the major reason for the RED development. I feel it is necessary to mention the theoretical foundations for RED development, e.g., the scaling theory. Although this study is mainly about model development, the explanation of the underlying mechanisms is necessary to facilitate the understanding of the model concept.

Response (18):

A valid point. We have now stated the theoretical foundations of metabolic scaling theory. Added onto the last description of the introduction:

Edit:

“This paper presents a simplified cohort model (*Robust Ecosystem Demography (RED)*) which updates the number of trees in each mass class, but does not separately track tree-age or patch-age. RED assumes that the tree size-distribution of a forest is determined by how the rates of tree growth and mortality vary with tree size (Kohyama et al., 2003; Coomes et al., 2003; Muller-Landau et al., 2006b; Lima et al., 2016). We follow many other studies in assuming that tree-growth rates vary with the three-quarter power of tree mass ($m^{3/4}$), as suggested by metabolic scaling theory (West et al., 1997). Where tree mortality rate can also be assumed to be approximately independent of tree mass, the demographic equation yields equilibrium tree-size distributions which follow a Weibull distribution. This is sometimes termed *Demographic Equilibrium Theory (DET)* (see Appendix B). These simplifications significantly reduce the number of free parameters in RED, but still enable it to fit forest inventory data in North America (Moore et al., 2018) and South America (Moore et al., 2020).”

Reviewer:

Description of the model: Overall, the equations should be carefully checked, and the units need to be added in an appropriate way.

Response (19):

The units and equations have been thoroughly checked for this study and other related papers (Moore et al., 2018, 2020). We have now moved the table of variables, definitions and units from appendix A to sit directly under the model description section.

Reviewer:

..Line 47-49: Check the symbol consistency between equ.1 and the corresponding descriptions. I suppose the equation has been simplified – it is assumed that gamma is independent from mass level already.

Response (20):

Edited for consistency.

Reviewer:

..Line 50: Any form of what?

Response (21):

Edited to say: “of relationship with size”.

Reviewer:

..Line 53: follows a power..

Response (22):

Corrected.

Reviewer:

..Line 59: Correct the reference format

Response (23):

Corrected.

Reviewer:

..Line 70: Is that a basic requirement to build a vegetation model?

Response (24):

Yes - in the context of the carbon cycle and Earth System Modelling.

Reviewer:

..Line 86: keep unit unified throughout the MS. why using per plant per unit area previously but using explicit unit here?

Response (25):

We now declare all model variables, descriptions and units in table 1.

Reviewer:

..Line 88: why it is a concern? To keep mass and energy balance is basic to develop a model.

Response (26):

We re-phrased this statement and have moved the discrete derivation into the appendix.

Reviewer:

..Line 66 the area term "a" does not appear before.

Response (27):

The mean crown area "a" - is defined in the previous paragraph.

Reviewer:

P3:

..Line 8: P has been defined before. Again, units miss

Response (28):

We have now added units in table 1.

Reviewer:

..Line 17: This part is mainly derived from PPA and TRIFFID, or new for RED? If it is former, I suggest to provide main equations and introduce them briefly.

Response (29):

These equations are developed for use in RED. We have removed the reference to PPA in response to other reviewer comments.

Reviewer:

P4:..Line 1: I'm concerned about the "coupling" here. Based on the description, I feel RED has not been coupled with the ESM. Using prescribed NPP means an implicit vegetation distribution in itself. From equ.16, higher NPP would mean higher baseline growth-rate.

Response (30):

RED was run offline using NPP and litter outputs from a UKESM run, there is no coupling. The UKESM runs were in terms of PFT area instead of grid-box area, therefore multiplying by coverage circumvents this issue. We have now clarified this point in the section 3.1:

Edit:

"The UKESM simulation provides NPP and local litterfall per unit area of each PFT. We multiply by PFT fraction to get the grid-box mean values required to drive RED (using ESA landcover data, as explained below)."

Reviewer:

..Line 53-54: What is the loss of vegetation C due to plants growing beyond the modelled mass classes

Response (31):

The truncated growth $g_I N_I$ as seen within the demographic litter equation. However, this term is negligibly small because we resolve a large mass class range that is very unlikely to be exceeded.

Reviewer:

P7:

For the first paragraph of "Modelling results", Should it be part of the method section?

Response (32):

No we don't think so. This paragraph is part of the explicit set-up rather than then the method and helps the results section have improved 'flow'.

Reviewer:

..Line 1: What tests?

Response (33):

Response: Changed "tests" to "run".

Reviewer:

..Line 2: Again, I'm concerned about the use of prescribed NPP. How you get NPP? Using which climate forcing? What period of NPP you used. And most importantly, how the NPP data from JULES defines the vegetation distribution? A predefined data or from a model? All the info needs to be added for a proper judgement. If fed a similar pattern from the data: ESA LC CCI

to RED, then it is not surprising that they would have the similar output as showed in Figure 7.

Response (34):

For the sake of clarity, we now state that the UKESM data is defined by unit of vegetation area rather than grid-box and include about the timescale of the dataset. We already state that this is a model inversion and is therefore essentially tuning the mortality rate within RED to fit the data.

Edit:

“The UKESM simulation ran on a yearly time-step, and provides NPP and local litterfall per unit PFT. We multiply by PFT fraction to get the grid-box mean values required to drive RED (using ESA landcover data, as explained below).”

Reviewer:

..Line 10: Why choose this grid-box

Response (35):

We choose this grid-box because it demonstrates a successional tropical sequence with many PFTs from bare soil. We could have shown many others.

Reviewer:

P16:

..Line 1: Discussion. The comparisons between RED and the other similar models are needed. But before that, I think the method description needs to be greatly improved, and the corresponding results should be further clarified.

Response (36):

Agreed. We have now included a comparison to other DGVMs which include forest demography within the discuss. Further we have tried be more clearer within the model description by keeping consistency in the equations and by moving some of more mathematically excessive sections into Appendix B. In addition to the above edits on the results, we have also reorientated the sections within the results section to improve the papers flow.

Edit:

“In a similar vein a few other models have limited the number of cohort dimensions, for example looking at using patch-age while using allometric relationships to capture size scale. Firstly the POP model (Haverd et al., 2014), uses stand-age cohorts as the dimension for population dynamics, every time-step applying crowding and resource limited mortality rates. Another example is the ORCHIDEE-MICT (Yue et al., 2018), which disaggrates the populations of a PFT into patch "Cohort" functional types, with transitions between cohorts diagnosed when the average basal diameter passes a threshold.”

Edit:

Finally, we assume that light-competition is only significant for the lowest ‘seedling’ mass class. This enables us to capture the impacts of light competition on seedling emergence through a simple ‘gap’ boundary condition. This represents a significant simplification compared to other approaches involving the Perfect Placidity Assumption (PPA), as used within other DGVMs such as LM3-PPA or CLM(ED) (Fisher et al., 2015; Weng et al., 2015), where canopies are assumed to perfectly fill gaps through photomorphism (Strigul et al., 2008). In LM3-PPA the radiative flux is limited by the available gap fraction in a given crown layer. PPA parallels our gap boundary condition at the lowest mass class (Equation (11)), but in RED the growth of a cohort is purely dictated by the the disaggregation of total growth assimilate assuming metabolic scaling (Equation (16)).

Reviews Bibliography

- Ahlström, A., Xia, J., Arneth, A., Luo, Y., and Smith, B. (2015). Importance of vegetation dynamics for future terrestrial carbon cycling. *Environmental Research Letters*, 10(5):054019.
- Allen, C. D., Macalady, A. K., Chenchouni, H., Bachelet, D., McDowell, N., Vennetier, M., Kitzberger, T., Rigling, A., Breshears, D. D., Hogg, E. T., et al. (2010). A global overview of drought and heat-induced tree mortality reveals emerging climate change risks for forests. *Forest ecology and management*, 259(4):660–684.
- Arora, V. K., Katavouta, A., Williams, R. G., Jones, C. D., Brovkin, V., Friedlingstein, P., Schwinger, J., Bopp, L., Boucher, O., Cadule, P., Chamberlain, M. A., Christian, J. R., Delire, C., Fisher, R. A., Hajima, T., Ilyina, T., Joetzjer, E., Kawamiya, M., Koven, C., Krasting, J., Law, R. M., Lawrence, D. M., Lenton, A., Lindsay, K., Pongratz, J., Raddatz, T., Séférian, R., Tachiiri, K., Tjiputra, J. F., Wiltshire, A., Wu, T., and Ziehn, T. (2019). Carbon-concentration and carbon-climate feedbacks in cmip6 models, and their comparison to cmip5 models. *Biogeosciences Discussions*, 2019:1–124.
- Brando, P. M., Balch, J. K., Nepstad, D. C., Morton, D. C., Putz, F. E., Coe, M. T., Silvério, D., Macedo, M. N., Davidson, E. A., Nóbrega, C. C., et al. (2014). Abrupt increases in amazonian tree mortality due to drought–fire interactions. *Proceedings of the National Academy of Sciences*, 111(17):6347–6352.
- Brovkin, V., Boysen, L., Arora, V. K., Boisier, J. P., Cadule, P., Chini, L., Claussen, M., Friedlingstein, P., Gayler, V., Van den hurk, B. J., Hurtt, G. C., Jones, C. D., Kato, E., De noblet ducoudre, N., Pacifico, F., Pongratz, J., and Weiss, M. (2013). Effect of anthropogenic land-use and land-cover changes on climate and land carbon storage in CMIP5 projections for the twenty-first century. *Journal of Climate*, 26(18):6859–6881.
- Brown, J. H., Gillooly, J. F., Allen, A. P., Savage, V. M., and West, G. B. (2004). Toward a metabolic theory of ecology. *Ecology*, 85(7):1771–1789.
- Burton, C., Betts, R., Cardoso, M., Feldpausch, T. R., Harper, A., Jones, C. D., Kelley, D. I., Robertson, E., and Wiltshire, A. (2019). Representation of fire, land-use change and vegetation dynamics in the joint uk land environment simulator vn4. 9 (jules). *Geoscientific Model Development*, 12(1):179–193.
- Chaturvedi, R., Raghubanshi, A., and Singh, J. (2012). Effect of grazing and harvesting on diversity, recruitment and carbon accumulation of juvenile trees in tropical dry forests. *Forest Ecology and Management*, 284:152–162.
- Chuvieco, E., Pettinari, M., Lizundia Loiola, J., Storm, T., and Padilla Parellada, M. (2019). Esa fire climate change initiative (fire_cci): Modis fire_cci burned area grid product, version 5.1. doi:10.5285/3628cb2fdb443588155e15dee8e5352.

- Ciais, P., Sabine, C., Bala, G., Bopp, L., Brovkin, V., Canadell, J., Chhabra, A., DeFries, R., Galloway, J., Heimann, M., et al. (2014). Carbon and other biogeochemical cycles. In *Climate change 2013: the physical science basis. Contribution of Working Group I to the Fifth Assessment Report of the Intergovernmental Panel on Climate Change*, pages 465–570. Cambridge University Press.
- Coomes, D. A., Duncan, R. P., Allen, R. B., and Truscott, J. (2003). Disturbances prevent stem size-density distributions in natural forests from following scaling relationships. *Ecology Letters*, 6(11):980–989.
- Coomes, D. A., Lines, E. R., and Allen, R. B. (2011). Moving on from metabolic scaling theory: hierarchical models of tree growth and asymmetric competition for light. *Journal of Ecology*, 99(3):748–756.
- Coutinho, L. M. (1990). Fire in the ecology of the brazilian cerrado. In *Fire in the tropical biota*, pages 82–105. Springer.
- Cox, P. M. (2001). Description of the "triffid" dynamic global vegetation model.
- Curran, L. M., Trigg, S. N., McDonald, A. K., Astiani, D., Hardiono, Y., Siregar, P., Caniago, I., and Kasischke, E. (2004). Lowland forest loss in protected areas of indonesian borneo. *Science*, 303(5660):1000–1003.
- Dorrough, J. and Moxham, C. (2005). Eucalypt establishment in agricultural landscapes and implications for landscape-scale restoration. *Biological conservation*, 123(1):55–66.
- Eller, C. B., Rowland, L., Mencuccini, M., Rosas, T., Williams, K., Harper, A., Medlyn, B. E., Wagner, Y., Klein, T., Teodoro, G. S., et al. (2020). Stomatal optimisation based on xylem hydraulics (sox) improves land surface model simulation of vegetation responses to climate. *New Phytologist*.
- Eller, C. B., Rowland, L., Oliveira, R. S., Bittencourt, P. R., Barros, F. V., da Costa, A. C., Meir, P., Friend, A. D., Mencuccini, M., Sitch, S., et al. (2018). Modelling tropical forest responses to drought and el niño with a stomatal optimization model based on xylem hydraulics. *Philosophical Transactions of the Royal Society B: Biological Sciences*, 373(1760):20170315.
- Esseen, P.-A. (1994). Tree mortality patterns after experimental fragmentation of an old-growth conifer forest. *Biological conservation*, 68(1):19–28.
- Farrior, C., Bohlman, S., Hubbell, S., and Pacala, S. W. (2016). Dominance of the suppressed: Power-law size structure in tropical forests. *Science*, 351(6269):155–157.
- Fischer, R., Bohn, F., de Paula, M. D., Dislich, C., Groeneveld, J., Gutiérrez, A. G., Kazmierczak, M., Knapp, N., Lehmann, S., Paulick, S., et al. (2016). Lessons learned from applying a forest gap model to understand ecosystem and carbon dynamics of complex tropical forests. *Ecological Modelling*, 326:124–133.
- Fisher, R. A., Koven, C. D., Anderegg, W. R., Christoffersen, B. O., Dietze, M. C., Farrior, C. E., Holm, J. A., Hurtt, G. C., Knox, R. G., Lawrence, P. J., Lichstein, J. W., Longo, M., Matheny, A. M., Medvigy, D., Muller-Landau, H. C., Powell, T. L., Serbin, S. P., Sato, H., Shuman, J. K., Smith, B., Trugman, A. T., Viskari, T., Verbeeck, H., Weng, E., Xu, C., Xu, X., Zhang, T., and Moorcroft, P. R. (2018). Vegetation demographics

- in Earth System Models: A review of progress and priorities. *Global Change Biology*, 24(1):35–54.
- Fisher, R. A., Muszala, S., Versteinstein, M., Lawrence, P., Xu, C., McDowell, N. G., Knox, R. G., Koven, C., Holm, J., Rogers, B. M., Spessa, A., Lawrence, D., and Bonan, G. (2015). Taking off the training wheels: the properties of a dynamic vegetation model without climate envelopes, *clm4.5*(ed). *Geoscientific Model Development*, 8(11):3593–3619.
- Friedlingstein, P., Meinshausen, M., Arora, V. K., Jones, C. D., Anav, A., Liddicoat, S. K., and Knutti, R. (2014). Uncertainties in CMIP5 climate projections due to carbon cycle feedbacks. *Journal of Climate*, 27(2):511–526.
- Haddad, N. M., Brudvig, L. A., Clobert, J., Davies, K. F., Gonzalez, A., Holt, R. D., Lovejoy, T. E., Sexton, J. O., Austin, M. P., Collins, C. D., et al. (2015). Habitat fragmentation and its lasting impact on earth’s ecosystems. *Science advances*, 1(2):e1500052.
- Haverd, V., Smith, B., Nieradzick, L. P., and Briggs, P. R. (2014). A stand-alone tree demography and landscape structure module for earth system models: integration with inventory data from temperate and boreal forests. *Biogeosciences*, 11(15):4039–4055.
- Higuchi, P., Oliveira-Filho, A. T., Bebbler, D. P., Brown, N. D., Silva, A. C., and Machado, E. L. (2008). Spatio-temporal patterns of tree community dynamics in a tropical forest fragment in south-east brazil. *Plant Ecology*, 199(1):125–135.
- Johnson, D. J., Needham, J., Xu, C., Massoud, E. C., Davies, S. J., Anderson-Teixeira, K. J., Bunyavejchewin, S., Chambers, J. Q., Chang-Yang, C.-H., Chiang, J.-M., et al. (2018). Climate sensitive size-dependent survival in tropical trees. *Nature ecology & evolution*, 2(9):1436–1442.
- Jones, S., Rowland, L., Cox, P., Hemming, D., Wiltshire, A., Williams, K., Parazoo, N. C., Liu, J., da Costa, A. C. L., Meir, P., Mencuccini, M., and Harper, A. (2019). The impact of a simple representation of non-structural carbohydrates on the simulated response of tropical forests to drought. *Biogeosciences Discussions*, 2019:1–26.
- Jönsson, M. T., Fraver, S., Jonsson, B. G., Dynesius, M., Rydgård, M., and Esseen, P.-A. (2007). Eighteen years of tree mortality and structural change in an experimentally fragmented norway spruce forest. *Forest Ecology and Management*, 242(2-3):306–313.
- Kinnaird, M. F. and O’Brien, T. G. (1998). Ecological effects of wildfire on lowland rainforest in sumatra. *Conservation Biology*, 12(5):954–956.
- Kohyama, T., Suzuki, E., Partomihardjo, T., Yamada, T., and Kubo, T. (2003). Tree species differentiation in growth, recruitment and allometry in relation to maximum height in a bornean mixed dipterocarp forest. *Journal of Ecology*, 91(5):797–806.
- Laurance, W. F., Ferreira, L. V., Rankin-de Merona, J. M., and Laurance, S. G. (1998). Rain forest fragmentation and the dynamics of amazonian tree communities. *Ecology*, 79(6):2032–2040.
- Levine, N. M., Zhang, K., Longo, M., Baccini, A., Phillips, O. L., Lewis, S. L., Alvarez-Dávila, E., de Andrade, A. C. S., Brienen, R. J., Erwin, T. L., et al. (2016). Ecosystem heterogeneity determines the ecological resilience of the amazon to climate change. *Proceedings of the National Academy of Sciences*, 113(3):793–797.

- Lewis, S. L., Phillips, O. L., Baker, T. R., Lloyd, J., Malhi, Y., Almeida, S., Higuchi, N., Laurance, W. F., Neill, D. A., Silva, J. N. M., et al. (2004). Concerted changes in tropical forest structure and dynamics: evidence from 50 south american long-term plots. *Philosophical Transactions of the Royal Society of London. Series B: Biological Sciences*, 359(1443):421–436.
- Li, W., MacBean, N., Ciais, P., Defourny, P., Lamarche, C., Bontemps, S., and Peng, S. (2019). Derivation of plant functional type (pft) maps from the esa cci land cover product [data set]. <http://doi.org/10.5281/zenodo.1048163>.
- Lima, R. A., Muller-Landau, H. C., Prado, P. I., and Condit, R. (2016). How do size distributions relate to concurrently measured demographic rates? evidence from over 150 tree species in panama. *Journal of Tropical Ecology*, 32(3):179–192.
- Lines, E. R., Coomes, D. A., and Purves, D. W. (2010). Influences of forest structure, climate and species composition on tree mortality across the eastern us. *PloS one*, 5(10).
- Longo, M., Knox, R. G., Levine, N. M., Swann, A. L. S., Medvigy, D. M., Dietze, M. C., Kim, Y., Zhang, K., Bonal, D., Burban, B., Camargo, P. B., Hayek, M. N., Saleska, S. R., da Silva, R., Bras, R. L., Wofsy, S. C., and Moorcroft, P. R. (2019b). The biophysics, ecology, and biogeochemistry of functionally diverse, vertically and horizontally heterogeneous ecosystems: the ecosystem demography model, version 2.2 – part 2: Model evaluation for tropical south america. *Geoscientific Model Development*, 12(10):4347–4374.
- Longo, M., Knox, R. G., Medvigy, D. M., Levine, N. M., Dietze, M. C., Kim, Y., Swann, A. L. S., Zhang, K., Rollinson, C. R., Bras, R. L., Wofsy, S. C., and Moorcroft, P. R. (2019a). The biophysics, ecology, and biogeochemistry of functionally diverse, vertically and horizontally heterogeneous ecosystems: the ecosystem demography model, version 2.2 – part 1: Model description. *Geoscientific Model Development*, 12(10):4309–4346.
- Medeiros, M. and Miranda, H. (2008). Post-fire resprouting and mortality in cerrado woody plant species over a three-year period. *Edinburgh Journal of Botany*, 65(1):53–68.
- Moore, J. R., Argles, A. P. K., Zhu, K., Huntingford, C., and Cox, P. M. (2020). Validation of demographic equilibrium theory against tree-size distributions and biomass density in amazonia. *Biogeosciences*, 17(4):1013–1032.
- Moore, J. R., Zhu, K., Huntingford, C., and Cox, P. M. (2018). Equilibrium forest demography explains the distribution of tree sizes across North America. *Environmental Research Letters*, 13(8).
- Muller-Landau, H. C., Condit, R. S., Chave, J., Thomas, S. C., Bohlman, S. A., Bunyavejchewin, S., Davies, S., Foster, R., Gunatilleke, S., Gunatilleke, N., et al. (2006a). Testing metabolic ecology theory for allometric scaling of tree size, growth and mortality in tropical forests. *Ecology letters*, 9(5):575–588.
- Muller-Landau, H. C., Condit, R. S., Harms, K. E., Marks, C. O., Thomas, S. C., Bunyavejchewin, S., Chuyong, G., Co, L., Davies, S., Foster, R., Gunatilleke, S., Gunatilleke, N., Hart, T., Hubbell, S. P., Itoh, A., Kassim, A. R., Kenfack, D., LaFrankie, J. V., Lagunzad, D., Lee, H. S., Losos, E., Makana, J. R., Ohkubo, T., Samper, C., Sukumar,

- R., Sun, I. F., Nur Supardi, M. N., Tan, S., Thomas, D., Thompson, J., Valencia, R., Vallejo, M. I., Muñoz, G. V., Yamakura, T., Zimmerman, J. K., Dattaraja, H. S., Esufali, S., Hall, P., He, F., Hernandez, C., Kiratiprayoon, S., Suresh, H. S., Wills, C., and Ashton, P. (2006b). Comparing tropical forest tree size distributions with the predictions of metabolic ecology and equilibrium models. *Ecology Letters*, 9(5):589–602.
- Nepstad, D. C., Stickler, C. M., Filho, B. S., and Merry, F. (2008). Interactions among amazon land use, forests and climate: prospects for a near-term forest tipping point. *Philosophical Transactions of the Royal Society B: Biological Sciences*, 363(1498):1737–1746.
- Pavlick, R., Drewry, D. T., Bohn, K., Reu, B., and Kleidon, A. (2013). The jena diversity-dynamic global vegetation model (jedi-dgvm): a diverse approach to representing terrestrial biogeography and biogeochemistry based on plant functional trade-offs. *Biogeosciences*, 10:4137–4177.
- Peterson, D. W. and Reich, P. B. (2001). Prescribed fire in oak savanna: fire frequency effects on stand structure and dynamics. *Ecological Applications*, 11(3):914–927.
- Prior, L. D., Murphy, B. P., and Russell-Smith, J. (2009). Environmental and demographic correlates of tree recruitment and mortality in north australian savannas. *Forest Ecology and Management*, 257(1):66–74.
- Pugh, T. A. M., Rademacher, T. T., Shafer, S. L., Steinkamp, J., Barichivich, J., Beckage, B., Haverd, V., Harper, A., Heinke, J., Nishina, K., Rammig, A., Sato, H., Arneth, A., Hantson, S., Hickler, T., Kautz, M., Quesada, B., Smith, B., and Thonicke, K. (2020). Understanding the uncertainty in global forest carbon turnover. *Biogeosciences Discussions*, 2020:1–44.
- Rüger, N. and Condit, R. (2012). Testing metabolic theory with models of tree growth that include light competition. *Functional Ecology*, 26(3):759–765.
- Russo, S. E., Wisser, S. K., and Coomes, D. A. (2007). Growth–size scaling relationships of woody plant species differ from predictions of the metabolic ecology model. *Ecology Letters*, 10(10):889–901.
- Sato, H., Itoh, A., and Kohyama, T. (2007). SEIB-DGVM: A new Dynamic Global Vegetation Model using a spatially explicit individual-based approach. *Ecological Modelling*, 200(3-4):279–307.
- Schleussner, C.-F., Rogelj, J., Schaeffer, M., Lissner, T., Licker, R., Fischer, E. M., Knutti, R., Levermann, A., Frieler, K., and Hare, W. (2016). Science and policy characteristics of the paris agreement temperature goal. *Nature Climate Change*, 6(9):827–835.
- Smith, B. (2001). Lpj-guess-an ecosystem modelling framework. *Department of Physical Geography and Ecosystems Analysis. INES, Sölvegatan*, 12:22362.
- Staver, A. C., Bond, W. J., Stock, W. D., Van Rensburg, S. J., and Waldram, M. S. (2009). Browsing and fire interact to suppress tree density in an african savanna. *Ecological applications*, 19(7):1909–1919.
- Strigul, N., Pristinski, D., Purves, D., Dushoff, J., and Pacala, S. (2008). Scaling from trees to forests: tractable macroscopic equations for forest dynamics. *Ecological Monographs*, 78(4):523–545.

- Swaine, M. (1992). Characteristics of dry forest in west africa and the influence of fire. *Journal of vegetation science*, 3(3):365–374.
- Van Nieuwstadt, M. G. and Sheil, D. (2005). Drought, fire and tree survival in a borneo rain forest, east kalimantan, indonesia. *Journal of Ecology*, 93(1):191–201.
- Van Uytvanck, J., Maes, D., Vandenhaute, D., and Hoffmann, M. (2008). Restoration of woodpasture on former agricultural land: the importance of safe sites and time gaps before grazing for tree seedlings. *Biological Conservation*, 141(1):78–88.
- Weng, E. S., Malyshev, S., Lichstein, J. W., Farris, C. E., Dybzinski, R., Zhang, T., Shevliakova, E., and Pacala, S. W. (2015). Scaling from individual trees to forests in an earth system modeling framework using a mathematically tractable model of height-structured competition. *Biogeosciences*, 12(9):2655–2694.
- West, G. B., Brown, J. H., and Enquist, B. J. (1997). A general model for the origin of allometric scaling laws in biology. *Science*, 276(5309):122–126.
- Yue, C., Ciais, P., Luyssaert, S., Li, W., McGrath, M. J., Chang, J., and Peng, S. (2018). Representing anthropogenic gross land use change, wood harvest, and forest age dynamics in a global vegetation model orchidee-mict v8.4.2. *Geoscientific Model Development*, 11(1):409–428.

Robust Ecosystem Demography (RED [version 1.0](#)): a parsimonious approach to modelling vegetation dynamics in Earth System Models

Arthur P. K. Argles¹, Jonathan R. Moore¹, Chris Huntingford², Andrew J. Wiltshire³, Anna B. Harper¹, Chris D. Jones³, and Peter M. Cox¹

¹College of Engineering, Mathematics, and Physical Sciences, University of Exeter, Exeter EX4 4QF, UK

²Centre for Ecology and Hydrology, Wallingford OX10 8BB, UK

³Met Office Hadley Centre, Fitzroy Road, Exeter EX1 3PB, UK

Correspondence: aa760@exeter.ac.uk, P.M.Cox@exeter.ac.uk, J.Moore3@exeter.ac.uk

Abstract. A significant proportion of the uncertainty in climate projections arises from uncertainty in the representation of land carbon uptake. Dynamic Global Vegetation Models (DGVMs) vary in their representations of regrowth and competition for resources, which results in differing responses to changes in atmospheric CO₂ and climate. More advanced cohort-based patch models are now becoming established in the latest DGVMs. These [models](#) typically attempt to simulate the size-distribution of trees as a function of both tree-size (mass or trunk diameter) and age (time since disturbance). This approach can capture the overall impact of stochastic disturbance events on the forest structure and biomass, but at the cost of [needing to update a increasing the number of parameters and ambiguity when updating the](#) probability density function ([pdf](#)) in two-dimensions. Here we present the *Robust Ecosystem Demography (RED)*, in which the pdf is collapsed on to the single dimension of tree mass. RED is designed to retain the ability of more complex cohort DGVMs to represent forest demography, while also being parameter sparse and analytically [soluble](#)[solvable for the steady-state](#). The population of each Plant Functional Type (PFT) is partitioned into mass classes with a fixed baseline mortality along with an assumed power-law scaling of [growth-rate](#) [growth rate](#) with mass. The analytical equilibrium solutions of RED allow the model to be calibrated against observed forest cover using a single parameter - the ratio of mortality to growth for a tree of a reference mass (μ_0). We show that RED can thus be calibrated to the ESA LC_CCI (European Space Agency Land Cover Climate Change Initiative) coverage dataset for nine PFTs. Using Net Primary Productivity and litter outputs from the UK Earth System Model (UKESM), we are able to diagnose the spatially varying disturbance rates consistent with this observed vegetation map. The analytical form for RED circumnavigates the need to spin-up the numerical model, making it attractive for application in Earth System Models (ESMs). This is especially so given that the model is also highly parameter-sparse.

1 Introduction

A key requirement of Earth System Science is to estimate how much carbon the land surface will take-up in the decades ahead ([Ciais et al., 2014](#)). This is an important component of the total carbon budget consistent with avoiding global warming thresholds, such as $2K2^{\circ}C$ ([Schleussner et al., 2016](#)). Unfortunately, projections of future land carbon storage still span a wide-range [-Using an ensemble of \(Brovkin et al., 2013; Friedlingstein et al., 2014; Arora et al., 2019\). Beyond the CO₂](#)

and nutrient fertilisation effects and land-use change, significant uncertainty also arises from the representation of vegetation demographics such as recruitment, competition and mortality (Brovkin et al., 2013; Ahlström et al., 2015). The representation of plant communities within Earth System Models (ESMs) is achieved through the use of Dynamic Global Vegetation Models (DGVMs), the Global Carbon Project estimates that the global land absorbed carbon at a rate of $3.2 \pm 0.8 \text{ GtC yr}^{-1}$ in 2018, which is approximately 30% of anthropogenic emissions (?). The cumulative uptake of land carbon across the Coupled Model Intercomparison Model Project 5 (CMIP5) under a common emissions scenario (RCP8.5) produced a range between -185 PgC (source) to 758 PgC (sink) by the end of . DGVMs employ a variety of biophysical, biogeographical and biochemical processes to simulate growth, competition and recruitment of vegetation. The variety in the number and resolution of the twenty-first century. This uncertainty arose in part from differences in how land-use change (LUC) was modelled, with eight of the eleven ESMs within CMIP5 including LUC (Friedlingstein et al., 2014) processes contributes to the differences found at the Earth System level.

Within the context of modelling vegetation at a global level, there is a trade-off between the complexity of ecological process representation and the necessity of parsimony at scale (Fisher et al., 2018). DGVMs range from the simplistic, older, top-down approaches to that of complex individual-based DGVMs. For example, in the first instance the TRIFFID model (Cox, 2001) simulates the fractional area of each Plant Functional Type (PFT) using phenomenological Lotka-Volterra equations. The benefit of the TRIFFID approach is its simplicity and robustness. However, even when focusing within CMIP5 ESMs including LUC the results are uncertain. Under RCP8.5, model runs had a range of $34 - 205 \text{ PgC}$ net emitted carbon by the land surface at the end of the century (Brovkin et al., 2013), which can be attributed to uncertainties in both regrowth and CO_2 fertilisation. Furthermore, models have been shown to have varying responses in climate-induced land cover change (Davies-Barnard et al., 2015; Pugh et al., 2015). DGVMs employ a variety of methods to simulate vegetation which contributes to the differences found at the Earth system level (Fisher et al., 2018). Complex models such as the SEIB-DGVM (Sato et al., 2007) stochastically represent individuals on a meter by meter grid which is scaled-up to hundreds of kilometres squared. the model suffers from the lack of size representation and other processes which results in the over-estimation of regrowth time (Burton et al., 2019). In the second-instance, individual based models can explicitly represent a multitude of biological and ecosystem processes at an individual plant level (Smith, 2001; Sato et al., 2007). The benefit of this is that size-dependent physiology and spatial heterogeneity can be explicitly represented. However, multiple ensemble-members are often needed to construct meaningful forest statistics, which makes such models computationally expensive to run at large scales. Top-down DGVMs, where all individuals of a Plant Functional Type (PFT) are essentially treated as of the same size, are significantly simpler and more computationally efficient. However, processes that are dependent on size cannot be represented, and forest regrowth times are often over-estimated. In the JULES-TRIFFID coupled model (Best et al., 2011), regrowth from disturbances is often unrealistically long, resulting in fast-growing PFTs becoming dominant in dynamical runs with fire and LUC (Burton et al., 2019). Compromises between the complexity of individual-individual-based and top-down DGVMs exists exist as a class of tree Cohort cohort models. In the ED model (Moorcroft et al., 2001; Medvigy et al., 2009) the tree population is partitioned between patch disturbance and biomass classes allowing for the scaling of process to be represented in both age and size. ED2 can realistically model forests around the world (boreal, rainforest and temperate) (Medvigy et al., 2009; Fisher et al., 2018). However, parameterisation of competition

within cohort DGVMs can result in a wide spread of outcomes when simulating climate change (Fisher et al., 2010; Scheiter et al., 2013). ~~Such patch models can also be numerically unwieldy, as new patches (or ‘tiles’) are created after each disturbance event.~~

In a similar vein other models have limited the number of cohort dimensions. The POP model (Haverd et al., 2014), uses stand-age cohorts as the dimension for population dynamics, every time-step applying crowding and resource limited mortality rates. Another example is the ORCHIDEE-MICT (Yue et al., 2018), which disaggregates the populations of a PFT into patch cohort functional types, with transitions between cohorts diagnosed when the average basal diameter passes a threshold.

This paper ~~represents~~ presents a simplified cohort model (~~Robust Ecosystem Demography (RED)~~) Robust Ecosystem Demography (RED) which updates the number of trees in each mass class, but does not separately track tree-age or patch-age. ~~This~~

~~simplification significantly reduces~~ RED assumes that the tree size-distribution of a forest is determined by how the rates of tree growth and mortality vary with tree size (Kohyama et al., 2003; Coomes et al., 2003; Muller-Landau et al., 2006; Lima et al., 2016)

. We follow many other studies in assuming that tree-growth rates vary with the three-quarter power of tree mass ($m^{3/4}$), as suggested by metabolic scaling theory (West et al., 1997). Where tree mortality rate can also be assumed to be approximately independent of tree mass, the demographic equation yields equilibrium tree-size distributions which follow a Weibull distribution.

This is sometimes termed *Demographic Equilibrium Theory (DET)* (see Appendix B). These simplifications significantly reduce the number of free parameters in ~~the model~~ RED, but still ~~enables~~ enable it to fit forest inventory data in North America (Moore et al., 2018) and South America ~~(?)~~.

(Moore et al., 2020).

2 Description of the Model

A full list of variables, parameters and units are given in Table 1.

Table 1. Model variables, parameters and units

<u>Symbol</u>	<u>Definitions</u>	<u>Units</u>
Dimensions		
t	<u>Time</u>	<u>year</u>
m	<u>Carbon mass of an individual within a PFT</u>	<u>kgC</u>
ESM Inputs		
P	<u>Total assimilate of Net Primary Productivity minus local (leaves, wood and roots) litterfall</u>	<u>kgC m⁻² yr⁻¹</u>
γ_d	<u>Disturbance mortality rate, the fraction of population dying over a year due to explicitly modelled reasons</u>	<u>yr⁻¹</u>
Individual		
m_0	<u>Lowest/sapling mass boundary</u>	<u>kgC</u>
g	<u>Structural growth of an individual at a given mass and time</u>	<u>kgC yr⁻¹</u>
g_0	<u>Structural growth of an individual at the lowest mass boundary at a specific time</u>	<u>kgC yr⁻¹</u>
a	<u>Crown area of an individual at a given mass</u>	<u>m²</u>
a_0	<u>Crown area of an individual at the lowest mass boundary</u>	<u>m²</u>
ϕ_a	<u>Constant describing the power law scaling of structural growth across mass</u>	<u>—</u>
ϕ_b	<u>Constant describing the power law scaling of height across mass</u>	<u>—</u>
ϕ_a	<u>Constant describing the power law scaling of crown area across mass</u>	<u>—</u>
α	<u>The fraction of total growth going into seedling recruitment</u>	<u>—</u>
Cohort		
n	<u>Number density across mass space, the derivative of N with respect to mass</u>	<u>(kgC)⁻¹ m⁻²</u>
N	<u>Number density</u>	<u>m⁻²</u>
G	<u>Growth density</u>	<u>kgC m⁻² yr⁻¹</u>
ν	<u>The fractional coverage</u>	<u>—</u>
γ	<u>Mortality rate, the summation of the baseline and additional mortalities across mass</u>	<u>yr⁻¹</u>
γ_b	<u>Baseline mortality rate, the fraction of population dying over a year due to non-explicitly modelled reasons</u>	<u>yr⁻¹</u>
s	<u>The fraction of space available for seedlings</u>	<u>—</u>
F	<u>The flux of population density over time</u>	<u>m⁻² yr⁻¹</u>
Λ_d	<u>Demographic litter, the loss of carbon due to competition and mortality</u>	<u>kgC m⁻² yr⁻¹</u>
M	<u>Biomass density</u>	<u>kgC m⁻²</u>
$c_{k,l}$	<u>Competition coefficient, the fraction a PFT, k, that is shaded by the canopy of PFT l</u>	<u>—</u>

<u>Symbol</u>	<u>Definitions</u>	<u>Units</u>
Equilibrium		
μ_0	The boundary turnover parameter - the ratio of mass lost to gained due to growth in the boundary mass class	—
λ_i	The proportional population of the i^{th} class to the $i^{\text{th}} - 1$ class at equilibrium	—
eq	Subscript denoting a variable in equilibrium	—
Numerical		
k, l	Indices representing the PFT number	—
i, j	Indices representing mass class number	—
I	The largest mass class	—
(k)	The current time-step	—
ξ	The size scaling coefficient, where mass classes are defined as $m_j = \xi m_{j-1}$, with $\xi > 1$	—

2.1 Theory

The underlying theoretical model for RED is a continuity equation, for each PFT and spatial location, which describes the time-evolution of the number density $n(m)$ of plants per unit area of mass m :

$$\frac{\partial n}{\partial t} + \frac{\partial}{\partial m} n g = -\gamma n \quad (1)$$

- 5 Here ~~$g(m)$ is the growth rate and $\gamma(m)$ is the mortality rate~~ g is the growth rate and γ is the mortality rate of a plant of mass m . In general, g and γ could take any form, ~~but of relationship with size, but for large-scale applications~~ we make simplifying assumptions for these functions consistent with observed $n(m)$ from forest inventory data (Moore et al., 2018; ?). ~~Simply,~~ (Moore et al., 2018, 2020). ~~By default~~ we assume that γ is independent of plant mass, and that ~~$g(m)$ is g~~ follows a power-law of plant mass:

$$10 \quad g = g_0 \left(\frac{m}{m_0} \right)^{\phi_g} \quad (2)$$

Here g_0 is the growth rate of a plant with the reference mass, m_0 . A value of $\phi_g = 0.75$ is assumed by default, consistent with (Niklas and Spatz, 2004) ~~the meta-analysis of field-based measurements by Niklas and Spatz (2004)~~. We also follow (Niklas and Spatz, 2004) ~~Niklas and Spatz (2004)~~ in assuming the scaling of plant canopy area a with plant mass:

$$a = a_0 \left(\frac{m}{m_0} \right)^{\phi_a} \quad (3)$$

- 15 where $\phi_a = 0.5$ by default.

Solutions for n can be integrated over mass to derive the total plant number, ~~$N = \int n dm$~~ $N = \int n dm$, the total ~~growth rate~~ growth rate, $G = \int g n dm$, the total biomass, $M = \int m n dm$, and the fractional area covered $\nu = \int a n dm$.

2.2 Discrete Mass Classes

We wish to produce a model of vegetation demography that can be updated numerically and which explicitly conserves vegetation carbon, providing a constraint on the number of plants moving between mass classes in the discrete form. In order to do this we integrate Eq. (1) over finite mass ranges:

$$5 \quad \frac{\partial N_i}{\partial t} + F_i - F_{i-1} = -\gamma N_i, \quad (4)$$

where i denotes the i^{th} mass class; F_i is the flux of plants growing out of the i^{th} mass class and into the $(i+1)^{th}$ mass class; F_{i-1} is the flux of plants growing out of the $(i-1)^{th}$ mass class and into the i^{th} mass class; and N_i is the number of plants per unit area in the i^{th} mass class. For clarity, Eq. (4) is deliberately presented as continuous in time at this stage, as the focus in this subsection is on discretization of the mass profile. The fully numerical version of RED, which includes discretization of time, is described in Section 2.4 and 2.5. In order to ~~conserve carbon (see below)~~ explicitly conserve carbon, the flux F_i must take the form ~~:(see Appendix A):~~

$$F_i = \frac{N_i g_i}{(m_{i+1} - m_i)}, \quad (5)$$

where m_i is the mean mass of a plant in the i^{th} mass class, and g_i is the ~~growth rate~~ growth rate per plant of the i^{th} mass class [$\text{kgC yr}^{-1} \text{ plant}^{-1}$].

15 ~~For large-scale application in ESMs, a primary concern is to ensure that the total vegetation carbon obeys carbon balance (i.e. only changes due to the net impact of total growth minus total mortality). The total vegetation carbon in each mass class is $M_i = m_i N_i$. The update equation for M_i is therefore Eq. multiplied by m_i :~~

$$\frac{\partial M_i}{\partial t} + m_i (F_i - F_{i-1}) = -\gamma M_i.$$

~~The total carbon in the vegetation, M , is the sum of the carbon in each of the mass classes:~~

$$20 \quad M = \sum_i M_i.$$

~~Thus the update equation for the total carbon is:~~

$$\frac{\partial M}{\partial t} + \sum_i m_i (F_i - F_{i-1}) = -\gamma M,$$

~~which can be rewritten as:~~

$$\frac{\partial M}{\partial t} + \sum_i F_i (m_i - m_{i+1}) = -\gamma M.$$

25 ~~Now substituting Eq. into Eq. gives:~~

$$\frac{\partial M}{\partial t} = \sum_i N_i g_i - \gamma M.$$

The first term on the righthand-side of this equation is the total carbon uptake due to growth, and the second term represents the total carbon loss due to mortality, which is the required carbon conservation equation.

2.3 Seedling production and gap competition

To solve Eq. (4) we also require a lower boundary condition which represents the rate at which seedlings of mass m_0 are introduced into the cohort. Here we assume that a fixed fraction, α , of the total assimilate available to a PFT (P), is devoted to producing new seedlings, with the remainder $G = (1 - \alpha)P$ being allocated to the growth of existing plants. In addition, we assume that only those seedlings growing in 'gaps' will survive. Spreading is homogeneous across the entirety of the grid-box, but only seedlings established within 'unoccupied' space will survive to join the plant cohort. The net incoming flux of seedlings of mass m_0 is therefore:

$$F_0 = \frac{\alpha P}{m_0} s = \frac{\alpha}{(1 - \alpha)} \frac{G}{m_0} s, \quad (6)$$

where s is the fractional gap area available for seedlings. The definition of s is assumed to differ by PFT to reflect an underlying tree-shrub-grass dominance hierarchy, as shown schematically in Figure 1.

Equation assumes a random overlap between seedlings and the existing vegetation. This lower boundary condition is the only place within RED where there is significant competition. Minimum overlap, which is broadly consistent with 'perfect plasticity' (Strigul et al., 2008), is assumed once seedlings have been injected into the cohort according to Eq. .

Therefore, the rate of recruitment F_0 is the ratio of a fraction of the carbon assimilate allocated to reproduction, αP , and m_0 , multiplied by the gap area s .

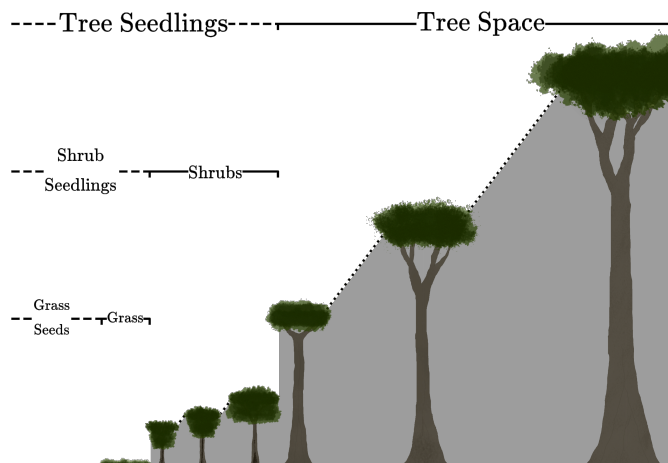


Figure 1. Illustration-Schematic depicting the hierarchical PFT functional group regime within RED. Trees shade Treestrees, Shrubs-shrubs and Grasses-grasses. Shrubs shade Shrubs-shrubs and Grasses-grasses, while grasses only shade grasses.

The space available to the seedlings of the k^{th} PFT is calculated from the area fractions of the PFTs to which it is subdominant:

$$s_k = 1 - \sum_l c_{kl} \nu_l, \quad (7)$$

where ν_l is the area fraction of the l^{th} PFT, and c_{kl} is the competition coefficient for the impact of PFT l on PFT k . If PFT l is within the same plant functional group (trees, shrubs or grasses) as PFT k , or dominant over it, $c_{kl} = 1$. If PFT k is dominant over PFT l , $c_{kl} = 0$ (Figure ??1). This is similar to the competition regime in the ‘gap’ boundary condition results in there being no equilibrium solution where the amount of coverage exceeds 1. Doing so would halt the recruitment flux such that mortality processes would bring the fractional coverage back below unity. This is a similar competition regime to the Lotka-inspired TRIFFID model (Cox, 2001), and allows for the co-existence between inter-functional groups (trees, shrubs and grasses) of PFTs. For instance, a PFT such as Broadleaf Deciduous Tree can co-exist with a Deciduous Shrub and C3 Grass. The hierarchy also enables the simulation of succession during regrowth. Faster growing species of grasses will not be able to expand into space occupied by trees and shrubs, unless there is space created by disturbance. A summary of the competition coefficients is given in table 2.

Table 2. The competition coefficients values assumed for different Plant Functional Groups. A more detailed example of this is given with for specific PFTs in table 3.

c_{kl}	l		
	Trees	Shrubs	Grasses
Trees	1	0	0
k Shrubs	1	1	0
Grasses	1	1	1

15 2.4 Coupling to Earth System Models

RED updates plant size distributions, biomass, and fractional areal coverage for an arbitrary number of PFTs at each spatial location, and can be driven by variables provided by a land carbon cycle model, an Earth System Model, or observations (see Figure ??2). For each PFT, the minimum required input is a time-series of net carbon assimilate (P), defined as the difference between Net Primary Productivity (Π_N), and local litter production due to turnover of leaves, stems and roots (Λ_l):

$$20 \quad P = \Pi_N - \Lambda_l. \quad (8)$$

Where available, additional mortality due to disturbance events such as droughts, fires and anthropogenic deforestation (γ_d) can be added to the baseline mortality rates (γ_b), for each PFT:

$$\gamma = \gamma_b + \gamma_d \quad (9)$$

These Disturbance rates γ_d values can in principle be both PFT-dependent and mass-dependent (e.g. to capture forestry practices).

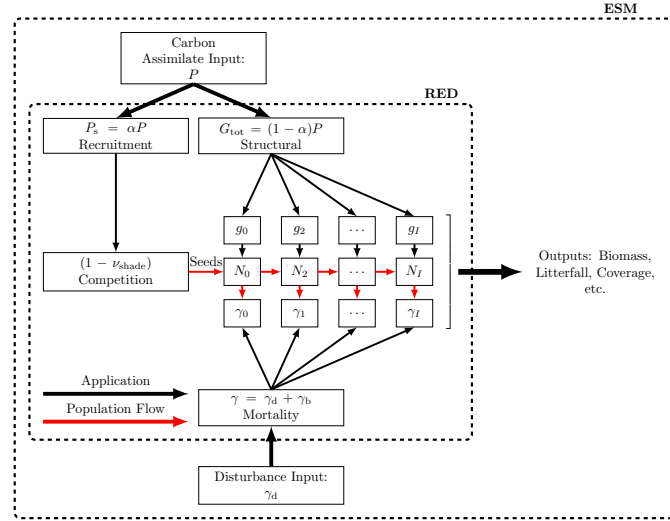


Figure 2. Schematic of RED coupled to an ESM ~~en-or~~ land carbon cycle model. RED is driven by a time-series of net carbon assimilate, P , which is then split between seedling production, αP , and the growth of existing plants, $G = (1 - \alpha) P$. The seedling flux is limited by the available free space, s . Additional mortality rates diagnosed from disturbance models, γ_d , can be added on to an assumed baseline mortality, γ_b , as a function of both PFT and ~~mass-class~~ mass class.

5

The input values of net assimilate for each PFT (P), define the total structural ~~growth-rate~~ growth rate, $G = (1 - \alpha) P$, and the seedling flux F_0 (via Eq. (6)), using PFT-specific values of the parameter α (see table 3). The definition of the total structural ~~growth-rate~~ growth rate at a given time-step t is:

$$G = \sum_i N_i g_i \quad (10)$$

can be combined with the growth-scaling given by Eq. (2), to derive the reference ~~growth-rate~~ growth rate, g_0 , from the net assimilate, P , which is a driving input:

$$g_0 = \frac{(1 - \alpha) P}{\sum_i N_i \left(\frac{m_i}{m_0} \right)^{\phi_g}} \quad (11)$$

This in turn enables the growth-rate-growth rate of each mass class to be calculated using Eq. (2). For each PFT, the number of plants in mass class (N_i) is updated using a discretised form of Eq. (4):

$$N_i^{(j+1)} = N_i^{(j)} + \Delta t \left(F_{i-1}^{(j)} - F_i^{(j)} - \gamma^{(j)} N_i^{(j)} \right) \quad (12)$$

where Δt is the RED timestep-time-step (typically 1 month), and the superscript (j) denotes the j^{th} timestep-time-step. The lower boundary seedling flux is calculated from Eq. (6) using Eq. (7). We ~~do not~~ impose a zero-flux condition out of the upper mass class, under the assumption that there will be enough mass classes to ensure that this flux is negligible. However, to ensure carbon conservation on the land we add any plants that grow out of the upper mass class into a demographic litterfall term for each PFT, which is a RED output. This demographic litterfall term, Λ_d , keeps track of the carbon lost from the vegetation due to competition, mortality and the carbon in any such plants that grow out of the largest resolved mass-class-mass class (class I):

$$\Lambda_d = \alpha P(1 - s) + \sum_i \gamma_i M_i + g_I N_I \quad (13)$$

The first term on the righthand-side of this equation represents carbon loss due to the shading of seedlings; the second term represents mortality of the resolved mass classes (which may include disturbance events); and the third term, which is normally very small, is the loss of vegetation carbon due to plants growing beyond the modelled mass classes. In order to initiate regrowth from bare soil, RED also assumes a minimum effective fractional area of each PFT. Where the net assimilate would be sufficiently negative to take the vegetation fraction below this minimum, the minimum value is maintained by subtraction from the demographic litter. The demographic litterfall term therefore represents the net addition litter production consistent with the prescribed net assimilate flux, the disturbance rate, and the change in vegetation carbon modelled by RED. When coupling to an ESM or land carbon model, the demographic litterfall term (Λ_d) should be added to the input local litterfall (Λ_l) (as used in Eq. (8)), to calculate the total litterfall flux into the soil/litter system.

2.5 Steady-State

The steady-state-steady-state of the continuum model defined by Eq. (1) and Eq. (2) can be solved analytical for each PFT ([Moore et al., 2018; ?](#)) ([Moore et al., 2018, 2020](#)). The continuum analytical solutions for the equilibrium mass distribution ($n_{\text{eq}}(m)$), the total plant number (N_{eq}), biomass (M_{eq}), growth-rate-growth rate (G_{eq}) and fractional area (ν_{eq}) are summarised in Appendix B. The shape of the mass distribution and each of these parameters depend on the ratio of plant mortality to growth, which we choose to define for the reference mass class m_0 :

$$\mu_0 = \frac{\gamma m_0}{g_0} \quad (14)$$

In order to initialise the numerical RED model in a drift-free initial state, we also derive the steady-state of the discrete model (Equation-of equation (12)), which will differ slightly from the continuum model for a finite number of mass classes. The equilibrium solution of Eq. (12) ~~defines a recursive relationship for the number of plants N_i in each mass-class:-~~

$$N_i = \lambda_i N_{i-1},$$

where-

$$\lambda_i = \frac{(m_{i-1}/m_0)^{\phi_g} m_0/(m_i - m_{i-1})}{(m_i/m_0)^{\phi_g} m_0/(m_{i+1} - m_i) + \mu_0}.$$

Thus for the discrete model the shape of the mass-number distribution also depends on the mortality-to-growth parameter, is derived in Appendix B2, based on the balance between seedling recruitment and total cohort mortality that defines the equilibrium state. The discretised version of RED thus yields formulae for the coverage (equation (B.28)) and biomass densities (equation (B.30)) which depend on the lowest mass class through the value of μ_0 . Repeated action of Eq. gives an equation for the Similarly, analytical expressions can be derived for total plant number in terms of the number of plants in the lowest mass-class, N_0 :-

$$N_{eq} = \sum_{i=0}^I N_i = N_0 X_N.$$

10 Where X_N :-

$$X_N = 1 + \sum_{i=1}^I \prod_{j=1}^i \lambda_j,$$

and I is the top mass-class. Where i and j are class indices over the sum product. Likewise, we can calculate: and total growth rate of each PFT at equilibrium:

1. the total structural growth at equilibrium:- N_{eq} , the total equilibrium stand density:

$$15 \quad N_{eq} = N_0 X_N \quad (15)$$

2. The total equilibrium structural growth, G_{eq} :

$$G_{eq} = \sum_{i=0}^I N_i g_i = N_0 g_0 X_G, \quad (16)$$

where Eq. implies: $X_G = 1 + \sum_{i=1}^I \frac{m_i \phi_g}{m_0} \prod_{j=1}^i \lambda_j$.

3. the total biomass at equilibrium:- The total equilibrium coverage, ν_{eq} :

$$20 \quad M \nu_{eq} = \sum_{i=0}^I N_i m_i \prod_{j=1}^i a_j = N_0 m_0 X_{M,\nu} \quad (17)$$

where:-

$$X_M = 1 + \sum_{i=1}^I \frac{m_i}{m_0} \prod_{j=1}^i \lambda_j.$$

4. ~~the fractional area covered by the PFT at equilibrium~~: The total equilibrium carbon mass:

$$\nu M_{\text{eq}} = \sum_{i=0}^I N_i a_i^I N_i m_i = N_0 \underline{a m_0} X_{\nu, M} \quad (18)$$

where Eq. implies:-

$$X_{\nu} = 1 + \sum_{i=1}^I \left(\frac{m_i}{m_0} \right)^{\phi_a} \prod_{j=1}^i \lambda_{jz}$$

- 5 ~~We can use an observation to constrain (red dashed arrow) μ_0 giving us an equilibrium coverage. If the addition of total growth is known (black double-headed arrow), we can rearrange μ_0 to find an equilibrium mortality rate (or vice-versa). Here X_N , X_G , X_{ν} and X_M , are functions of μ_0 (see Appendix B2). This equilibrium state is derived by setting $N_i^{(j+1)} = N_i^{(j)}$ in equation (B.17), such that the flux entering into a mass class is equal to the flux leaving that class plus the loss of plants due to mortality.~~
- 10 The equations above therefore define the equilibrium state of the discrete system for given values of N_0 and μ_0 . The value of μ_0 can be estimated from forest demographic data where this is available (~~Moore et al., 2018; ?~~)(Moore et al., 2018, 2020) . However, for global applications we rarely have more observations than the fractional coverage of each PFT. ~~Under these circumstances, we use the condition that at equilibrium the rate of injection of seedlings (Equation) must balance the rate of loss of plants due to mortality (γN_{eq}):~~

$$15 \quad \underline{\gamma N_{\text{eq}} = \frac{\alpha}{(1-\alpha)} \frac{G}{m_0} s.}$$

~~Now substituting in Eq., Eq. Starting from the derived forms for N_{eq} (equation (15)) and G_{eq} (equation (16) and Eq. yields a balance), and requiring that the recruitment flux ($\alpha/(1-\alpha)G_{\text{eq}}s$) is equal to that of the total population dying (γN_{eq}), we can derive an equation for the k^{th} PFT: total equilibrium coverage (full details in Appendix B2):~~

$$\underline{\nu_{\text{eq},k} = 1 - \left(\frac{1-\alpha}{\alpha} \right) \frac{1 - \sum_l c_{kl} \nu_l \equiv \mu_0}{X_G} \frac{X_N}{X_G} = f(\mu_0), \frac{X_N}{X_G} - \sum_{l \neq k} c_{kl} \nu_l} \quad (19)$$

- 20 ~~where X_N and X_G are given by Eq. and Eq. respectively. As the righthand-side~~ As the lefthand-side of this equation depends only on prescribed constants and μ_0 , Eq. (19) can be inverted (by numerical iteration) to estimate μ_0 for observed values of the PFT fractions (~~$\nu_{\nu,k}$, ν_l~~) and an assumed value of α (see Table 3). Once the value of μ_0 has been derived in this manner, it can be used to calculate X_{ν} ~~via Eq.~~, and therefore N_0 by inversion of Eq. ~~(B.28):~~

$$N_0 = \frac{\nu_{\text{eq}}}{a_0 X_{\nu}} \quad (20)$$

- 25 Equations ~~and~~ (19) and (20) therefore allow us to define an initial equilibrium state (N_i) which is consistent with observed area fractions of each PFT (~~Figure ??~~). Furthermore, when paired with an estimate of the net carbon assimilate (from a model or observations), the μ_0 estimate can be converted into a map of the implied mortality (γ) by PFT. We demonstrate this capability ~~as part of the global tests of RED described~~ globally in the next section.

3 Modelling Results

For these [tests runs](#), the numerical RED model is [set-up set up](#) to use the 9 PFTs which are currently used in JULES (Harper et al., 2018). This enables us to directly use driving data - [time-series time series](#) of the rate of net assimilation (P) - from a previous UKESM model simulation that includes JULES (Sellar et al., 2019). RED is integrated forward using a one month

5 time-step and successive [mass-classes mass classes](#) that differ by a multiplicative constant ξ , so that $m_i = \xi m_{i-1}$. The value of ξ was chosen to optimally fit the analytical equilibrium solutions assuming 10 mass classes for trees, 8 mass classes for shrubs and 1 mass class for grasses, assuming $\mu_0 = 0.25$ (see Appendix B3). Other PFT-specific parameters are assumed as summarised in Table 3.

Table 3. [The List of PFT list-names](#) and [their corresponding assumed allometric scaling](#) parameters (m_0, a_0, h_0), seedling fraction (α) and competition coefficient ($c_{\text{pft},j}$). The growth allometry of trees and shrubs across size is assumed to follow ([Niklas and Spatz, 2004](#)) [Niklas and Spatz \(2004\)](#) ($\phi_g = 0.75, \phi_a = 0.5, \phi_h = 0.25$). The competition coefficients given describe which PFT functional group shades the current PFT, if $c_{\text{pft},j} = 1$, the PFT is shaded, otherwise it is not (Table 2).

Long name	Abbrev	Classes	Scaling (ξ)	α	m_0 (kgC)	a_0 (m ²)	$c_{\text{pft},j}$		
							Tree	Shrub	Grass
Broadleaf Evergreen Tree Tropical	BET-Tr	10	2.32	0.10	1.00	0.50	3.00	0	0
Broadleaf Evergreen Tree Temperate	BET-Te	10	2.32	0.10	1.00	0.50	3.00	0	0
Broadleaf Deciduous Tree	BDT	10	2.35	0.10	1.00	0.50	3.00	0	0
Needleleaf Evergreen Tree	NET	10	2.35	0.10	1.00	0.50	3.00	0	0
Needleleaf Deciduous Tree	NDT	10	2.32	0.10	1.00	0.50	3.00	0	0
Cool Season Grasses	C3	1	1.50	0.60	0.10	0.25	0.05	1	1
Tropical Grasses	C4	1	1.50	0.60	0.15	0.25	0.05	1	1
Evergreen Shrub	ESh	8	2.80	0.35	0.15	0.25	3.00	1	0
Deciduous Shrub	DSh	8	2.80	0.35	0.50	0.25	3.00	1	0

3.1 [LocalGlobal: Simulating Succession Diagnosed Plant Mortality Rates](#)

We begin by demonstrating the vegetation succession simulated by RED in an idealised spin-up from bare soil (a minimum vegetation fraction of 0.001 occupying the lowest class.), in this case for a grid-box at the edge of the Amazonian rainforest (Figure ??). Under these circumstances, the diagnosed initial state is indeed the long-term equilibrium state, as evidenced by the horizontal dashed lines in panels a and b of Figure ??.

5 Dynamical run of two RED simulations at grid-box level, dashed transparent lines initialised with the equilibrium solutions, the other (solid lines), initialises from bare soil. Both use the same constant assimilate rate from the UKESM dataset per coverage. (a) is the total vegetation fractions among each of the PFTs. (b) is the corresponding biomass. (c), (d) and (e) provide snapshots of the number density distribution of the PFTs across mass classes at different times. Lines marked as + are the equilibrium runs while X indicates the spin-up run.

10 Faster growing grass PFTs dominate the grid-box within the first twelve years, before being replaced by evergreen shrubs which shade the grass seedlings. Eventually, Broad-leaf Evergreen Tropical trees replace much of the shrub and grass, on a timescale determined in large part by the parameter α and the reference mass class m_0 . With the parameters used here, the vegetation fraction reaches close to its equilibrium value after about 20 years (panel a), but full spin-up of the biomass takes around 150 years (panel b). Having a fixed rate of growth per coverage results in a changing g_0 , as the allometric scaling for growth and coverage differs.

15 The modelled evolution of the plant number versus mass distribution for each PFT is shown in panel c (after 6 years), panel d (after 13 years) and panel (after 100 years), with the eventual demographic equilibrium profiles shown by the dashed lines. It is clear that grass PFTs are close to their demographic equilibrium after only 6 years, but tree PFTs need more than 100 years to reach equilibrium.

20 The dashed lines in Figure ?? represent a dynamical RED simulation from the diagnosed demographic equilibrium state. This state is derived using the methodology described in Section 2.5, with one significant change. The competition rules given by Eq. and Table 2 result ultimately in equilibria which have a single dominate PFT in each class of co-competing types (trees, shrubs, grasses). To avoid drifts associated with the competitive exclusion of the subdominant PFTs in each vegetation class, we choose to initialise the dominant PFT to have the total area fraction of all the PFTs in that vegetation class.

25 3.2 Global: Simulation of Current Vegetation Map

~~In this section we use a similar procedure to diagnose the~~ Here we use the analytical forms for the equilibrium state (Section 2.5) and observations of global vegetation cover, to diagnose the corresponding map of PFT-specific mortality rates. These mortality rates are therefore consistent with the current observed vegetation state, and rates of net assimilation (P) provided ~~by from~~ UKESM (Sellar et al., 2019). The UKESM simulation provides NPP and local litterfall per unit area of each PFT.

30 We multiply by PFT fraction to get the grid-box mean values required to drive RED (using ESA landcover data, as explained below). The observed maps of PFTs are provided by the ESA LC_CCI dataset for 2008-2012 (Poulter et al., 2015), projected onto the 9 JULES PFTs (Figure ??3). Maps of the prescribed annual mean values of the rate of net assimilation (P) are shown in Figure ??4.

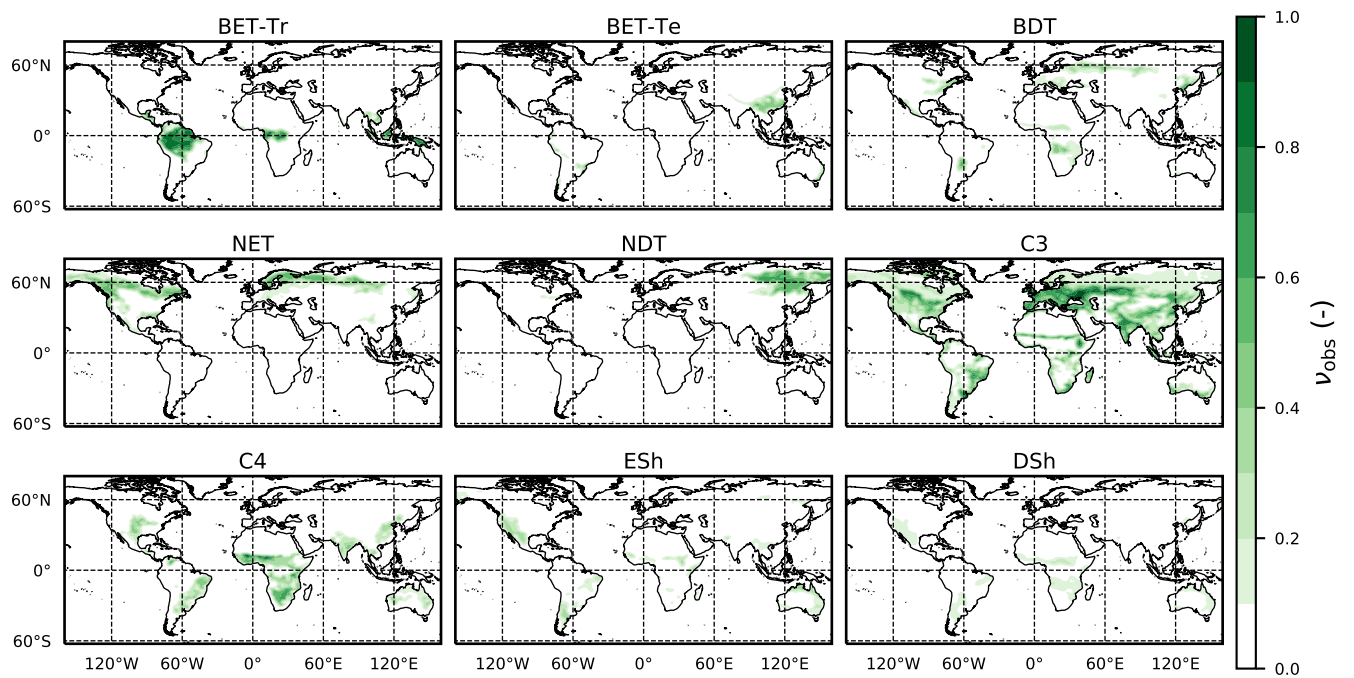


Figure 3. Observed-Observation-based dataset of the PFT fraction-area fractions for the nine JULES PFTs (Harper et al., 2016) ,as given by the title abbreviations listed in Table 3.

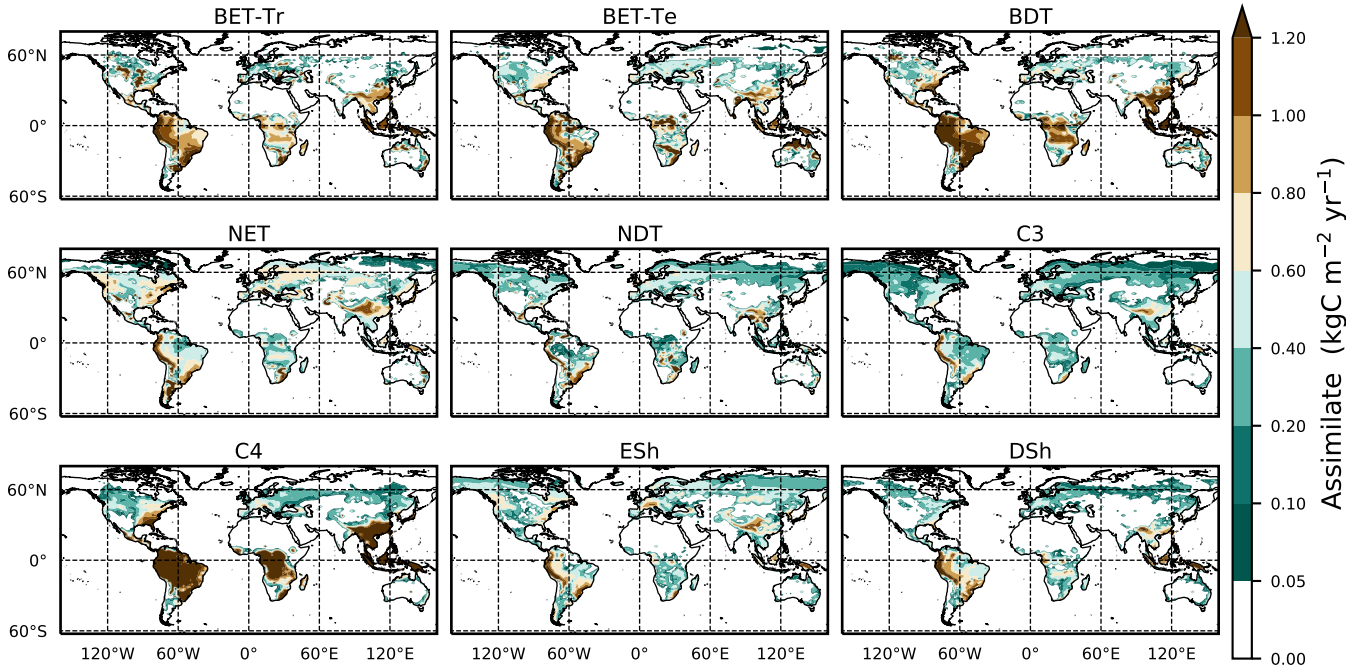


Figure 4. Driving Mean net assimilate $P_{\text{assimilate}}$ (Equation-equation (8)) from UKESM $\bar{\cdot}$ averaged between 2000-2010. The average mean is constructed by truncating setting any negative growth rates to zero.

We use the procedure outlined in Section 2.5 to estimate spatially-varying values of μ_0 for each PFT, using Eq. (B.32), and then Eq. (B.34) to estimate N_0 . This method successfully reproduces the ESA map of dominant PFT to good accuracy, as shown in Figure ??-5 and Table 4.

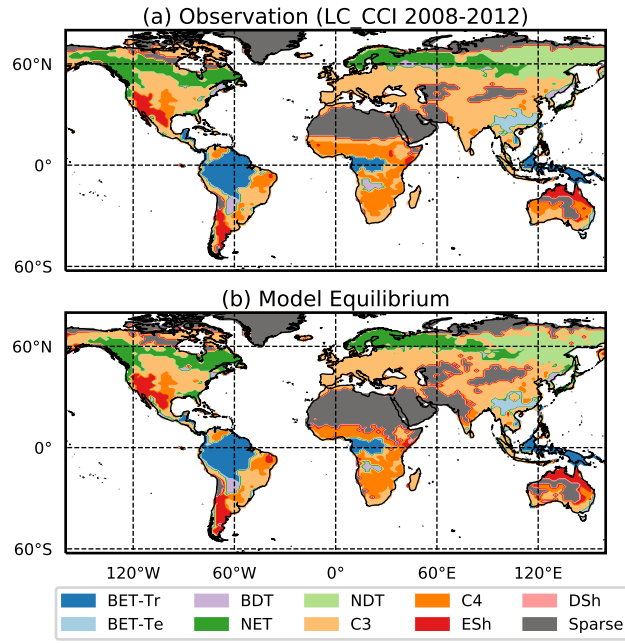


Figure 5. Maps of dominant PFT for (a) Map of observed PFT cover ESA LC_CCI dataset and (b) RED model equilibrium fractions assigned to the nine PFTs Harper et al. (2016). Colour-coded are the PFTs possessing the largest fraction within the grid-box. Sparse area is defined as where the total vegetation coverage of is less than 10%.

Table 4. Goodness of fits for the RED equilibrium coverages to that of the coverages from ESA LC_CCI dataset across the PFTs. r represents the Person's Pearson Correlation Coefficient. The RMSE has been weighted, after weighting by the grid-box area to the mean grid-box area to account for latitudinal variations-variation of grid-box areas.

PFT	r	RMSE
BET-Tr	0.990	0.030
BET-Te	0.935	0.030
BDT	0.783	0.053
NET	0.905	0.051
NDT	0.928	0.033
C3	0.895	0.129
C4	0.818	0.088
ESh	0.854	0.051
DSht	0.525	0.049

There are a few reasons why the model-equilibrium fractions are not an identical fit with the observed fractions. Firstly, the two datasets are not necessarily consistent – there are a few places (The fit of the RED equilibrium vegetation coverage to the ESA observations is generally very good (Table 4). However, it is imperfect in some areas (e.g. Central Asia, Sahel) where the average UKESM-assimilates-used is zero, not aligning with the positive coverage from the ESA dataset. Secondly, areas of mixed where the driving net assimilate from UKESM is zero or negative. Also, areas where the observational dataset indicates co-existing PFTs within the same vegetation class, as previously stated, will have an adjusted RED equilibrium fraction where the dominant PFT equilibrium will be the sum of the vegetation class.

3.2 Global: Diagnosed Plant Mortality Rates

As (e.g. broadleaf trees and needleleaf trees) are not well simulated by this first version of RED, which leads to competitive exclusion in the equilibrium state (see Discussion). Since we now have diagnosed values of μ_0 and N_0 , along with prescribed values of P , we can also diagnose the mean plant mortality rate γ , for each location and for each PFT, from Eq. (14) :

$$\gamma = \frac{\mu_0 g_0}{m_0} \quad (21)$$

where g_0 is given by Eq. (11) combined with Eq. (B.18) and Eq. (B.20). The maps of γ values, derived in this way, are shown in Figure 6.

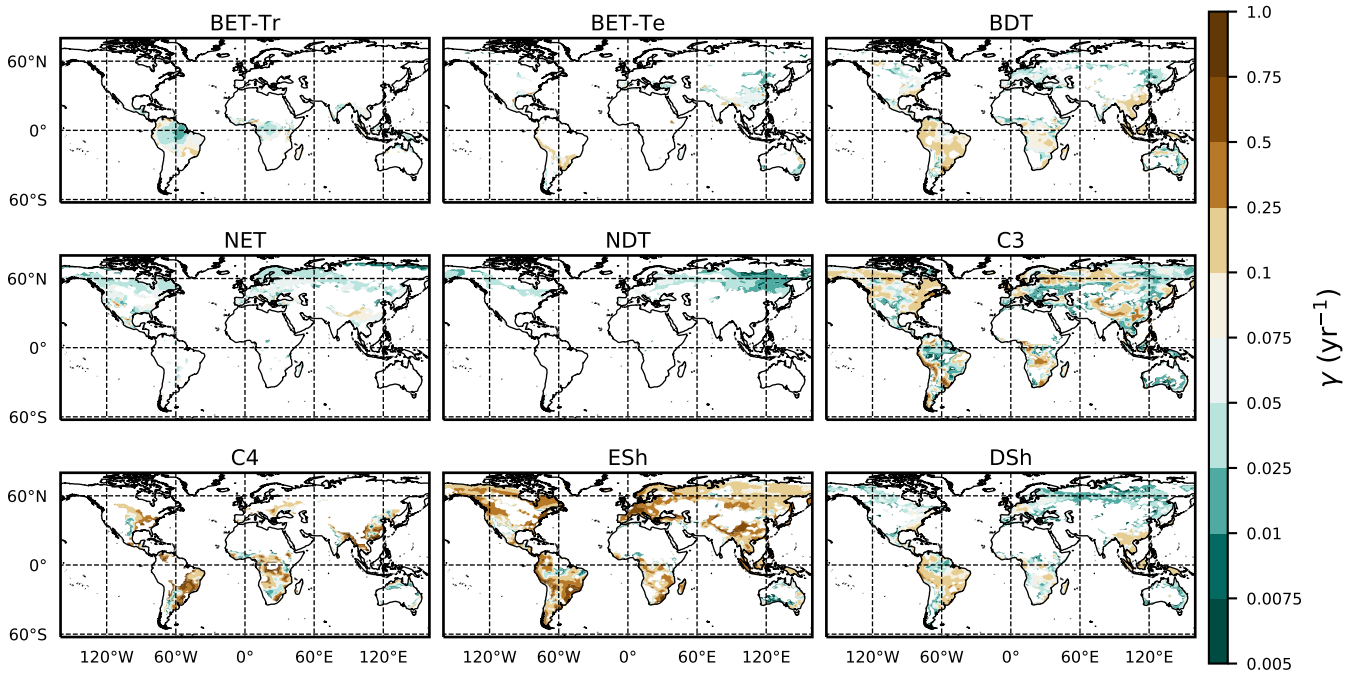


Figure 6. Diagnosed maps of mortality rates γ for each PFT, as required for consistency with the ESA observations and the UKESM growth rates. White areas correspond with zero coverage and/or zero growth –mortality is assumed infinite within RED.

The mortality rate derived is ~~very~~ dependent on the ~~overall-assumed areal~~ coverage and the total assimilate. ~~Having a~~ high coverage with a low growth rate will result in ~~RED-compensating through having a low-a compensating low diagnosed~~ mortality rate (and vice-versa). ~~This explains why some mortality rates of PFTs seem to posses large variations (Figure ??).~~ Furthermore, the choice of α (~~Equation equation~~ (11)) and ~~the~~ m_0 ~~is also influential when it comes to the~~ ~~also influence the diagnosed~~ value of γ . ~~An analysis of the sensitivity of the inferred value of γ to these factors is presented in Appendix C. Assuming $\pm 20\%$ uncertainty on assimilate, α , m_0 and $\pm 5\%$ on the coverage gives an uncertainty bound of $\pm 35\%$ on γ .~~ Under the assumption that high coverages are ~~close to a ‘healthy’ environment for a PFT. We can indicative of the baseline mortality for a given PFT, we~~ take a sub-sample of the grid-boxes that are within the top quartile of non-zero coverages ($\nu_{eq} > 0.01$) (Table 5). The median μ_0 value diagnosed from the top quartile of BET-Tr of $0.232_{-0.007}^{+0.008}$ (Table 45), is ~~very~~ close to the ~~values-calculated~~ ~~by-value calculated in~~ our previous paper ~~(?)~~ (Moore et al., 2020) of approximately 0.235 for all of South America. ~~The-value within the paper 0.198 is converted to dry carbon mass through Eq. . Carbon dry mass constitutes approximate half of the total dry mass (Thomas and Martin, 2012). In addition to parametrisations (such as α), some of the differences between these μ_0 values can arise from the discretization of the model, as the discretised form will underestimate the diagnosed μ_0 values to meet the same observation – when compared with the continuous form (Figure ??).a). A possible usage of RED might be to~~ ~~diagnose a μ_0 , fix a baseline mortality rate from surveys and diagnose the required carbon assimilate to match an additional observation (Figure ??).~~ Potentially providing a future constraint on ESM growth rates for PFTs. ~~using the RAINFOR sites.~~

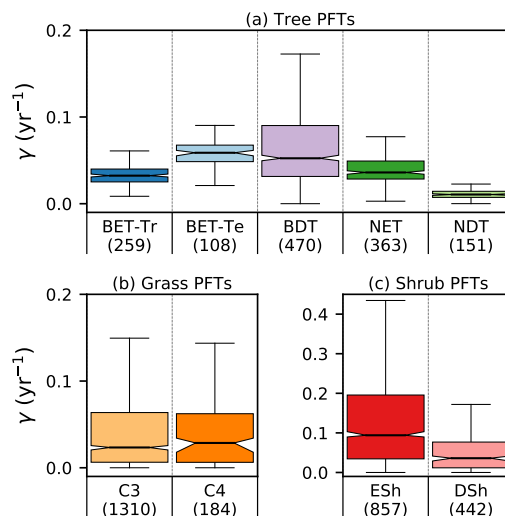


Figure 7. ~~Diagnosed~~ ~~Diagnosed~~ mortality rates for (a) trees, (b) grasses and (c) shrubs ~~for non-zero in the top quartile of~~ coverage ($\nu_{eq} > 0.01$). ~~Hatches~~ ~~Notches~~ within the box represent the confidence bounds of the median. The confidence bounds are estimated using a bootstrap method. Bracketed numbers represent the number of grid-points.

~~There have been multiple site-level assessments of the rates of stand mortality within pan-tropical forests – typically the background rate is between 1 yr^{-1} to 4 yr^{-1} (Lugo and Seaten, 1996; Phillips, 1996; Phillips et al., 2004). (Phillips, 1996) estimates 60 mortality rates collected across 40 pan-tropical sites for tree sizes greater than 10–25 cm dbh. Later work by~~

Phillips in 2004 used the demographic data from the RAINFOR dataset of trees $\geq 10\text{cm dbh}$. Using these site assessments, we can make a comparison to BET-Tr equilibrium mortality rates by looking at the values of γ in areas where we would expect to see old growth forests. Within the top 25% of coverages, we assume represent areas of undisturbed forest. BET-Tr captures the baseline mortality rates seen post 2000 in the Amazon from site data (Figure ??).

Table 5. The ~~area-weighted~~ ~~area-weighted~~ median values of ~~driving~~ ~~observed~~ coverage and ~~driving net~~ assimilate against μ_0 and γ for the upper quartile of grid-boxes of greater than 0.01 for each PFT.

PFT	Area weighted median			
	ν_{obs}	P (kgC m ⁻² yr ⁻¹)	μ_0	γ (yr ⁻¹)
BET-Tr	0.793 ^{+0.019} _{-0.023}	0.731 ^{+0.054} _{-0.041}	0.232 ^{+0.008} _{-0.007}	0.032 ^{+0.002} _{-0.001}
BET-Te	0.402 ^{+0.020} _{-0.030}	0.349 ^{+0.022} _{-0.028}	0.340 ^{+0.006} _{-0.004}	0.059 ^{+0.003} _{-0.003}
BDT	0.238 ^{+0.011} _{-0.011}	0.143 ^{+0.018} _{-0.014}	0.377 ^{+0.013} _{-0.011}	0.052 ^{+0.003} _{-0.003}
NET	0.471 ^{+0.009} _{-0.011}	0.281 ^{+0.005} _{-0.013}	0.328 ^{+0.008} _{-0.009}	0.036 ^{+0.002} _{-0.002}
NDT	0.597 ^{+0.010} _{-0.015}	0.112 ^{+0.009} _{-0.008}	0.298 ^{+0.008} _{-0.007}	0.011 ^{+0.001} _{-0.001}
C3	0.566 ^{+0.011} _{-0.007}	0.124 ^{+0.008} _{-0.006}	0.163 ^{+0.017} _{-0.013}	0.023 ^{+0.002} _{-0.003}
C4	0.545 ^{+0.043} _{-0.053}	0.123 ^{+0.084} _{-0.040}	0.189 ^{+0.044} _{-0.027}	0.029 ^{+0.006} _{-0.010}
ESh	0.142 ^{+0.009} _{-0.007}	0.028 ^{+0.002} _{-0.001}	0.744 ^{+0.019} _{-0.021}	0.094 ^{+0.010} _{-0.004}
DSh	0.116 ^{+0.010} _{-0.015}	0.024 ^{+0.006} _{-0.004}	0.713 ^{+0.046} _{-0.027}	0.036 ^{+0.005} _{-0.007}

- 5 [Site-level assessments of the rates of stand mortality within pan-tropical forests conclude a range of background rates \(Lugo and Scatena, 1996\). Phillips \(1996\) estimates mortality rates collected across 40 pan-tropical sites for tree sizes greater than 10 – 25 cm dbh. Later work by Phillips et al. \(2004\) used the demographic data from the RAINFOR dataset of trees \$\geq 10\text{cm dbh}\$. Using these site assessments, we can make a comparison to BET-Tr equilibrium mortality rates by looking at the values of \$\gamma\$ in areas where we would expect to see old growth forests. We use the top 25% of coverages of the BET-Tr PFT to represent plausible areas of undisturbed forest. Figure 7 shows that the diagnosed baseline mortality rates are in reasonable agreement with these observational estimates for Amazonia.](#)
- 10

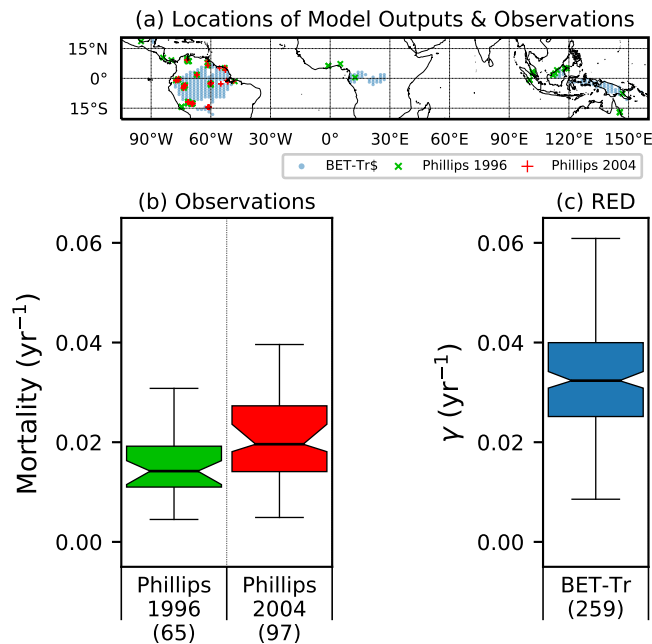


Figure 8. Comparison of observed observation-based estimates of tropical tree mortality with γ . Comparing datasets presented in (Phillips, 1996; Phillips et al., 2004) to γ values diagnosed from RED for an adjusted estimate of observed stand mortality with the equilibrium mortality rates for BET-Tr within PFT (for the largest top 25% of fractions for this PFT). (a) shows the observations locations location of observational sites (blue and green crosses) versus the chosen RED grid-points (red circles); (b) shows the distribution of mortality across grid-boxes, while; (c) shows the mortality distribution across the BET-Tr grid-points. Red diamonds represent the mean, while the bracketed Bracketed numbers in panel (b) represent the number of measurements from, and in panel (c) the datasets number of gridpoints.

Next There is a need to better understand the influence of mortality arising from disturbance events such as droughts and fire in order to constrain model projections (Pugh et al., 2020). Here we investigate if the equilibrium mortality rates implicitly capture areas of disturbances. We compare the mean woody equilibrium, by comparing the mean tree mortality rate to fire and land-use surveys. The woody (the mean mortality is defined as the sum of here by weighting grid-box γ weighted against the coverage of Trees and Shrubs to their collective coverage. Areas with large rates of disturbances area generally not expected to conform to the equilibrium assumptions, such as DET, used to initialise RED. Generally, biomes, that are humid and dry such as savannah or grassland, wildfires play a natural part in maintaining the balance of vegetation (Bond et al., 2005), therefore for woody PFTs we expect to see a raised mortality/higher μ_0 values by grid-box fractional coverages). There are a number of surveys relating stand mortality in regions prone to wildfires (Swaine, 1992; Kinnaid and O'Brien, 1998; Peterson and Reich, 2001; Van N
 5
 10
 . In a broad sense, post-fire mortality rates can range from 0.06 yr^{-1} to catastrophic rates around 0.8 yr^{-1} and can vary quite considerably depending on tree species, fire frequency and drought severity. The drought-fire interaction is responsible for significantly increasing mortality post-fire and can be a driving cause of regional die-back (Allen et al., 2010; Brando et al., 2014)

. Using the ESA FIRE_CCI dataset (Chuvieco et al., 2019) we can estimate the rate of burnt burnt vegetation fraction per year:

$$BF = \frac{\text{Burnt Area}}{\text{Burnable Fraction} \times \text{Area}} \times \frac{1}{\Delta t},$$

where Burnt Area and Burnable Fraction are given from the dataset. Area is inferred from the longitude, latitude quadrant.

5 The resolution of FIRE_CCI is $0.25^\circ \times 0.25^\circ$ is bi-linearly interpolated onto the simulated grid-boxes. Taking the averages of the burnt fraction rate between Taking the average burnt vegetation fraction for the months between 2000 and 2010, and converting into an annual burn rate we gain an estimate of fire severity.

We also carry out a comparison with agriculture, we expect that in area of Another key issue is anthropogenic land-use we will see raised mortality for woody PFTs as the industry will use the space for crops and pasture. There is difficulty in

10 getting an explicit rate of clearance from and land-use, however, by comparing with the fraction of cropland we achieve a non-direct geographic comparison to the to change (Nepstad et al., 2008; Haddad et al., 2015). Fragmentation of natural forests is understood to raise the mortality of the dataset (Figure ??). For the crop fraction we use remaining forest and to decrease the overall resilience of the ecosystem (Esseen, 1994; Laurance et al., 1998; Jönsson et al., 2007). In order to maintain a near-constant agricultural fraction, regular disruption such as grazing is needed to prevent re-colonisation and secondary

15 succession (Dorrough and Moxham, 2005; Van Uytvanck et al., 2008; Chaturvedi et al., 2012). We carry out a comparison with land-use using the 2000 ESA LC_CCI inferred PFT from (Li et al., 2019) of half a degree resolution – again interpolating onto the RED grids. Comparison of the mean grid-box baseline mortality rate for ‘Woody’ PFTs (BET-Tr, BET-Te, BDT, ESh, DSh) (a) to disturbances – With fractional rate of burnt area (area burnt divided by burnable area) from ESA FIRE_CCI (b) and with a crop coverage from the PFT classification of the ESA LC_CCI 2000 Dataset (c). (d) describes where we see higher rates of mortality (condition i, $\gamma > 0.05 \text{ yr}^{-1}$) overlapped with areas of fire (condition ii, $BF > 0.05 \text{ yr}^{-1}$) and land-use (condition iii, $\geq 10\%$). Comparison of the mean woody baseline mortality rate within areas of remotely sensed fire fractions from the FIRE_CCI and crop-land areas. There crop coverages (Li et al., 2019).

In Figure 9, we see the derived observations for burn area (a) and crop fraction (b), along with the derived mean γ for the tree PFTs (c). From Figure 9 (d), we see that there are areas of spatial overlap of disturbance with that larger mortality rates (defined

25 as $\gamma \geq 0.05 \text{ yr}^{-1}$ and a similar burn rate) with Figure ?? . d. This would be expected, as areas of increased disturbances typically have PFTs with faster demographic turnovers with large mortality ($\gamma > 0.075 \text{ yr}^{-1}$) that do correspond to areas where we see large fire activity (burn rate $> 0.1 \text{ yr}^{-1}$) and increased crop fraction (> 0.25). However, large burn rates are seen to overlap in parts of central Brazil around the Cernado region, Southern Africa and North Western Australia where fires are understood to play a significant part within the ecosystem (Coutinho, 1990; Medeiros and Miranda, 2008; Prior et al., 2009; Staver et al., 2009)

30 There are also some areas of agriculture which correspond to deforestation, such as in the Atlantic forests of Brazil and in Indonesia (Higuchi et al., 2008; Curran et al., 2004). Areas of increased disturbances result in grasses and shrubs, dominating the environment, with the local areas either being more fire prone, or under agriculture. We see this clearly in areas such as South-Eastern Brazil and around Central Africa, there are areas of high mortality overlapping with areas of high land-use and /or fire. Furthermore, we see in Europe and parts of China there are large mortality rates overlapping with high fractions of

~~pastures-dominating (Figure 3).~~

~~If the carbon assimilate is similar to that of forests, to compensate for the lower observed coverage of woody PFTs the trees will possess higher mortality rates. Such compensation will be a non-direct approach to estimating mortality of disturbance-prone areas. We see that in comparison to~~

- 5 ~~Analysis of the RED equilibrium is an indirect approach to estimating tree mortality based on simple yet mechanistic principles of demography, and relying on few inputs (vegetation cover and assimilate). It is however conditional on the assumed estimates of vegetation coverage and net rates of assimilation.~~

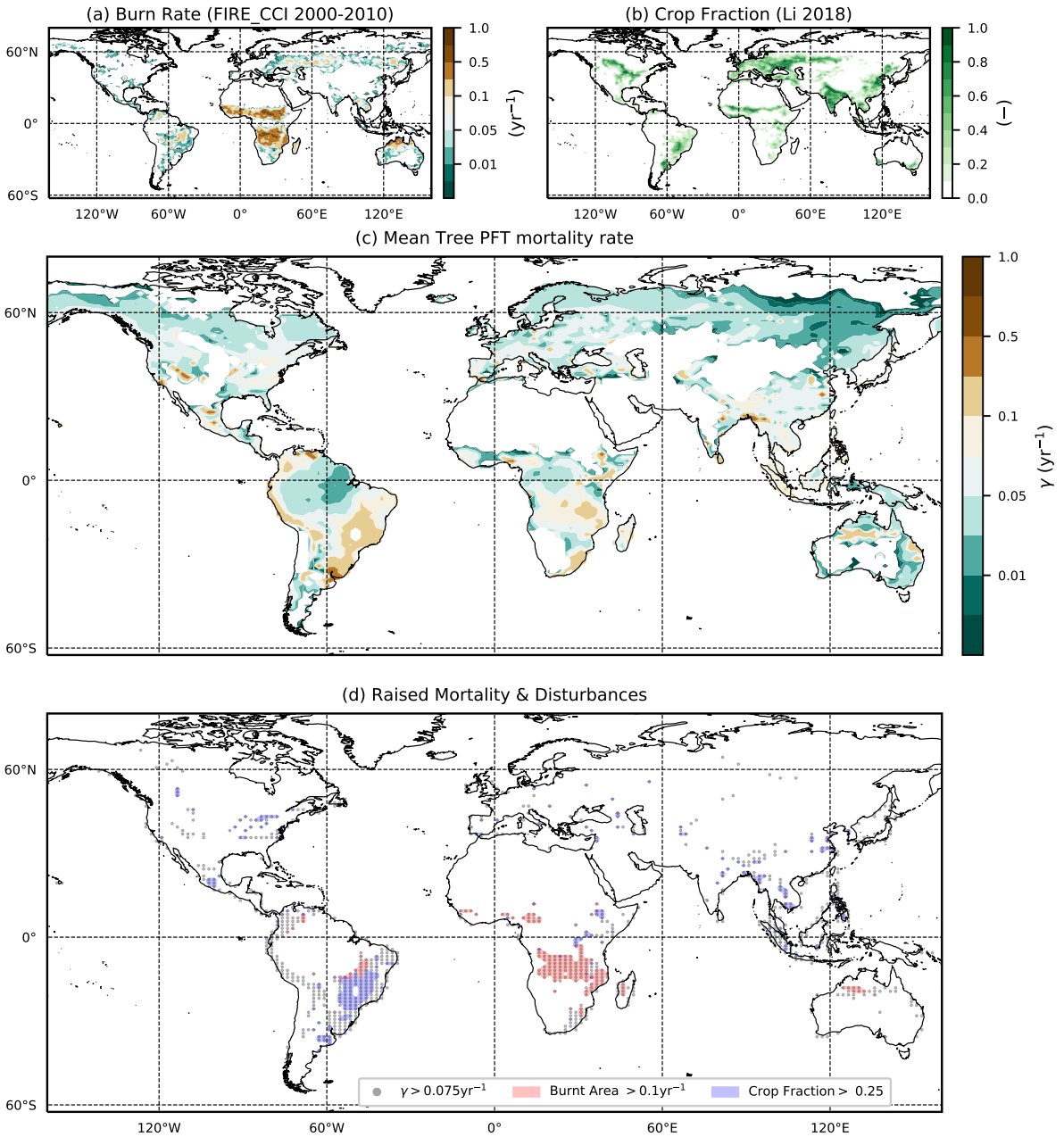


Figure 9. Comparison of diagnosed mortality rates, with observation-based maps of fire and land-use. (a) annual burnt area fraction from the ESA FIRE_CCI dataset; (b) crop fraction from the ESA LC_CCI 2000 dataset; (c) diagnosed mortality rate γ for the tree PFTs (BET-Tr, BET-Te, BDT, NET, NDT); (d) overlap of areas of higher tree mortality rates ($\gamma > 0.075 \text{ yr}^{-1}$) with areas of fire (Burnt Area $> 0.1 \text{ yr}^{-1}$) and agriculture (Crop Fraction $> 30\%$).

3.2 Dynamical Simulations

3.2.1 Local: Simulating Succession

In this subsection we demonstrate the vegetation successional dynamics simulated by RED in an idealised spin-up from bare-soil, for a grid-box at the edge of the Amazonian rainforest (Figure 10). Under these circumstances, the diagnosed initial state is indeed the long-term equilibrium state, as evidenced by the horizontal dashed lines in panels a and b of Figure 10.

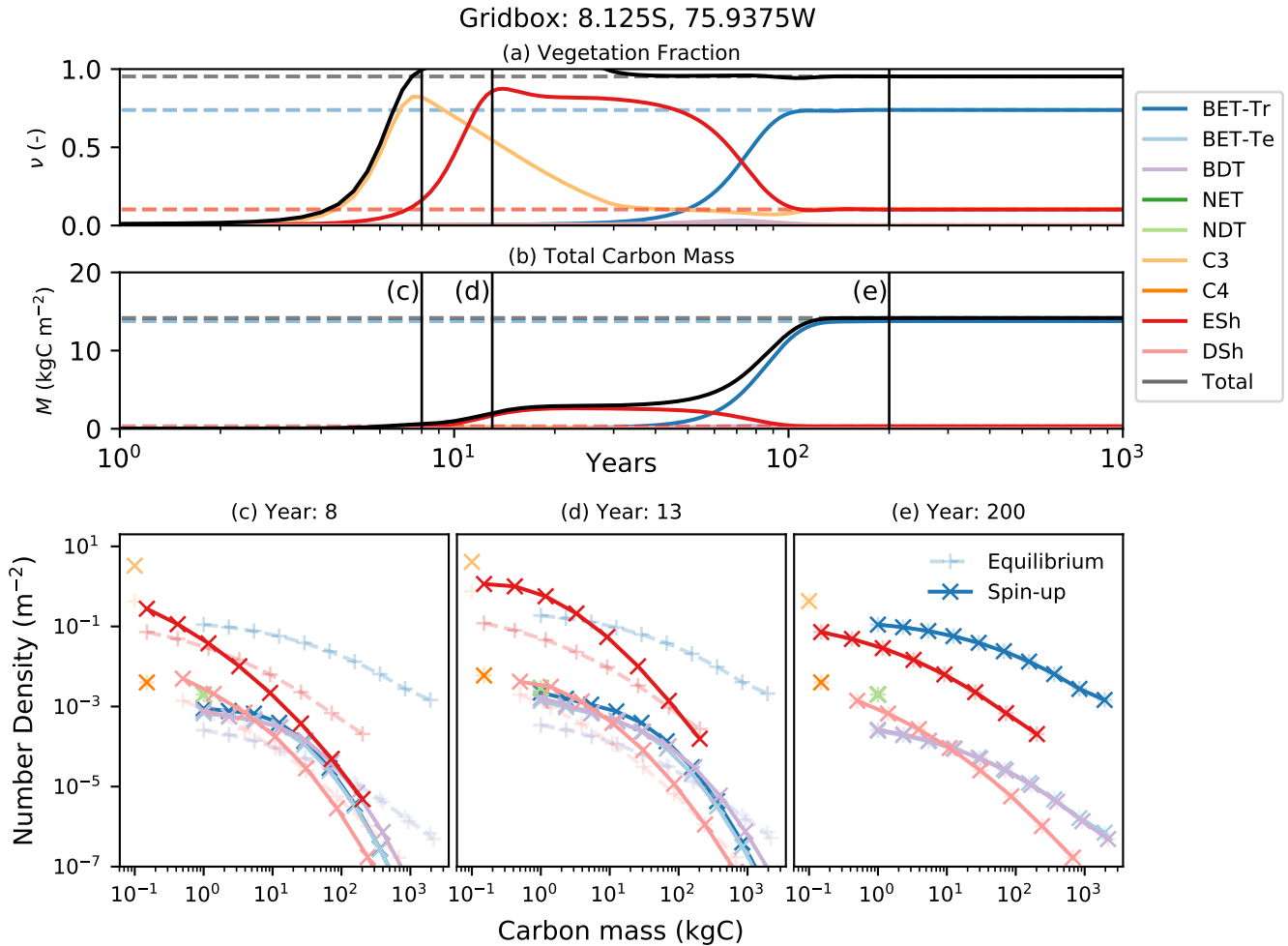


Figure 10. Dynamical runs of RED for a grid-box at the edge of the Amazonian rainforest, starting from bare soil (solid lines) and the diagnosed equilibrium state (dashed lines). (a) PFT fractions versus time; (b) biomass versus time; (c), (d) and (e) snapshots of the number density distribution of the PFTs across mass classes at different times. Lines marked as + are the equilibrium runs while X indicates the spin-up run. The ultimate steady-state is determined by the balance between recruitment and mortality (equation (6)). Intra- and inter-PFT occurs here through the shading of seedlings, which implies that just a fraction of the gridbox (s, 'space' or 'gap' fraction) is available to grow seedlings (equation (7)).

Faster growing grass PFTs dominate the grid-box within the first twelve years, before being replaced by evergreen shrubs which shade the grass seedlings. Eventually, Broad-leaf Evergreen Tropical Trees replace much of the shrub and grass, on a timescale determined in large part by the parameter α and the reference mass class m_0 . With the parameters used here, the vegetation fraction reaches close to its equilibrium value after about 20 years (panel (a)), but full spin-up of the biomass takes

5 around 150 years (panel (b)).

The modelled evolution of number density versus mass distribution for each PFT is shown in panel (c) (after 6 years), panel (d) (after 13 years) and panel (e) (after 100 years), with the eventual demographic equilibrium profiles shown by the dashed lines. It is clear that grass PFTs are close to their demographic equilibrium after only 6 years, but tree PFTs need more than 100 years to reach equilibrium.

10 The dashed lines in Figure 10 represent a dynamical RED simulation from the diagnosed demographic equilibrium state. This state is derived using the methodology described in Section 2.5, with one significant change. The competition rules given by Eq. (7) and Table 2 result ultimately in equilibria which have a single dominate PFT in each class of co-competing types (trees, shrubs, grasses). To avoid drifts associated with the competitive exclusion of the subdominant PFTs in each vegetation class, we choose to initialise the dominant PFT to have the total area fraction of all the PFTs in that vegetation class.

15 3.2.2 Global: Spin-up from Bare Soil

Transient simulations of global vegetation will be the subject of a future paper, but in the final subsection of this paper we wish to demonstrate the utility of the ~~distribution of mortalities increases in areas of observed land-use and fire (Figure ??), however it does underestimate the annual burn rate.~~ semi-analytical equilibrium for initialisation of global model runs. Figure 11 shows the time-evolution of global mean PFT fractions and biomass from a global run driven by net assimilation rates from

20 the UKESM model. Once again, two RED simulations are shown, one started from bare soil (solid lines) and the other from the semi-analytical equilibrium state (dashed lines). Using a constant assimilate rate (Figure 4) and the mortality distribution (Figure 7), we see convergence of these two runs, but only after more than 1000 years of simulated time. The ability to diagnose the equilibrium state therefore has the potential to reduce model spin-up time hugely, especially for Earth System Models (ESMs) applications.

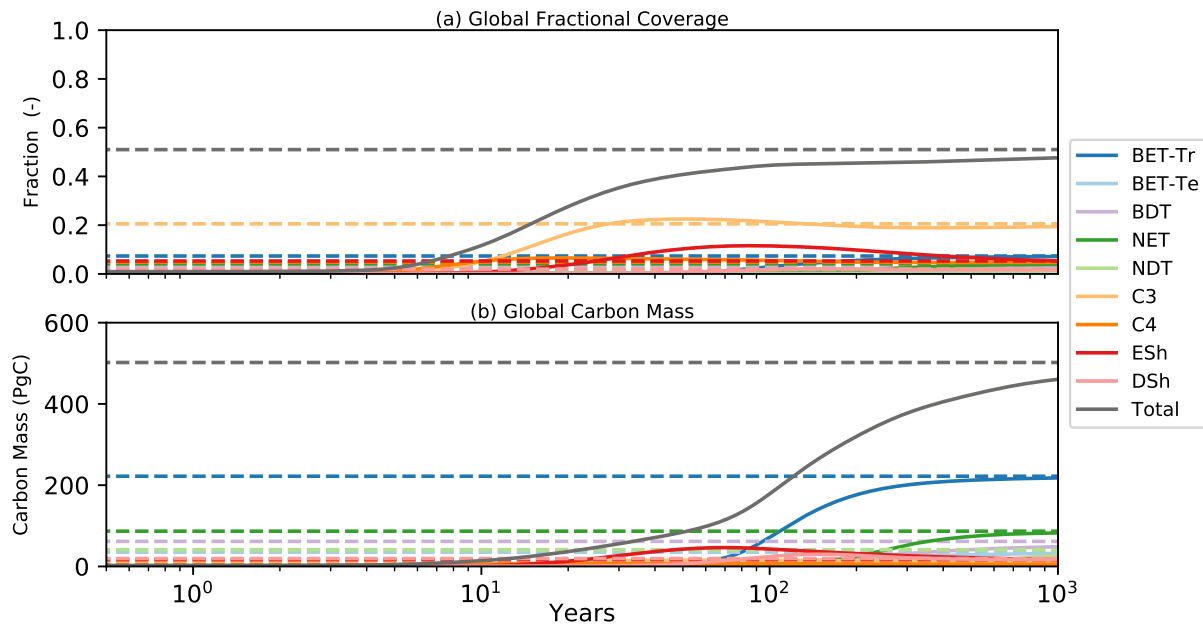


Figure 11. Global model spin-up from bare soil. As for figure 10, solid lines are spin-up from bare soil, dashed lines are the equilibrium instillation run. Panel (a) represents the fractional global coverage relative to the total land area; panel (b) represents the total biomass of the vegetation.

4 Discussion

The response of the land surface to climate change is a key uncertainty in climate projections. Ambitious climate targets also rely on land management practices such as reforestation and afforestation to increase the storage of carbon on land. First-generation Dynamic Global Vegetation Models (DGVMs) attempted to model the the land surface in terms of bulk properties such as mean vegetation cover, vegetation carbon and leaf area index. These models lack information about the plant size-distribution, which compromised their ability to represent recovery from disturbance and the impact of land-managementland management. Providing useful guidance on these issues requires improved DGVMs which can represent changes in tree size distributions within forests (so called ‘demography’). A number of much more sophisticated second-generation DGVMs are now under development. These models often explicitly simulate the number of plants within different size or mass classes, and on different patches of land, which are defined by the time since a disturbance event. Such second generation models are therefore in principle able to simulate variations in plant number density as both a function of patch age and plant size. However, this completeness is at the expense of much computational complexity. In principle, the number of age-defined patches grows indefinitely, and this can only be managed by arbitrarily merging patches of different ages after a certain age. and parameter complexity.

15 In this paper, we represent an intermediate complexity second generation DGVM (‘RED’), which is designed to capture

~~important features of plant demography~~ Our previous work in evaluating demographic equilibrium theory for regional forest inventory datasets in North America (Moore et al., 2018) and using RAINFOR sites for South America (Moore et al., 2020), has provided the theoretical basis for the development of RED. In those studies we found that tree-size distributions within observed forests can be satisfactorily understood in terms of demographic equilibrium in the size dimension alone. This is a reduction in complexity compared to other cohort models which are based on patch age, and yet ~~avoid unwieldy computation.~~ Our guiding principles in the development of RED have been that the model should: (i) simulate forest tree-size distributions; (ii) be globally applicable for ESM applications; (iii) be parameter sparse to minimise parameter uncertainties; (iv) be analytically soluble for steady-states to aid model initialisation. These design criteria, along with evaluation exercises against observed tree-size distributions in North America (Moore et al., 2018) and South America (?), has led us to an improvement in ecological fidelity compared to older phenomenological DGVMs such as TRIFFID (Cox, 2001). The modular design of RED allows for easy coupling to land-surface schemes, merely requiring the per unit grid-box total carbon assimilate rate and any additional mortality disturbance rates as inputs for each grid-box (Figure 2). In principle, RED allows scope for more complex tree size-dependent processes, although in this first study we chose to assume size-independent (but spatially varying) mortality rates for each PFT. Our previous work suggests that this is a good first-order assumption (Moore et al., 2018, 2020).

~~Internally within the model we~~ make a number of simplifications. Firstly, the number density for each PFT is treated as a function of plant mass alone. This immediately eliminates the need to explicitly represent patches, and therefore removes age as an independent dimension. This is a distinct approach relative to cohort DGVMs which are based on patches defined by time since disturbance, such as the POP or ORCHIDEE-MICT models (Haverd et al., 2014; Yue et al., 2018). Secondly, we assume that plant ~~growth rates~~ growth rates vary as a power of plant mass. By default we assume a power of $\phi_g = 3/4$, which is consistent with Metabolic Scaling Theory (Enquist et al., 1998) and the empirically determined allometric relationships of (Niklas and Spatz, 2004). ~~Niklas and Spatz (2004).~~

Finally, we assume that ~~light-competition~~ competition is only significant for the lowest ‘seedling’-‘seedling’ mass class. This enables us to ~~capture the impacts of light competition on seedling emergence through a simple ‘gap’ boundary condition~~ represent gap dynamics among plants and resultant stages in succession. This represents a significant simplification compared to other approaches involving the Perfect Plasticity Assumption (PPA), as used within DGVMs such as LM3-PPA or CLM(ED) (Fisher et al., 2015; Weng et al., 2015), where canopies are assumed to perfectly fill gaps through photomorphism (Strigul et al., 2008). In LM3-PPA the radiative flux is limited by the available gap fraction in a given crown layer. PPA parallels our gap boundary condition at the lowest mass class (equation (6)), but in RED the growth of a cohort is purely dictated by the the disaggregation of total growth assimilate assuming metabolic scaling (equation (11)).

These simplifications allow RED to be solved analytically for the ~~steady-state~~ steady-state vegetation cover given information on the mortality and growth rates per unit area for each PFT. Such analytical steady-state solutions mean that RED can be easily initialised in drift-free pre-industrial states, which is vital to avoid spurious sources and sinks in climate-carbon cycle projections. The analytical solutions also enable RED to be calibrated to the observed vegetation cover, via a single parameter (μ_0) which represents the ratio of mortality to growth for a tree of an arbitrary reference mass. ~~The existence of analytical steady-state solutions for RED also opens up other promising research avenues. For example, these solutions imply~~

relationships between the fractional coverage of each PFT, total plant biomass, and the ratio of mortality-to-growth. This in turn allows RED to be calibrated using observations of any two of these quantities. The analytical solutions also allow optimality hypotheses to be explored (e.g. the hypothesis that the fraction of net assimilate allocated to seed production maximises stand-density and/or biomass).

5 Aside from the existence of analytical ~~stead-state~~ steady-state solutions, RED is attractive for large-scale applications because it is both parameter sparse (‘parsimonious’) and requires very few driving variables. The main driving variable is the time-varying net plant ~~growth-rate~~ growth rate for each PFT, which is defined as net primary production minus the local ~~litter-fall~~ litterfall. These driving data can be provided by a land-surface scheme, as we do in this study, or from observations. The only other driving variable for RED is the mortality rate, which we treat in this study as a geographically-varying PFT-specific constant that
10 is independent of mass, ~~but which could be dependent~~. However, in principle RED could utilise mortality rates that depend on plant mass and time to represent individual disturbance events (e.g. forest fires, disease outbreaks). Despite its simplicity, the RED ~~modelling model~~ is able to fit the global distribution of vegetation types (Figure ??5), and ~~simulates realistic succession~~ simulate successional dynamics, including changes in forest demography (Figure ??10).

There are inevitably weaknesses with any particular modelling approach. For RED, a current limitation is for competition to
15 lead to a single PFT at each location within each co-competing vegetation class (i.e. tree, shrub, grass). The PFT with the highest equilibrium fraction will ~~end-up~~ end up excluding sub-dominant PFTs within the same vegetation class. It was necessary for us to account for this eventual competitive exclusion to derive zero-drift ~~steady-states~~ steady-states for the global runs presented in Section 3.2.1. Such competitive exclusion is a common problem in DGVMs (Fisher et al., 2018). ~~Adapting the ‘gap’~~ Currently, RED would therefore not be the most appropriate DGVM to answer important questions regarding the role
20 of biodiversity in ecosystem function (Pavlick et al., 2013; Levine et al., 2016). More sophisticated DGVMs are required to simulate plant diversity, such as individual-based models (Fischer et al., 2016), and DGVMs specifically-designed to capture sub-gridscale patch dynamics (Longo et al., 2019a, b). Adapting our ‘gap’ boundary condition (Equation equation (7)) appears to be a promising way to ~~deal with this issue~~ allow greater PFT diversity in RED, without unduly increasing model complexity. We see this as a key priority for future research.

25 ~~The existence of analytical steady-state solutions for RED also opens up other promising research avenues. For example, these solutions imply relationships between the fractional coverage of each PFT, total plant biomass, mean canopy height, and the ratio of mortality-to-growth. This in turn allows RED to be calibrated using observations of any two of these quantities (Figure ??). The analytical solutions also allow optimality hypotheses to be explored (e.g. the hypothesis that the fraction of net assimilate allocated to seed production maximises stand-density and/or biomass)~~ RED is currently being coupled to the JULES
30 Land Surface Model, replacing TRIFFID as the default DGVM within that framework. In parallel, significant improvements are being made to the representation of physiological processes in JULES, most notably through the representation of non-structural carbohydrate (‘SUGAR’, Jones et al. (2019)), and through the inclusion of a coupled model of stomatal conductance and hydraulic failure under drought stress (‘SOX’, Eller et al. (2018, 2020)). Plans are also being made to derive the mortality rates for RED from the INFERNO forest-fire model (Burton et al., 2019). These developments will allow us to simulate the effects
35 of size-dependent tree mortality rates within the near future.

5 Conclusions

In this paper we have presented a new intermediate complexity second generation Dynamic Global Vegetation Model (DGVM), which captures important changes in forest demography. The *Robust Ecosystem Demography (RED)* model makes a number of important simplifications to achieve this. These simplifications are ~~based-on-theoretical-ideas-based-on-theoretical~~ concepts (e.g. metabolic scaling theory to estimate how plant ~~growth-rate~~ growth rate varies with plant mass, and ~~perfect crown plasticity to minimise light competition~~ minimum crown overlap) and also comparison to observed forest demography (~~Moore et al., 2018; ?~~) (Moore et al., 2018, 2020). As a result, RED is parameter sparse, and can be driven with time-series of net plant growth rate (and optionally disturbance rates) for each Plant Functional Type (PFT). We have demonstrated that RED can be calibrated effectively to observed global vegetation maps, using a single fitting parameter (representing the ratio of mortality to growth for a plant of an arbitrary reference mass). The next stage will be to use RED in coupled climate-carbon cycle projections so to assess how changes in vegetation demography impact future ~~CO2~~ CO₂ and climate. We have made the prototype RED code publically available, and we hope that Earth System and land-surface modellers will make good use of this framework to further their own research.

Code availability. The RED model Python Code is archived at <https://doi.org/10.5281/zenodo.3548678>. Furthermore, RED is currently being coupled into JULES, where a basic integration currently exists as branch (vn5.4_veg3_ctrl) - this requires registration for the JULES repository (<https://code.metoffice.gov.uk/trac>).

Appendix A: ~~Definitions~~ Functional Form of Flux F_i in Discretised RED

~~List of Model Variables and Parameters Symbol Definitions Units t Time, year m Carbon mass of an individual within a PFT. kgC P Total assimilate of Net Primary Productivity minus Local (Leaves, Wood and roots) Litterfall kgC $m^{-2} yr^{-1} \gamma_d$ Disturbance Mortality rate, the fraction of population dying over a year due explicitly modelled reason. $yr^{-1} m_0$ Lowest/Sapling mass boundary. kgC g_0 (Sapling) Structural growth of an individual at the lowest mass boundary at a specific time. kgC $yr^{-1} g$ Structural growth of an individual at a given mass and time. kgC $yr^{-1} h_0$ (Sapling) Height of an individual at the lowest mass boundary. m/h (Height of an individual at a given mass. $m a_0$ (Sapling) Crown area of an individual at the lowest mass boundary. $m^2 a$ Crown area of an individual at a given mass. $m^2 \phi_g$ Constant describing the power law scaling of structural growth across mass. For large-scale application in ESMs a primary concern is to ensure that the total vegetation carbon obeys carbon balance (i.e. only changes due to the net impact of total growth minus total mortality). $-\phi_n$ Constant describing the power law scaling of height across mass. $-\phi_g$ Constant describing the power law scaling of crown area across mass. $-\alpha$ The fraction of total growth going into seedling recruitment. $-n$ Number density across mass space, the differential of N with respect to mass. $(kgC)^{-1} m^{-2} N$ Number density. $m^{-2} G$ Growth density. kgC $m^{-2} yr^{-1} \nu$ The fractional coverage. γ Mortality rate, the summation of the baseline and additional mortalities across mass. $yr^{-1} \gamma_b$ Baseline Mortality rate, the fraction of population dying over a year due non-explicit reasons. $yr^{-1} s$ The fraction of available space open for seedlings.~~

— F The flux of population density over time. $\text{m}^{-2}\text{yr}^{-1}$ Λ_d Demographic litter, the loss of carbon due to competition and mortality. $\text{kgC m}^{-2} \text{yr}^{-1}$ Here we use that requirement to derive the functional form for F_i as given in equation (5).

The total vegetation carbon in each mass class is $M_i = m_i N_i$. The update equation for M_i is therefore Eq. (4) multiplied by m_i :

$$5 \quad \frac{\partial M_i}{\partial t} + m_i (F_i - F_{i-1}) = -\gamma M_i. \quad (\text{A1})$$

The total carbon in the vegetation, M Biomass density. kgC m^{-2} $c_{k,l}$ Competition coefficient, the fraction a PFT, k , is shaded by the canopy of PFT l . — μ_0 The boundary turnover parameter — the ratio of mass lost to growth gained in the boundary mass class. — λ_i The proportional population of the i^{th} class to, is the sum of the i^{th} — 1 class at equilibrium. — e_j Subscript denoting a variable in equilibrium. — k, l Indices representing the PFT number. — i, j Indices representing mass class number. — I The largest mass class. — (k) The current time step. — ξ The size scaling coefficient, mass classes are defined as $m_j = \xi m_{j-1}$, with $\xi > 1$. — carbon in each of the mass classes:

$$M = \sum_i M_i. \quad (\text{A2})$$

Thus the update equation for the total carbon is:

$$\frac{\partial M}{\partial t} + \sum_i m_i (F_i - F_{i-1}) = -\gamma M, \quad (\text{A3})$$

15 which can be rewritten as:

$$\frac{\partial M}{\partial t} + \sum_i F_i (m_i - m_{i+1}) = -\gamma M. \quad (\text{A4})$$

Now substituting Eq. (5) into Eq. (A4) gives:

$$\frac{\partial M}{\partial t} = \sum_i N_i g_i - \gamma M. \quad (\text{A5})$$

20 The first term on the righthand-side of this equation is the total carbon uptake due to growth, and the second term represents the total carbon loss due to mortality, which is the required carbon conservation equation.

Appendix B: ~~RED~~ Continuum Solutions and Demographic Equilibrium Theory

Equation (1), can be solved for the ~~steady-state~~ steady-state if we assume metabolic scaling of growth using Eq. (2) and a size-independent mortality μ_0 (Moore et al., 2018, 2020):

$$n = n_0 \left(\frac{m}{m_0} \right)^{-\phi_g} \exp \left\{ \frac{\mu_0}{(1 - \phi_g)} \left[1 - \left(\frac{m}{m_0} \right)^{1 - \phi_g} \right] \right\}, \quad \mu_0 = \frac{\gamma m_0}{g_0}. \quad (\text{B.1})$$

The scaling variable does not necessarily have to be biomass and can be any size dimension with a power-scaling relationship with growth (height, basal diameter, etc.). The variable μ_0 can be thought of a parameter tied to the rate of biomass lost to biomass gained. The larger μ_0 is the greater the associated cost of replacing lost biomass – the smaller the total population density. Where n_0 is a boundary condition that describes the number density at the mass m_0 .

- 5 describes the number density at the mass m_0 . The parameter μ_0 is the ratio of the rate biomass loss due to mortality to the rate of biomass gain due to growth, for the reference mass class m_0 . Similar analytical solutions can be derived for other measures of tree-size, such as basal diameter or height (Moore et al., 2018, 2020).

Integrating Eq. (B.1) from m_0 to ∞ gives ~~us estimates for~~ the total number density:

$$N_{\text{eq}} = \frac{n_0 g_0}{\gamma} = \frac{n_0 m_0}{\mu_0}. \quad (\text{B.2})$$

- 10 We can also gain estimates of the total growth and biomass values by integrating with the allometric relationships: Other cohort integrals can be derived by integrating over the number density distribution, such as total growth rate ($\int g n dm$):

$$G_{\text{eq}} = g_0 N_{\text{eq}} \left(\frac{\mu_0}{1 - \phi_g} \right)^{\frac{\phi_g}{\phi_g - 1}} \exp \left\{ \frac{\mu_0}{1 - \phi_g} \right\} \Gamma \left(\frac{1}{1 - \phi_g}, \frac{\mu_0}{1 - \phi_g} \right) \quad (\text{B.3})$$

~~the total biomass ÷ total biomass~~ ($\int m n dm$):

$$M_{\text{eq}} = m_0 N_{\text{eq}} \left(\frac{\mu_0}{1 - \phi_g} \right)^{\frac{1}{\phi_g - 1}} \exp \left\{ \frac{\mu_0}{1 - \phi_g} \right\} \Gamma \left(\frac{1}{1 - \phi_g} + 1, \frac{\mu_0}{1 - \phi_g} \right) \quad (\text{B.4})$$

- 15 and ~~the total vegetation cover ÷~~ ($\int a n dm$):

$$\nu_{\text{eq}} = a_0 N_{\text{eq}} \left(\frac{\mu_0}{1 - \phi_g} \right)^{\frac{\phi_a}{\phi_g - 1}} \exp \left\{ \frac{\mu_0}{1 - \phi_g} \right\} \Gamma \left(\frac{\phi_a}{1 - \phi_g} + 1, \frac{\mu_0}{1 - \phi_g} \right) \quad (\text{B.5})$$

~~Where where~~ $\Gamma(a, b)$ is the incomplete upper gamma function. ~~When~~

As we assume the constants presented in (Niklas and Spatz, 2004) – $\phi_g = \frac{3}{4}$, $\phi_a = \frac{1}{3}$ – simplifies towards: allometric exponents presented in Niklas and Spatz (2004) ($\phi_g = 3/4$, $\phi_a = 1/3$), these functional forms simplify to:

- 20 $G_{\text{eq}} = g_0 N_{\text{eq}} \left(1 + \frac{3}{4\mu_0} + \frac{3}{8\mu_0^2} + \frac{3}{32\mu_0^3} \right)$ (B.6)

$$M_{\text{eq}} = m_0 N_{\text{eq}} \left(1 + \frac{1}{\mu_0} + \frac{3}{4\mu_0^2} + \frac{3}{8\mu_0^3} + \frac{3}{32\mu_0^4} \right) \quad (\text{B.7})$$

$$\nu_{\text{eq}} = a_0 N_{\text{eq}} \left(1 + \frac{1}{2\mu_0} + \frac{1}{8\mu_0^2} \right) \quad (\text{B.8})$$

For converting Finally, to convert a μ_0 found using total dry mass biomass ($\mu_{0,\text{tdm}}$) of 1 kg to that of dry carbon mass:-

$$\mu_0 = 2^{1-\phi_g} \mu_{0,\text{tdm}}.$$

to one based on carbon mass, we use the formula:

$$\mu_0 = 2^{1-\phi_g} \mu_{0,\text{tdm}} \quad (\text{B.9})$$

5 B1 Closed Continous Form

assuming that biomass is twice the carbon mass.

B1 Closed Continuous Form

Using Eq. and Eq. with the competitive constraint, we find that the equilibrium fraction is given by: The lowest population flux, $n_0 g_0$, is equal to the seedling boundary condition, F_0 , in equation (6):

$$10 \quad \nu_{\text{eq}} n_0 g_0 = 1 - \frac{1-\alpha}{\alpha} \frac{\mu_0}{1 + \frac{3}{4\mu_0} + \frac{3}{8\mu_0^2} + \frac{3}{32\mu_0^3}} \cdot \frac{\alpha}{1-\alpha} \frac{G}{m_0} s \quad (\text{B.10})$$

We can rearrange Eq. into Eq. allowing for the substitution of ν_{eq} into the equilibrium solutions (Equation and Eq.). For instance, the exact Substituting the total number density, N_{eq} , equation (B.2), into the lefthand-side, and total growth, G_{eq} , Eq. (B.6), into the righthand-side, yields a solution for the equilibrium coverage, assuming $s = 1 - \nu_{\text{eq}}$:

$$\gamma N_{\text{eq}} = \left(\frac{\alpha}{1-\alpha} \right) \frac{g_0}{m_0} N_{\text{eq}} (1 - \nu_{\text{eq}}) \left(1 + \frac{3}{4\mu_0} + \frac{3}{8\mu_0^2} + \frac{3}{32\mu_0^3} \right) \quad (\text{B.11})$$

15 which simplifies:

$$\nu_{\text{eq}} = 1 - \left(\frac{1-\alpha}{\alpha} \right) \frac{\mu_0}{1 + \frac{3}{4\mu_0} + \frac{3}{8\mu_0^2} + \frac{3}{32\mu_0^3}} \quad (\text{B.12})$$

Using equation (B.8) we can write the total number density is given as: at equilibrium in terms of ν_{eq} :

$$N_{\text{eq}} = \frac{\nu_{\text{eq}}}{a_0} \left(\frac{1}{1 + \frac{1}{2\mu_0} + \frac{1}{8\mu_0^2}} \right); \quad (\text{B.13})$$

enables the calculation of total growth to Eq. This enables equation (B.6) to be rewritten:

$$20 \quad G_{\text{eq}} = \frac{\nu_{\text{eq}} g_0}{a_0} \left(\frac{1 + \frac{3}{4\mu_0} + \frac{3}{8\mu_0^2} + \frac{3}{32\mu_0^3}}{1 + \frac{1}{2\mu_0} + \frac{1}{8\mu_0^2}} \right) \quad (\text{B.14})$$

This equation in turn defines the total assimilate:

$$\underline{G_{\text{eq}}} P_{\text{eq}} = \frac{\nu_{\text{eq}} g_0}{a_0 (1-\alpha)} \left(\frac{1}{1-\alpha} \right); \underline{G_{\text{eq}}} \quad (\text{B.15})$$

and the biomass: Finally the total biomass can be written in closed form as:

$$M_{\text{eq}} = \frac{\nu_{\text{eq}} m_0}{a_0} \left(\frac{1 + \frac{1}{\mu_0} + \frac{3}{4\mu_0^2} + \frac{3}{8\mu_0^3} + \frac{3}{32\mu_0^4}}{1 + \frac{1}{2\mu_0} + \frac{1}{8\mu_0^2}} \right) \quad (\text{B.16})$$

B2 Continuous-Discrete Convergence Discrete Steady-State

To solve for the discrete model equilibrium, we start from the flow equation from Eq. (4) with the term $\partial N/\partial t \rightarrow 0$:

$$5 \quad \gamma N_i + F_i = F_{i-1} \quad (\text{B.17})$$

considering the population flux - equation (5), we find N_i in relation to the lower mass class, N_{i-1} :

$$N_i = N_{i-1} \left[\frac{g_{i-1}/(m_i - m_{i-1})}{g_i/(m_{i+1} - m_i) + \gamma} \right] = N_{i-1} \lambda_i \quad (\text{B.18})$$

Assuming no population grows out of the top class, λ_I is given as:

$$\lambda_I = \frac{g_{i-1}}{(m_i - m_{i-1})\gamma} \quad (\text{B.19})$$

- 10 λ_i can be simplified to depend only on μ_0 , by using $\mu_0 = (\gamma m_0/g_0)$ (equation (14)) and applying the mass scaling of growth rates $g_i = g_0(m_i/m_0)^{\phi_g}$. We can show that λ_i and λ_I are:

$$\lambda_i = \frac{(m_{i-1}/m_0)^{\phi_g} m_0/(m_i - m_{i-1})}{(m_i/m_0)^{\phi_g} m_0/(m_{i+1} - m_i) + \mu_0}, \quad \lambda_I = \frac{(m_{i-1}/m_i)^{\phi_g} m_0}{(m_i - m_{i-1})\mu_0} \quad (\text{B.20})$$

An expression for the total stand density at equilibrium, N_{eq} , can be derived. Using equation (B.18), we can represent any

- 15 population of mass class i in terms of the lowest mass class N_0 :

$$N_i = N_0 \prod_{j=1}^i \lambda_j \quad (\text{B.21})$$

Therefore, when finding the total number of stands relative to N_0 we get:

$$N_{\text{eq}} = N_0 \left[1 + \sum_{i=1}^I \prod_{j=1}^i \lambda_j \right] = N_0 X_N \quad (\text{B.22})$$

where X_N describes the sum of the all mass classes as a proportion of N_0 . We can describe the total class growth rate in

- 20 relation to N_0 as:

$$G_i = N_0 g_i \prod_{j=1}^i \lambda_j \quad (\text{B.23})$$

By using the allometric relationship (equation (2)):

$$G_i = N_0 g_0 \left(\frac{m_i}{m_0} \right)^{\phi_g} \prod_{j=1}^i \lambda_j \quad (\text{B.24})$$

we describe the total class growth rate in relation to the lowest class growth rate, $N_0 g_0$. Like N_{eq} , we can show the total growths across all classes is therefore:

$$5 \quad G_{\text{eq}} = N_0 g_0 \left[1 + \sum_{i=1}^I \left(\frac{m_i}{m_0} \right)^{\phi_g} \prod_{j=1}^i \lambda_j \right] = N_0 g_0 X_G \quad (\text{B.25})$$

We can repeat the same process for coverage:

$$\nu_i = N_0 a_i \prod_{j=1}^i \lambda_j \quad (\text{B.26})$$

and using allometric relationship (equation (3)):

$$\nu_i = N_0 a_0 \left(\frac{m_i}{m_0} \right)^{\phi_a} \prod_{j=1}^i \lambda_j \quad (\text{B.27})$$

10 This gives the total coverage, ν_{eq} as:

$$\nu_{\text{eq}} = N_0 a_0 \left[1 + \sum_{i=1}^I \left(\frac{m_i}{m_0} \right)^{\phi_a} \prod_{j=1}^i \lambda_j \right] = N_0 a_0 X_\nu \quad (\text{B.28})$$

Finally, for the total carbon mass within the class:

$$M_i = N_0 m_i \prod_{j=1}^i \lambda_j \quad (\text{B.29})$$

with the total carbon density equalling:

$$15 \quad M_{\text{eq}} = N_0 m_0 \left[1 + \sum_{i=1}^I \frac{m_i}{m_0} \prod_{j=1}^i \lambda_j \right] = N_0 m_0 X_M \quad (\text{B.30})$$

In equilibrium, the rate of the recruitment of seedlings (equation (6)) must balance the rate of loss of plants due to total mortality (γN_{eq}):

$$\gamma N_{\text{eq}} = \frac{\alpha}{(1-\alpha)} \frac{G_{\text{eq}}}{m_0} s \quad (\text{B.31})$$

Substituting in equation (B.22), Eq. (B.25) yields a balance equation for the k^{th} PFT:

$$\left(\frac{\alpha}{1-\alpha}\right) \left(1 - \sum_l c_{kl} \nu_l\right) = \mu_0 \frac{X_N}{X_G} \quad (\text{B.32})$$

We can get the equilibrium fraction of a PFT, k , by rearranging the above equation, assuming $c_{kk} = 1$:

$$\nu_{\text{eq},k} = 1 - \left(\frac{1-\alpha}{\alpha}\right) \mu_0 \frac{X_N}{X_G} - \sum_{l \neq k} c_{kl} \nu_l \quad (\text{B.33})$$

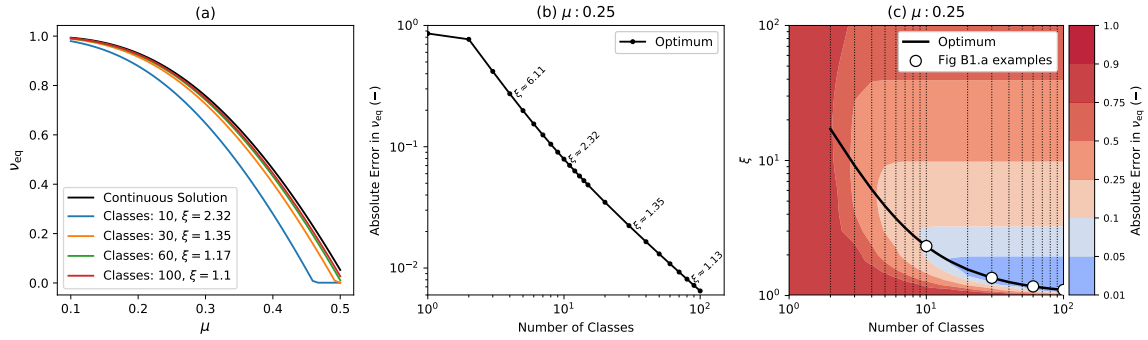
5 Once the value of μ_0 has been derived in this manner, we can find N_0 by inversion of equation (B.28):

$$N_0 = \frac{\nu_{\text{eq}}}{a_0 X_\nu} \quad (\text{B.34})$$

Substituting equation (B.33) into Eq.(B.34) allows us to determine N_0 and hence most other total densities in terms of purely μ_0 and prescribed constants.

B3 Continuous-Discrete Convergence

10 Inevitably discretised models will not exactly reproduce exact continuum analytical solutions, as a result of numerical inaccuracies that arise from using a finite number of mass classes. However, where exact analytical solutions exist they can be used to benchmark numerical models and optimise discretisation schemes, which is what we set out to do in this appendix. We compare the continuum analytical solution for the equilibrium coverage (equation B.12) to results from RED with differing numbers of mass classes m_i and a geometric mass class scaling, $m_{i+1} = \xi m_i$. Figure B2(a) shows how the relationship between ν_{eq} varies
 15 with μ_0 for the exact continuum solution (black line) and variants of the numerical version of RED with different numbers of mass classes (coloured lines). As hoped, results from the discretised model converge on the exact solution as the number of mass classes increases.



Showing the convergence of the numerical model towards the analytical equilibrium for Broadleaf Evergreen Tropical (BET-Tr) for coverage. With $\phi_g = 0.75, \alpha = 0.1$. (a) demonstrates over given μ_0 values the convergence. (b-c) shows that the differences is minimised when the bin scaling, $\xi \rightarrow 1$, while the number of mass classes goes towards infinity. The black lines on (b,c) denote the optimum from Eq. . The white dots on (c) correspond with the discrete lines on (a):

Figure B2. Comparison of the discretised model to the continuum analytical solution, showing convergence for higher numbers of mass classes. This example uses parameters for Broadleaf Evergreen Tropical trees (BET-Tr PFT) with $\alpha = 0.1$: (a) equilibrium coverage ν_{eq} versus μ_0 for the exact continuum solution (black line) and discretisations of the mass dimension with varying numbers of mass classes and mass class width scaling (ξ); (b) absolute error in the modelled value of ν_{eq} against the number of mass classes using the optimum value of ξ for each case; (c) optimum ξ versus number of mass classes, with contours showing the absolute error in ν_{eq} . Panels (b) and (c) assume $\mu_0 = 0.25$. The white dots in (c) have the same number of classes and scaling as the discrete lines in (a).

There are a few differences between the numerical steady state and the continuous form of RED. Firstly, the truncation point The numerical versions of RED shown in Figure B2(a) each use a value of ξ that is near optimum for the number of the top mass class results in a underestimation of the total coverage, biomass and number density for an identical μ_0 . The second source of difference arises from the binning of the mass classes. Discretising results in the continuous scaling of the growth and mass is not fully captured. In the current scheme a number density between the masses m_j of m_{j+1} will have its physiological characteristics represented at the m_j mass, this can lead to underestimating the total growth/biomass/coverage within the class. This is demonstrated in figure ?? . a, where the total coverage of the biomass is lower in the discrete model than the continuous solution . There is also convergence when the bins between the methods when the number of classes goes towards infinity ($I \rightarrow \infty$) and class widths goes towards zero ($\xi \rightarrow 1$) . mass classes, as shown in panels (b) and (c) of Figure B2. Optimum ξ values reduce from about 2.3 for 10 mass classes to 1.1 for 100 mass classes. This variation results from a trade-off. For a given number of mass classes, small values of ξ give greater numerical accuracy, but explicitly model less of the mass range, and the opposite is true of large ξ values. As a result, optimum values of ξ can be defined for each number of mass classes as outlined below.

For geometric scaling any mass can be expressed in terms of m_0 , by writing $m_i = m_0(\xi)^i$. Therefore, by using $m_{i+1} - m_i = m_0(\xi)^i(\xi - 1)$ we find that our equilibrium form of λ_i is reduced to:

$$\lambda_i = \frac{\xi^{(\phi_g-1)(i-1)}}{\xi^{i(\phi_g-1)} + \mu_0(\xi-1)}, \quad \lambda_I = \frac{\xi^{(\phi_g-1)(i-1)}}{\mu_0(\xi-1)} \quad (\text{B.35})$$

- 5 From Figure ??eFrom figure B2 (c), we see that there is a clear optimum amount of an optimum value for ξ , the geometric scaling for a given number of classes which minimise, which minimises the difference between the continuous and discrete forms. This can be found by taking the difference of the continuous and discrete coverages and differentiating with respect to ξ to find the minima. It should be noted that the as the continuous form is not dependent on ξ , we get:

$$\frac{\partial}{\partial \xi} [\nu_{\text{eq,continuous}} - \nu_{\text{eq}}] = -\frac{\partial}{\partial \xi} [\nu_{\text{eq}}] \quad (\text{B.36})$$

- 10 Where where ν_{eq} corresponds with the discrete equilibrium (Equation equation (B.32), with $\nu_{\text{eq}} = (1 - s)$). Setting Eq. (B.36) equal to zero we reduce the relationship to just a dependence of only a dependence on X_N and X_G :

$$0 = \frac{\partial}{\partial \xi} \left[\frac{X_N}{X_G} \right] = X_G X'_N - X'_G X_N \quad (\text{B.37})$$

Finding the partial derivative of X_N , using the geometric form of equation (B.18), we get:

$$X'_N = \sum_{j=1}^I \left[\left(\prod_{i=1}^j \lambda_i \right) \left(\sum_{i=1}^j \frac{\lambda'_i}{\lambda_i} \right) \right] \quad (\text{B.38})$$

- 15 and for X_G :

$$X'_G = \sum_{j=1}^I \left[\xi^{j\phi_g} \left(\prod_{i=1}^j \lambda_i \right) \left(j\phi_g \xi^{-1} + \sum_{i=1}^j \frac{\lambda'_i}{\lambda_i} \right) \right] \quad (\text{B.39})$$

Finding λ'_i we get:

$$\lambda'_i = \lambda_i \left[(1-i)(\phi_g-1)\xi^{-1} - \lambda_i \left(i(\phi_g-1)\xi^{\phi_g-2} + \mu_0\xi^{(i-1)(1-\phi_g)} \right) \right] \quad (\text{B.40})$$

and for λ'_I : the top class, λ'_I :

$$\lambda'_{iI} = \left(\frac{(1-\xi^{-1})(I-1)(\phi_g-1)-1}{\xi-1} \right) \lambda_{iI} \quad (\text{B.41})$$

To numerically solve for the minimum, we must differentiate Eq. (B.37), with respect to ξ . Through the product rule we get:

$$\frac{\partial^2}{\partial \xi^2} \left[\frac{X_N}{X_G} \right] = X_G X''_N - X''_G X_N \quad (\text{B.42})$$

Eq. Differentiating equation (B.38) differentiated simplifies towards: and simplifying gives:

$$X''_N = \sum_{j=1}^I \left[\left(\prod_{i=1}^j \lambda_i \right) \left(\sum_{i=1}^j \frac{\lambda''_i}{\lambda_i} \right) \right] \quad (\text{B.43})$$

and doing the same for Eq. (B.39) ~~÷~~ gives:

$$\underline{X''_G} = \sum_{j=1}^I \left[\underline{\xi^{j\phi_g}} \left(\prod_{i=1}^j \lambda_i \right) \left(\underline{j\phi_g \xi^{-2} (j\phi_g - 1)} + \sum_{i=1}^j \frac{2j\phi_g \xi^{-1} \lambda_i - \lambda_i''}{\lambda_i} \right) \right] \quad (\text{B.44})$$

λ_i'' is given ~~as:~~ by:

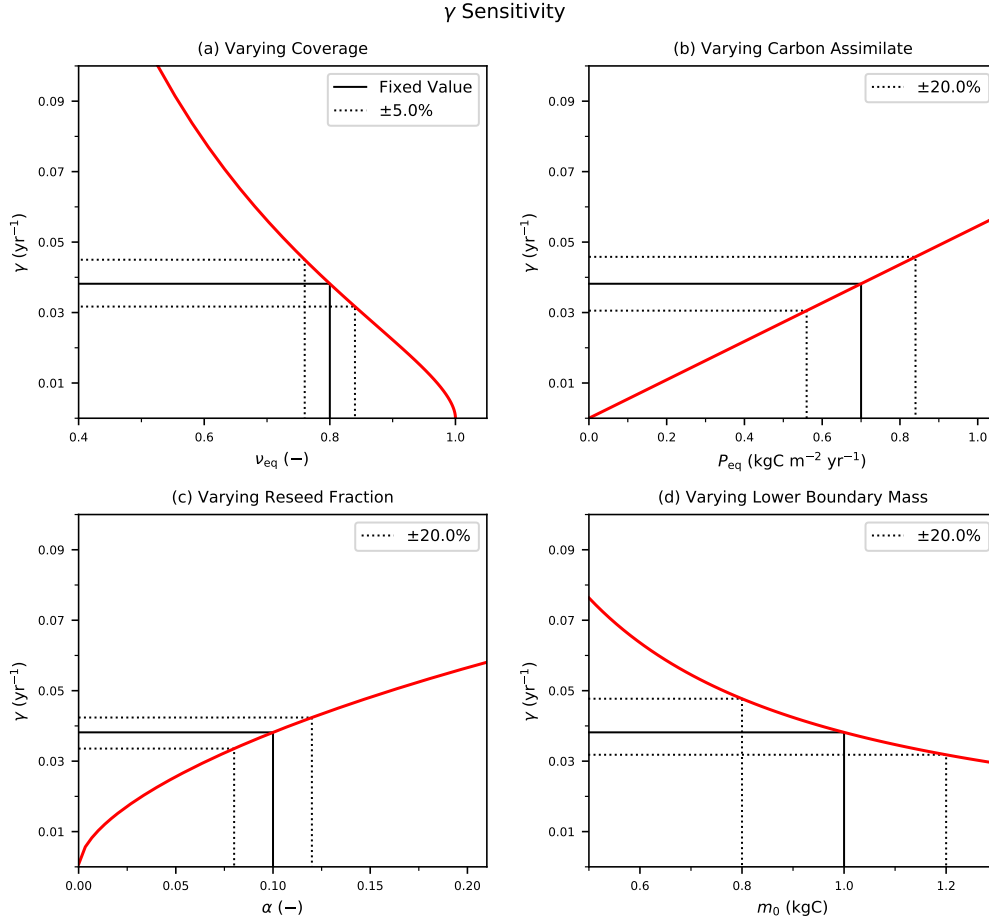
$$\underline{\lambda_i''} = \lambda_i \left[\underline{\frac{\lambda_i'}{\lambda_i}} \left(\underline{(i-1)(\phi_g - 1)\xi^{-1}} \right) \underline{-(i-1)(\phi_g - 1)\xi^{-2} - \lambda_i(\phi_g - 1)\xi^{-1}} \left(\underline{i(\phi_g - 1)\xi^{\phi_g - 2} - \mu_0(i-1)\xi^{(i-1)(1-\phi_g)}} \right) \right] \quad (\text{B.45})$$

5 For the double differential of λ_i we get:

$$\underline{\lambda_i''} = \frac{\lambda_i'^2}{\lambda_i} \underline{+} \frac{\lambda_i}{\xi - 1} \underline{\times} \left(\frac{(I-1)(\phi-1)}{\xi^2} \underline{-} \frac{\lambda_i'}{\lambda_i} \right) \quad (\text{B.46})$$

We now possess the identities needed to ~~perform a numerical root finding algorithm for~~ numerically find the optimum bin scaling for a given ~~class.~~ Using a Newton root finding method for Eq number of classes. In figure B2 (c), the optimum scaling, ξ , is shown as the solid black line.

Appendix C: Sensitivity of Diagnosed Mortality Rates to Model Parameters



Fixed Values: $\nu_{eq} = 0.8$, $P_{eq} = 0.7 \text{ kgC m}^{-2} \text{ yr}^{-1}$, $\alpha = 0.1$, $m_0 = 1.0 \text{ kgC}$, $a_0 = 0.5 \text{ m}^2$

Figure C1. The sensitivity of the mortality rate to assumed input variables: coverage, ν_{eq} (a) and carbon assimilate rate, P_{eq} (b), and model parameters: reseed fraction, α (c) and boundary mass, m_0 (d). The solid black line indicates the fixed values with corresponding $\pm 20\%$ (b,c,d) or $\pm 5\%$ (a) variation (dotted black lines).

The diagnosed mortality rates in figure 6 are sensitive to variation in model inputs and parameters. The mortality rate, γ , can be found for the continuous solutions by rearranging the boundary condition equation (6), and substituting in Eq.(B.2) and Eq.(B.13):

$$5 \quad \gamma = \frac{\alpha P_{eq} a_0}{m_0} \left(\frac{1 - \nu_{eq}}{\nu_{eq}} \right) \left[1 + \frac{1}{2\mu_0} + \frac{1}{8\mu_0^2} \right] \quad (\text{C.1})$$

The key external inputs to this equation are the observed PFT fraction ν_{eq} and the net assimilate P_{eq} . In addition, our estimates of γ are dependent on the internal model parameters, α and m_0 .

5 The red lines in Figure C1 demonstrate how the estimate of γ depends on these four inputs. The black dashed lines in Figure C1 indicate how uncertainties in each input relate to uncertainties in γ , for 'true' values typical of a tree PFT. We estimate uncertainties in the observed PFT fraction (e.g. from remote-sensing) to be $\pm 5\%$, and uncertainties in P (e.g. from JULES) to be $\pm 20\%$, leading to errors of $\pm 17\%$ and $\pm 20\%$ respectively. Likewise, $\pm 20\%$ uncertainties in the internal parameters α and m_0 lead to $\pm 12\%$ and $\pm 20\%$ uncertainties in γ . Combining these sources of uncertainty leads to an overall uncertainty in our inferred estimate of γ of about $\pm 35\%$. with it's differential; Eq., we find the optimum. On figure ?? the optimum line is shown as the bright dashed black line.

Author contributions. Originally the model framework in JRM's thesis (Moore, 2016) under the supervision of PMC and CH. The description of PFT competition, the numerical model and the equilibrium solutions has been further developed by APKA, JRM, ABH, and PMC. Currently RED is being integrated into JULES with the supervision of AJW and CJ. AJW also provided and processed the UKESM growth rates needed to drive RED globally within this paper.

5 *Competing interests.* The authors declare that they have no conflict of interest.

Acknowledgements. This work has been funded as part of the Newton Fund with the Met Office Climate Science for Service Partnership Brazil (CSSP-Brazil) and by the European Research Council (ERC) ECCLES project. A.A was funded through the CASE studentship from the University of Exeter and the Met Office. We are grateful to the Met Office for considering implementation in JULES, via a ticket 902 within a branch of the code repository.

References

- Ahlström, A., Xia, J., Arneeth, A., Luo, Y., and Smith, B.: Importance of vegetation dynamics for future terrestrial carbon cycling, *Environmental Research Letters*, 10, 054019, 2015.
- Allen, C. D., Macalady, A. K., Chenchouni, H., Bachelet, D., McDowell, N., Venetier, M., Kitzberger, T., Rigling, A., Breshears, D. D.,
5 Hogg, E. T., et al.: A global overview of drought and heat-induced tree mortality reveals emerging climate change risks for forests, *Forest ecology and management*, 259, 660–684, 2010.
- Arora, V. K., Katavouta, A., Williams, R. G., Jones, C. D., Brovkin, V., Friedlingstein, P., Schwinger, J., Bopp, L., Boucher, O., Cadule, P., Chamberlain, M. A., Christian, J. R., Delire, C., Fisher, R. A., Hajima, T., Ilyina, T., Joetzjer, E., Kawamiya, M., Koven, C., Krasting, J., Law, R. M., Lawrence, D. M., Lenton, A., Lindsay, K., Pongratz, J., Raddatz, T., Séférian, R., Tachiiri, K., Tjiputra, J. F., Wiltshire, A.,
10 Wu, T., and Ziehn, T.: Carbon-concentration and carbon-climate feedbacks in CMIP6 models, and their comparison to CMIP5 models, *Biogeosciences Discussions*, 2019, 1–124, <https://doi.org/10.5194/bg-2019-473>, <https://www.biogeosciences-discuss.net/bg-2019-473/>, 2019.
- Best, M. J., Pryor, M., Clark, D. B., Rooney, G. G., Essery, R. L. H., Ménard, C. B., Edwards, J. M., Hendry, M. A., Porson, A., Gedney, N., Mercado, L. M., Sitch, S., Blyth, E., Boucher, O., Cox, P. M., Grimmond, C. S. B., and Harding, R. J.: The Joint UK Land
15 Environment Simulator (JULES), model description – Part 1: Energy and water fluxes, *Geoscientific Model Development*, 4, 677–699, <https://doi.org/10.5194/gmd-4-677-2011>, <https://www.geosci-model-dev.net/4/677/2011/>, 2011.
- Bond, W. J., Woodward, F. I., and Midgley, G. F.: The global distribution of ecosystems in a world without fire, *New phytologist*, 165, 525–538, 2005.
- Brando, P. M., Balch, J. K., Nepstad, D. C., Morton, D. C., Putz, F. E., Coe, M. T., Silvério, D., Macedo, M. N., Davidson, E. A., Nóbrega,
20 C. C., et al.: Abrupt increases in Amazonian tree mortality due to drought–fire interactions, *Proceedings of the National Academy of Sciences*, 111, 6347–6352, 2014.
- Brovkin, V., Boysen, L., Arora, V. K., Boisier, J. P., Cadule, P., Chini, L., Claussen, M., Friedlingstein, P., Gayler, V., Van den hurk, B. J., Hurtt, G. C., Jones, C. D., Kato, E., De noblet ducouudre, N., Pacifico, F., Pongratz, J., and Weiss, M.: Effect of anthropogenic land-use and land-cover changes on climate and land carbon storage in CMIP5 projections for the twenty-first century, *Journal of Climate*, 26,
25 6859–6881, <https://doi.org/10.1175/JCLI-D-12-00623.1>, 2013.
- Burton, C., Betts, R., Cardoso, M., Feldpausch, T. R., Harper, A., Jones, C. D., Kelley, D. I., Robertson, E., and Wiltshire, A.: Representation of fire, land-use change and vegetation dynamics in the Joint UK Land Environment Simulator vn4. 9 (JULES), *Geoscientific Model Development*, 12, 179–193, 2019.
- Chaturvedi, R., Raghubanshi, A., and Singh, J.: Effect of grazing and harvesting on diversity, recruitment and carbon accumulation of juvenile
30 trees in tropical dry forests, *Forest Ecology and Management*, 284, 152–162, 2012.
- Chuvieco, E., Pettinari, M., Lizundia Loiola, J., Storm, T., and Padilla Parellada, M.: ESA Fire Climate Change Initiative (Fire_cci): MODIS Fire_cci Burned Area Grid product, version 5.1., doi:10.5285/3628cb2fdb443588155e15dee8e5352, 2019.
- Ciais, P., Sabine, C., Bala, G., Bopp, L., Brovkin, V., Canadell, J., Chhabra, A., DeFries, R., Galloway, J., Heimann, M., et al.: Carbon and other biogeochemical cycles, in: *Climate change 2013: the physical science basis. Contribution of Working Group I to the Fifth Assessment Report of the Intergovernmental Panel on Climate Change*, pp. 465–570, Cambridge University Press, 2014.
- Coomes, D. A., Duncan, R. P., Allen, R. B., and Truscott, J.: Disturbances prevent stem size-density distributions in natural forests from following scaling relationships, *Ecology Letters*, 6, 980–989, <https://doi.org/10.1046/j.1461-0248.2003.00520.x>, 2003.

- Coutinho, L. M.: Fire in the ecology of the Brazilian cerrado, in: Fire in the tropical biota, pp. 82–105, Springer, 1990.
- Cox, P. M.: Description of the "TRIFFID" dynamic global vegetation model, 2001.
- Curran, L. M., Trigg, S. N., McDonald, A. K., Astiani, D., Hardiono, Y., Siregar, P., Caniago, I., and Kasischke, E.: Lowland forest loss in protected areas of Indonesian Borneo, *Science*, 303, 1000–1003, 2004.
- 5 Davies-Barnard, T., Valdes, P., Singarayer, J. S., Wiltshire, A., and Jones, C.: Quantifying the relative importance of land cover change from climate and land use in the representative concentration pathways, *Global Biogeochemical Cycles*, 29, 842–853, 2015.
- Dorrough, J. and Moxham, C.: Eucalypt establishment in agricultural landscapes and implications for landscape-scale restoration, *Biological conservation*, 123, 55–66, 2005.
- Eller, C. B., Rowland, L., Oliveira, R. S., Bittencourt, P. R., Barros, F. V., da Costa, A. C., Meir, P., Friend, A. D., Mencuccini, M., Sitch, S., et al.: Modelling tropical forest responses to drought and El Niño with a stomatal optimization model based on xylem hydraulics, *Philosophical Transactions of the Royal Society B: Biological Sciences*, 373, 20170315, 2018.
- 10 Eller, C. B., Rowland, L., Mencuccini, M., Rosas, T., Williams, K., Harper, A., Medlyn, B. E., Wagner, Y., Klein, T., Teodoro, G. S., et al.: Stomatal optimisation based on xylem hydraulics (SOX) improves land surface model simulation of vegetation responses to climate, *New Phytologist*, 2020.
- 15 Enquist, B. J., Brown, J. H., and West, G. B.: Allometric scaling of plant energetics and population density, *Nature*, 395, 163, 1998.
- Esseen, P.-A.: Tree mortality patterns after experimental fragmentation of an old-growth conifer forest, *Biological conservation*, 68, 19–28, 1994.
- Fischer, R., Bohn, F., de Paula, M. D., Dislich, C., Groeneveld, J., Gutiérrez, A. G., Kazmierczak, M., Knapp, N., Lehmann, S., Paulick, S., et al.: Lessons learned from applying a forest gap model to understand ecosystem and carbon dynamics of complex tropical forests, *Ecological Modelling*, 326, 124–133, 2016.
- 20 Fisher, R., McDowell, N., Purves, D., Moorcroft, P., Sitch, S., Cox, P., Huntingford, C., Meir, P., and Woodward, F. I.: Assessing uncertainties in a second-generation dynamic vegetation model caused by ecological scale limitations, *New Phytologist*, 187, 666–681, 2010.
- Fisher, R. A., Muszala, S., Versteinstein, M., Lawrence, P., Xu, C., McDowell, N. G., Knox, R. G., Koven, C., Holm, J., Rogers, B. M., Spessa, A., Lawrence, D., and Bonan, G.: Taking off the training wheels: the properties of a dynamic vegetation model without climate envelopes, *CLM4.5(ED), Geoscientific Model Development*, 8, 3593–3619, <https://doi.org/10.5194/gmd-8-3593-2015>, <https://www.geosci-model-dev.net/8/3593/2015/>, 2015.
- 25 Fisher, R. A., Koven, C. D., Anderegg, W. R., Christoffersen, B. O., Dietze, M. C., Farrior, C. E., Holm, J. A., Hurtt, G. C., Knox, R. G., Lawrence, P. J., Lichstein, J. W., Longo, M., Matheny, A. M., Medvigy, D., Muller-Landau, H. C., Powell, T. L., Serbin, S. P., Sato, H., Shuman, J. K., Smith, B., Trugman, A. T., Viskari, T., Verbeeck, H., Weng, E., Xu, C., Xu, X., Zhang, T., and Moorcroft, P. R.: Vegetation demographics in Earth System Models: A review of progress and priorities, *Global Change Biology*, 24, 35–54, <https://doi.org/10.1111/gcb.13910>, 2018.
- 30 Friedlingstein, P., Meinshausen, M., Arora, V. K., Jones, C. D., Anav, A., Liddicoat, S. K., and Knutti, R.: Uncertainties in CMIP5 climate projections due to carbon cycle feedbacks, *Journal of Climate*, 27, 511–526, <https://doi.org/10.1175/JCLI-D-12-00579.1>, 2014.
- Haddad, N. M., Brudvig, L. A., Clobert, J., Davies, K. F., Gonzalez, A., Holt, R. D., Lovejoy, T. E., Sexton, J. O., Austin, M. P., Collins, C. D., et al.: Habitat fragmentation and its lasting impact on Earth's ecosystems, *Science advances*, 1, e1500052, 2015.
- 35 Harper, A. B., Cox, P. M., Friedlingstein, P., Wiltshire, A. J., Jones, C. D., Sitch, S., Mercado, L. M., Groenendijk, M., Robertson, E., Kattge, J., Bönsch, G., Atkin, O. K., Bahn, M., Cornelissen, J., Niinemets, Ü., Onipchenko, V., Peñuelas, J., Poorter, L., Reich, P. B., Soudzilovskaia, N. A., and Van Bodegom, P.: Improved representation of plant functional types and physiology in the

- Joint UK Land Environment Simulator (JULES v4.2) using plant trait information, *Geoscientific Model Development*, 9, 2415–2440, <https://doi.org/10.5194/gmd-9-2415-2016>, 2016.
- Harper, A. B., Wiltshire, A. J., Cox, P. M., Friedlingstein, P., Jones, C. D., Mercado, L. M., Sitch, S., Williams, K., and Duran-Rojas, C.: Vegetation distribution and terrestrial carbon cycle in a carbon cycle configuration of JULES4.6 with new plant functional types, *Geoscientific Model Development*, 11, 2857–2873, <https://doi.org/10.5194/gmd-11-2857-2018>, 2018.
- 5 Haverd, V., Smith, B., Nieradzik, L. P., and Briggs, P. R.: A stand-alone tree demography and landscape structure module for Earth system models: integration with inventory data from temperate and boreal forests, *Biogeosciences*, 11, 4039–4055, 2014.
- Higuchi, P., Oliveira-Filho, A. T., Bebbler, D. P., Brown, N. D., Silva, A. C., and Machado, E. L.: Spatio-temporal patterns of tree community dynamics in a tropical forest fragment in South-east Brazil, *Plant Ecology*, 199, 125–135, 2008.
- 10 Jones, S., Rowland, L., Cox, P., Hemming, D., Wiltshire, A., Williams, K., Parazoo, N. C., Liu, J., da Costa, A. C. L., Meir, P., Mencuccini, M., and Harper, A.: The Impact of a Simple Representation of Non-Structural Carbohydrates on the Simulated Response of Tropical Forests to Drought, *Biogeosciences Discussions*, 2019, 1–26, <https://doi.org/10.5194/bg-2019-452>, <https://www.biogeosciences-discuss.net/bg-2019-452/>, 2019.
- Jönsson, M. T., Fraver, S., Jonsson, B. G., Dynesius, M., Rydgård, M., and Esseen, P.-A.: Eighteen years of tree mortality and structural change in an experimentally fragmented Norway spruce forest, *Forest Ecology and Management*, 242, 306–313, 2007.
- 15 Kinnaird, M. F. and O'Brien, T. G.: Ecological effects of wildfire on lowland rainforest in Sumatra, *Conservation Biology*, 12, 954–956, 1998.
- Kohyama, T., Suzuki, E., Partomihardjo, T., Yamada, T., and Kubo, T.: Tree species differentiation in growth, recruitment and allometry in relation to maximum height in a Bornean mixed dipterocarp forest, *Journal of Ecology*, 91, 797–806, 2003.
- 20 Laurance, W. F., Ferreira, L. V., Rankin-de Merona, J. M., and Laurance, S. G.: Rain forest fragmentation and the dynamics of Amazonian tree communities, *Ecology*, 79, 2032–2040, 1998.
- Levine, N. M., Zhang, K., Longo, M., Baccini, A., Phillips, O. L., Lewis, S. L., Alvarez-Dávila, E., de Andrade, A. C. S., Brienen, R. J., Erwin, T. L., et al.: Ecosystem heterogeneity determines the ecological resilience of the Amazon to climate change, *Proceedings of the National Academy of Sciences*, 113, 793–797, 2016.
- 25 Li, W., MacBean, N., Ciais, P., Defourny, P., Lamarche, C., Bontemps, S., and Peng, S.: Derivation of plant functional type (PFT) maps from the ESA CCI Land Cover product [Data set]., <http://doi.org/10.5281/zenodo.1048163>, 2019.
- Lima, R. A., Muller-Landau, H. C., Prado, P. I., and Condit, R.: How do size distributions relate to concurrently measured demographic rates? Evidence from over 150 tree species in Panama, *Journal of Tropical Ecology*, 32, 179–192, 2016.
- Longo, M., Knox, R. G., Medvigy, D. M., Levine, N. M., Dietze, M. C., Kim, Y., Swann, A. L. S., Zhang, K., Rollinson, C. R., Bras, R. L., Wofsy, S. C., and Moorcroft, P. R.: The biophysics, ecology, and biogeochemistry of functionally diverse, vertically and horizontally heterogeneous ecosystems: the Ecosystem Demography model, version 2.2 – Part 1: Model description, *Geoscientific Model Development*, 12, 4309–4346, <https://doi.org/10.5194/gmd-12-4309-2019>, <https://www.geosci-model-dev.net/12/4309/2019/>, 2019a.
- 30 Longo, M., Knox, R. G., Levine, N. M., Swann, A. L. S., Medvigy, D. M., Dietze, M. C., Kim, Y., Zhang, K., Bonal, D., Burban, B., Camargo, P. B., Hayek, M. N., Saleska, S. R., da Silva, R., Bras, R. L., Wofsy, S. C., and Moorcroft, P. R.: The biophysics, ecology, and biogeochemistry of functionally diverse, vertically and horizontally heterogeneous ecosystems: the Ecosystem Demography model, version 2.2 – Part 2: Model evaluation for tropical South America, *Geoscientific Model Development*, 12, 4347–4374, <https://doi.org/10.5194/gmd-12-4347-2019>, <https://www.geosci-model-dev.net/12/4347/2019/>, 2019b.

- Lugo, A. E. and Scatena, F. N.: Background and catastrophic tree mortality in tropical moist, wet, and rain forests, *Biotropica*, pp. 585–599, 1996.
- Medeiros, M. and Miranda, H.: Post-fire resprouting and mortality in cerrado woody plant species over a three-year period, *Edinburgh Journal of Botany*, 65, 53–68, 2008.
- 5 Medvigy, D., Wofsy, S. C., Munger, J. W., Hollinger, D. Y., and Moorcroft, P. R.: Mechanistic scaling of ecosystem function and dynamics in space and time: Ecosystem Demography model version 2, *Journal of Geophysical Research: Biogeosciences*, 114, 1–21, <https://doi.org/10.1029/2008JG000812>, 2009.
- Moorcroft, P. R., Hurtt, G., and Pacala, S. W.: a Method for Scaling Vegetation Dynamics: the Ecosystem Demography Model (Ed), *Ecological Monographs*, 71, 557–586, [https://doi.org/doi:10.1890/0012-9615\(2001\)071\[0557:AMFSVD\]2.0.CO;2](https://doi.org/doi:10.1890/0012-9615(2001)071[0557:AMFSVD]2.0.CO;2), [https://doi.org/10.1890/0012-9615\(2001\)071\[0557:AMFSVD\]2.0.CO;2](https://doi.org/10.1890/0012-9615(2001)071[0557:AMFSVD]2.0.CO;2), 2001.
- 10 Moore, J. R.: Aspects of Land Surface Modelling: Role of Biodiversity in Ecosystem Resilience to Environmental Change and a Robust Ecosystem Demography Model, Ph.D. thesis, 2016.
- Moore, J. R., Zhu, K., Huntingford, C., and Cox, P. M.: Equilibrium forest demography explains the distribution of tree sizes across North America, *Environmental Research Letters*, 13, <https://doi.org/10.1088/1748-9326/aad6d1>, 2018.
- 15 Moore, J. R., Argles, A. P. K., Zhu, K., Huntingford, C., and Cox, P. M.: Validation of demographic equilibrium theory against tree-size distributions and biomass density in Amazonia, *Biogeosciences*, 17, 1013–1032, <https://doi.org/10.5194/bg-17-1013-2020>, <https://www.biogeosciences.net/17/1013/2020/>, 2020.
- Muller-Landau, H. C., Condit, R. S., Harms, K. E., Marks, C. O., Thomas, S. C., Bunyavejchewin, S., Chuyong, G., Co, L., Davies, S., Foster, R., Gunatilleke, S., Gunatilleke, N., Hart, T., Hubbell, S. P., Itoh, A., Kassim, A. R., Kenfack, D., LaFrankie, J. V., Lagunzad, D.,
- 20 Lee, H. S., Losos, E., Makana, J. R., Ohkubo, T., Samper, C., Sukumar, R., Sun, I. F., Nur Supardi, M. N., Tan, S., Thomas, D., Thompson, J., Valencia, R., Vallejo, M. I., Muñoz, G. V., Yamakura, T., Zimmerman, J. K., Dattaraja, H. S., Esufali, S., Hall, P., He, F., Hernandez, C., Kiratiprayoon, S., Suresh, H. S., Wills, C., and Ashton, P.: Comparing tropical forest tree size distributions with the predictions of metabolic ecology and equilibrium models, *Ecology Letters*, 9, 589–602, <https://doi.org/10.1111/j.1461-0248.2006.00915.x>, 2006.
- Nepstad, D. C., Stickler, C. M., Filho, B. S., and Merry, F.: Interactions among Amazon land use, forests and climate: prospects for a
- 25 near-term forest tipping point, *Philosophical Transactions of the Royal Society B: Biological Sciences*, 363, 1737–1746, 2008.
- Niklas, K. J. and Spatz, H.-C.: From The Cover: Growth and hydraulic (not mechanical) constraints govern the scaling of tree height and mass, *Proceedings of the National Academy of Sciences*, 101, 15 661–15 663, <https://doi.org/10.1073/pnas.0405857101>, <http://www.pnas.org/cgi/doi/10.1073/pnas.0405857101>, 2004.
- Pavlick, R., Drewry, D. T., Bohn, K., Reu, B., and Kleidon, A.: The Jena Diversity-Dynamic Global Vegetation Model (JeDi-DGVM): a
- 30 diverse approach to representing terrestrial biogeography and biogeochemistry based on plant functional trade-offs, *Biogeosciences*, 10, 4137–4177, 2013.
- Peterson, D. W. and Reich, P. B.: Prescribed fire in oak savanna: fire frequency effects on stand structure and dynamics, *Ecological Applications*, 11, 914–927, 2001.
- Phillips, O. L.: Long-term environmental change in tropical forests: increasing tree turnover, *Environmental Conservation*, 23, 235–248, <https://doi.org/10.1017/s0376892900038856>, 1996.
- 35 Phillips, O. L., Baker, T. R., Arroyo, L., Higuchi, N., Killeen, T. J., Laurance, W. F., Lewis, S. L., Lloyd, J., Malhi, Y., Monteagudo, A., Neill, D. A., Núñez Vargas, P., Silva, J. N., Terborgh, J., Vásquez Martínez, R., Alexiades, M., Almeida, S., Brown, S., Chave, J., Comiskey, J. A., Czimczik, C. I., Di Fiore, A., Erwin, T., Kuebler, C., Laurance, S. G., Nascimento, H. E., Olivier, J., Palacios, W., Patiño, S.,

- Pitman, N. C., Quesada, C. A., Saldias, M., Torres Lezama, A., and Vinceti, B.: Pattern and process in Amazon tree turnover, 1976-2001, *Philosophical Transactions of the Royal Society B: Biological Sciences*, 359, 381–407, <https://doi.org/10.1098/rstb.2003.1438>, 2004.
- Poulter, B., MacBean, N., Hartley, A., Khlystova, I., Arino, O., Betts, R., Bontemps, S., Boettcher, M., Brockmann, C., Defourny, P., Hagemann, S., Herold, M., Kirches, G., Lamarche, C., Lederer, D., Otlé, C., Peters, M., and Peylin, P.: Plant functional type classification for earth system models: Results from the European Space Agency’s Land Cover Climate Change Initiative, *Geoscientific Model Development*, 8, 2315–2328, <https://doi.org/10.5194/gmd-8-2315-2015>, 2015.
- Prior, L. D., Murphy, B. P., and Russell-Smith, J.: Environmental and demographic correlates of tree recruitment and mortality in north Australian savannas, *Forest Ecology and Management*, 257, 66–74, 2009.
- Pugh, T., Jones, C., Huntingford, C., Burton, C., Arneth, A., Brovkin, V., Ciais, P., Lomas, M., Robertson, E., Piao, S., et al.: A Large Committed Long-Term Sink of Carbon due to Vegetation Dynamics, *Earth’s Future*, 6, 1413–1432, 2018.
- Pugh, T. A. M., Rademacher, T. T., Shafer, S. L., Steinkamp, J., Barichivich, J., Beckage, B., Haverd, V., Harper, A., Heinke, J., Nishina, K., Rammig, A., Sato, H., Arneth, A., Hantson, S., Hickler, T., Kautz, M., Quesada, B., Smith, B., and Thonicke, K.: Understanding the uncertainty in global forest carbon turnover, *Biogeosciences Discussions*, 2020, 1–44, <https://doi.org/10.5194/bg-2019-491>, <https://www.biogeosciences-discuss.net/bg-2019-491/>, 2020.
- Sato, H., Itoh, A., and Kohyama, T.: SEIB-DGVM: A new Dynamic Global Vegetation Model using a spatially explicit individual-based approach, *Ecological Modelling*, 200, 279–307, <https://doi.org/10.1016/j.ecolmodel.2006.09.006>, 2007.
- Scheiter, S., Langan, L., and Higgins, S. I.: Next-generation dynamic global vegetation models: Learning from community ecology, *New Phytologist*, 198, 957–969, <https://doi.org/10.1111/nph.12210>, 2013.
- Schleussner, C.-F., Rogelj, J., Schaeffer, M., Lissner, T., Licker, R., Fischer, E. M., Knutti, R., Levermann, A., Frieler, K., and Hare, W.: Science and policy characteristics of the Paris Agreement temperature goal, *Nature Climate Change*, 6, 827–835, 2016.
- Sellar, A. A., Jones, C. G., Mulcahy, J., Tang, Y., Yool, A., Wiltshire, A., O’connor, F. M., Stringer, M., Hill, R., Palmieri, J., et al.: UKESM1: Description and evaluation of the UK Earth System Model, *Journal of Advances in Modeling Earth Systems*, 2019.
- Smith, B.: LPJ-GUESS-an ecosystem modelling framework, Department of Physical Geography and Ecosystems Analysis. INES, *Sölvegatan*, 12, 22 362, 2001.
- Staver, A. C., Bond, W. J., Stock, W. D., Van Rensburg, S. J., and Waldram, M. S.: Browsing and fire interact to suppress tree density in an African savanna, *Ecological applications*, 19, 1909–1919, 2009.
- Strigul, N., Pristinski, D., Purves, D., Dushoff, J., and Pacala, S.: Scaling from trees to forests: tractable macroscopic equations for forest dynamics, *Ecological Monographs*, 78, 523–545, 2008.
- Swaine, M.: Characteristics of dry forest in West Africa and the influence of fire, *Journal of vegetation science*, 3, 365–374, 1992.
- Thomas, S. C. and Martin, A. R.: Carbon content of tree tissues: a synthesis, *Forests*, 3, 332–352, 2012.
- Van Nieuwstadt, M. G. and Sheil, D.: Drought, fire and tree survival in a Borneo rain forest, East Kalimantan, Indonesia, *Journal of Ecology*, 93, 191–201, 2005.
- Van Uytvanck, J., Maes, D., Vandenhaute, D., and Hoffmann, M.: Restoration of woodpasture on former agricultural land: the importance of safe sites and time gaps before grazing for tree seedlings, *Biological Conservation*, 141, 78–88, 2008.
- Weng, E. S., Malyshev, S., Lichstein, J. W., Farrior, C. E., Dybzinski, R., Zhang, T., Shevliakova, E., and Pacala, S. W.: Scaling from individual trees to forests in an Earth system modeling framework using a mathematically tractable model of height-structured competition, *Biogeosciences*, 12, 2655–2694, <https://doi.org/10.5194/bg-12-2655-2015>, <https://www.biogeosciences.net/12/2655/2015/>, 2015.

West, G. B., Brown, J. H., and Enquist, B. J.: A general model for the origin of allometric scaling laws in biology, *Science*, 276, 122–126, 1997.

Yue, C., Ciais, P., Luysaert, S., Li, W., McGrath, M. J., Chang, J., and Peng, S.: Representing anthropogenic gross land use change, wood harvest, and forest age dynamics in a global vegetation model ORCHIDEE-MICT v8.4.2, *Geoscientific Model Development*, 11, 409–428,

5 <https://doi.org/10.5194/gmd-11-409-2018>, <https://www.geosci-model-dev.net/11/409/2018/>, 2018.